

Universität für Bodenkultur Wien



University of Natural Resources and Life Sciences, Vienna

Department für Biotechnologie
Institut für angewandte Mikrobiologie

Leiterin: Univ.Prof. Dipl.-Ing. Dr.rer.nat. techn. Reingard Grabherr

Separation of HIV-1 gag Virus-Like Particles and Viruses from Cell Culture Supernatants

Dissertation

Zur Erlangung des akademischen Grades
„Doktor der Bodenkultur“

Vorgelegt von

Dipl. Ing. Tobias Amadeus Schneider

Betreut durch:

Univ.Prof. Dipl.-Ing. Dr.nat.techn. Alois Jungbauer

Wien, 01.04.2020

For Ylvie.

Abstract

Enveloped virus-like particles are considered promising candidates for next generation vaccines or immunotherapy. However, their purification remains a challenge because of a limited amount of suitable purification methods for preparative and analytical scale. Also, their size and structural similarity to host cell derived impurities like extracellular vesicles, or other bio-nanoparticles adds to this difficult task. This work shows the development of two purification protocols for the purification of HIV-1 gag H1 particles produced in a baculovirus insect cell system with *Tnms42* cells and fluorescent HIV-1 gag-gfp VLPs produced in a HEK293 cell culture by transient transfection. For the purification a monolithic QA anion-exchange chromatography column was chosen. Both processes allow a direct capture of the cell culture supernatant after filtration and nuclease treatment. The final processes were able to deplete the majority of impurities such as host cell derived proteins, DNA and other bio-nanoparticles. Assuming a particle concentration of 1×10^9 particles/vaccination dose, 450 vaccination doses could be produced from 100 mL cell culture supernatant produced in BEVS. The HEK293 process could produce 390 vaccination doses from the same amount of cell culture supernatant with similar purity and quality. Furthermore, an at-line particle monitoring method was developed that allows direct in-process tracking of particles. The method uses the intensity of the scattered light from a multi-angle light scattering detector, which is directly proportional to particle concentration and size. Additionally, the light scattering data was used to calculate the relative form factors of elution fractions that allowed the differentiation of particle morphologies directly from elution samples. In summary it can be stated, that the two developed methods have shown the practicability of convective chromatography media such as monoliths for the purification of large bio-nanoparticles. Further, we showed that light scattering detectors are a valuable contribution in the detector setup for process development and that the implementation of these newly developed methods allows an accelerated process development for bio-nanoparticle downstream processing.

Keywords: Virus-like particle, VLP, Virus, Chromatography, purification, MALS, SAXS, NTA

Kurzfassung

Umhüllte virusartige Partikel (VLP) werden als vielversprechende Kandidaten für Gentherapie oder Impfstoffe der nächsten Generation angesehen. Aufgrund der eingeschränkten Auswahl von geeigneten Analytik- und Aufreinigungsmethoden stellt die Aufreinigung dieser Partikel noch eine anspruchsvolle Aufgabe dar. Eine weitere Herausforderung ist die Größe der Partikel und ihre Ähnlichkeit zu anderen von der Wirtszelle herrührenden Verunreinigungen wie extrazelluläre Partikel oder andere Nanopartikel biologischen Ursprungs wie zum Beispiel Viren. Diese Arbeit beschreibt die Entwicklung von zwei Aufreinigungsprozessen. Der erste VLP ist ein HIV-1 gag H1 Partikel, der in *Tnms42* Zellen und einem Baculovirus-Insektenzellen Expressionssystem produziert wurde. Bei dem anderen aufgereinigten Partikel handelt es sich um einen fluoreszierenden HIV-1 gag-gfp VLP und wurde mit Hilfe von HEK293 Zellen produziert. Für die Aufreinigung wurde eine Monolith QA-Anionentauscher-Chromatographiesäule gewählt. Beide Prozesse erlauben das direkte Laden des Zellkultur-Überstands, nachdem die Wirtszellen abgetrennt und der Überstand mit Nukleasen behandelt und filtriert wurde. Der jeweils finale Prozess reichert Protein und DNA der Wirtszelle zu hohem Anteil ab und reduziert andere partikuläre Verunreinigungen signifikant. Bei einer angenommenen Partikelmenge von 1×10^9 Partikeln pro Impfdosis, konnten 450 Impfdosen aus 100 mL Zellkulturüberstand im Baculovirus Expressionssystem gewonnen werden. Aus dem HEK293 Prozess konnten 390 Impfdosen aus der gleichen Menge an Zellkultur-Überstand mit vergleichbarer Produktqualität und Reinheit produziert werden. Weiter wurde eine Methode für die In Prozess-Kontrolle für Bio-Nanopartikeln entwickelt, die die direkte Verfolgung der Partikel durch den Aufreinigungsprozess ermöglicht. Die Methode nutzt die Intensität von Streulicht in Multi-Winkel Streulichtdetektoren, welches direkt proportional zur Partikel-Konzentration und Partikelgröße ist. Das Detektorsignal wurde überdies noch genutzt um die relativen Form-Faktoren von Elutions-Fractionen zu berechnen. Diese Methode ermöglicht die Unterscheidung von Partikeln aufgrund ihrer geometrischen Form direkt in den Elutions-Fractionen. Zusammengefasst lässt sich sagen, dass die beiden entwickelten Prozesse die erfolgreiche Verwendbarkeit von konvektiver Chromatographie Material wie Monolithen für die Aufreinigung von großen Bio-Nanopartikeln wie VLPs oder Viren zeigen. Weiter haben wir gezeigt, dass die Implementierung von Streulichtdetektoren einen wertvollen Beitrag für die Prozessentwicklung leistet und eine signifikante Beschleunigung der Entwicklung von Aufreinigungsprozessen für Bio-Nanopartikel darstellt.

Schlagwörter: Virusartige Partikel, VLP, Viren, Chromatographie, Aufreinigung, MALS, SAX, NTA

Statutory Declaration

Statutory Declaration

I hereby declare that I have developed and written the enclosed doctoral thesis entirely by myself and have not used any sources or means without unambiguous declaration in this text. This thesis was not submitted in the same or in a substantially similar version, not even partially, to any other authority to achieve an academic grading. I am also aware, that an incorrect statutory declaration will have legal effects.

Wien, 01.04.2020

(Ort, Datum)



(Signature)

Eidesstattliche Erklärung

Ich versichere, dass die vorliegende Doktorarbeit selbständig und ohne Benutzung anderer als der angegebenen Quellen und Hilfsmittel angefertigt und die den benutzten Quellen, wörtlich oder inhaltlich, entnommenen Stellen als solche kenntlich gemacht wurden. Diese Arbeit wurde in gleicher oder ähnlicher Form noch keiner Prüfungsbehörde vorgelegt. Ich bin mir bewusst, dass eine falsche Erklärung rechtliche Folgen haben wird.

Wien, 01.04.2020

(Ort, Datum)



(Unterschrift)

Acknowledgements

To begin with, I want to thank Mr. Univ.Prof. Dipl.-Ing. Dr.nat.techn. Alois Jungbauer for the opportunity to write my doctoral thesis in his working group. I also want to especially thank him for his patience, his mentoring not only on a scientific, but also personal level.

Thank you Alois!

Furthermore, I owe gratitude and special thanks to the “VLP-Gang”: Patricia, Petra and Katrin for their excellent assistance, patience and support during the development of this thesis.

I would also like to thank everyone else who supported me in developing the experiments and work during my wonderful time at Boku. Special thank goes to Mrs. Eva Berger for her excellent assistance with the TEM pictures and to Dipl.-Ing. Dr. Rupert Tscheließnig for supporting me with excellent input for the fractal dimension analysis.

Above all, I owe my greatest gratitude to my family. My companion Anna Mareike, my daughter Ylvie Ophelia, my parents Beate and Franz-Joseph and my sister Maximiliane for their unending love and support... Thank you!

Thank you!

Table of Contents

Abstract	III
Kurzfassung	IV
Statutory Declaration	V
Acknowledgements.....	6
Table of Contents	VII
List of Symbols and Abbreviations	IX
Index of Figures	XI
Table Directory.....	XV
1 Introduction and Theoretical Background	17
1.1 Brief Summary on the History and Development of Vaccination	17
1.2 Virus-Like Particles	19
1.2.1 VLP assembly & Budding-Process of HIVLPs	19
1.2.2 Distinction of VLPs to other extracellular vesicles	21
1.3 Manufacturing of VLPs	22
1.4 Purification of VLPs	25
1.5 Methodology of VLP Analytics	31
2 Aim of this Work.....	37
3 Materials and Methods.....	38
3.1 Chemicals	38
3.2 Production of VLPs	38
3.2.1 Production of HIV-1 Gag-GFP VLP Supernatants in HEK-293 Cell Culture	38
3.2.2 Production of HIV-1 Gag H1 VLP Supernatants in <i>Tnms42</i> Insect Cell Culture	39
3.2.3 Production of HIV-1 Gag VLPs in CHO Cell Culture	40
3.2.4 Endonuclease treatment.....	40
3.3 Liquid Chromatography.....	40
3.3.1 Preparative Scale Chromatography Equipment.....	40
3.3.2 Preparative Scale Chromatography	40
3.3.3 High-Performance Liquid Chromatography (HPLC) Equipment.....	41
3.3.4 At-line Multi Angle Light Scattering as Fraction Analytics	42

3.4	Protein Concentration and dsDNA Content	42
3.5	Sodium Dodecyl Sulfate-Polyacrylamide Gel Electrophoresis (SDS-PAGE).....	42
3.6	Western Blot Analysis	43
3.7	Tissue Culture Infective Dose (TCID ₅₀).....	43
3.8	Nanoparticle tracking analysis (NTA)	43
3.9	Transmission Electron Microscopy (TEM)	44
3.10	Fractal Dimension Analysis and Calculation from MALS Data	44
3.10.1	Conceptual MALS Computation using Characteristic Tailing of Scattering Curves.....	44
3.10.2	Conceptual MALS Computation using Truncated Forms of Pair Densities	47
4	Results and Discussion	48
4.1	Purification Method Development for HIV-1 gag H1 VLPs Expressed in BVES	49
4.1.1	Characterization of Expression Levels of <i>TnmsS42</i>	49
4.1.2	Linear Gradient Purification of HIV-1 gag H1 VLPs.....	60
4.1.3	Step Gradient Purification.....	64
4.2	Purification Method Development for HIV-1 Gag-GFP VLPs Expressed in HEK-293.....	70
4.2.1	Linear Gradient Purification of HIV-1 Gag-GFP VLPs.....	70
4.2.2	Step Gradient Purification of HIV-1 Gag-GFP VLPs	73
5	Summary and Conclusion.....	77
6	References.....	79

List of Symbols and Abbreviations

eVLP	Enveloped Virus-like Particle
VLP	Virus-like Particle
HBsAg	Hepatitis B virus surface antigen
Hpv	Human papillomavirus
HIV-1	Human immunodeficiency virus type 1
EV	Extracellular vesicle
PTMs	Postranslational modifications
USP	Upstream processing
DSP	Downstream processing
CHO	Chinese hamster ovaries
GOI	Gene of interest
PEI	Polyethyleneimine
GOI	Gene of interest
BEVS	Baculovirus Expression Vector System
B/IC	Baculovirus Insect Cell System
BV	Baculovirus
DF	Depth filtration
TFF	Tangential flow filtration
UF/DF	Ultra filtration / diafiltration
PEG	Polyethylene glycol
AC	Affinity chromatography
IEC	Ion exchange chromatography
AIEX	Anion exchange chromatography
CIEX	Cation exchange chromatography
HIC	Hydrophobic interaction chromatography
MMC	Mixed mode chromatography
SEC	Size exclusion chromatography
MW	Molecular weight
RGD	Rayleigh-Gans-Debye
WB	Western blot

SDS-PAGE	Sodium dodecyl sulfate polyacrylamide gel electrophoresis
NTA	Nanoparticle tracking analysis
MALS	Multi-angle light scattering
TCID ₅₀	Tissue culture infection Dose 50%,
SAXS	Small-angle X-ray scattering
(Cryo)-TEM	(Cryogenic-) Transmission electron-microscope
CV	Column volumes
RMSq	Root mean square radius
r_g	Radius of gyration
<i>Tnms42</i>	<i>Trichoplusia ni</i>
M	Molecular weight marker
S	Supernatant
L	Load
FT	Flow-through
W	Wash
P1 – n	Pooled elution Peak 1 – n
FE	Pooled full elution

Index of Figures

- Figure 1-1: Schematic overview over the evolution of vaccine design with the advancements in technology adapted from [6]. In the 18 – 19th century inoculation techniques were used and later developing into tissue- and cell-culture techniques in the middle of the 20th century. After the pioneering work in the field of recombinant DNA and PCR sequencing recombinant vaccines could be developed. Since the 2000s the era of synthetic biology has further advanced and with genetic engineering, a high amount of different vaccine designs are in development. 17
- Figure 1-2: Possible conformational assemblies of enveloped and unenveloped VLPs built from one or two structural proteins. 19
- Figure 1-3: A) Schematic overview over the gag polyprotein gene and its monomers. B) Summary of the VLP formation and budding process, illustrated in three steps. After translation and expression of the gag polyprotein gene the native gag proteins accumulate at the plasma membrane of the host cell, which finally leads to a bud formation and release of an assembled enveloped VLP into the extracellular space. Gag proteins are on the inner surface of the VLP with a host cell derived membrane as outer layer. On the right side, a cryo-TEM picture shows the budding process in a *Tnms42* cell expressing HIV-1 gag H1 VLPs. 20
- Figure 1-4: Schematic flow chart for manufacturing of secreted VLPs. After the initial production and clarification, the typical three stage purification strategy is used. The purification starts with a capture step followed by the intermediate purification and final polishing. On the left side, the potential purification techniques are shown for each step. The right side of the process shows the depleted impurities for each step. DF: depth filtration; TFF: tangential flow filtration; UF/DF: ultrafiltration / diafiltration; PEG: polyethylene glycol; AC: affinity chromatography; IEC: ion exchange chromatography; HIC, hydrophobic interaction chromatography; MM, mixed mode chromatography; SEC, size-exclusion chromatography..... 25
- Figure 1-5: Schematic examples of chromatography stationary phases: A) Column with packed bed B) Chromatography Resin bead particle C) Monolith column with radial flow and continuous flow channel network D) Stacked membrane adsorber sheets. (adapted from: [79])..... 26
- Figure 1-6: Left: Schematic drawing of the measurement principle of NTA. The laser light of the focused laser beam is scattered as it passes through the measuring chamber. Right: The illuminated particles are filmed in a video clip and later analyzed by the tracking software..... 33
- Figure 1-7: The principle of a Multi-angle light scattering detector. A) Detector setup with a laser light source providing polarized light and a flow cell. Particles scatter the light which is collected at fixed detectors at specific angles around the flow cell. B) Calculation principle of the root mean square radius (RMS) or radius of gyration (r_g): The distance r_i from the center of mass to the isotropic scattering center is needed to calculate the root mean square radius (RMS). 34
- Figure 1-8: Illustration of the measuring principle of small angle X-ray scattering. A) Experimental setup for light scattering experiment. The X-ray beam passes the sample chamber and is scattered by

particles. The X-ray detector measures the intensity as well as the position. B) Different sample properties can be extracted from the three regions of a SAXS profile (Guinier, Fourier and Porod) in a double logarithmic plot, depending on slope and shape of the curve [134].....	35
Figure 3-1: Graphical description, how the fractal bodies are built from the equation $p(r)$ to compute the possible pair densities of particles representing hollow spheres.....	45
Figure 3-2: Theoretical scattering curve for a spherical hollow particle.	46
Figure 4-1: Chromatogram of the linear gradient of the <i>Tnms42</i> mock fermentation using a QA monolith. The loading material was 100 mL of clarified, nuclease treated and 0.8 μm filtered cell culture supernatant. Bars represent the area under the curve of the light scattering intensity (grey) at-line measurements. FT: flow-through; W: wash; P1-P4: pooled fractions for peaks 1–4.....	50
Figure 4-2: A) SDS-PAGE and Western blots of linear gradient purification of the mock fermentation supernatant (Figure 4-1) B) gp64 Western blot and C) HIV-1 p24 Western blot. M: molecular weight marker; S: supernatant; FT: flow-through; W: wash; P1 – P4: pooled peaks 1 – 4; CIP: cleaning-in-place	51
Figure 4-3: Chromatogram of the linear gradient of the virus expression in <i>Tnms42</i> cells using a QA monolith. The loading material was 100 mL of clarified, nuclease treated and 0.8 μm filtered cell culture supernatant. Bars represent the area under the curve of the light scattering intensity (grey) at-line measurements. FT: flow-through; W: wash; P1-P4: pooled fractions for peaks 1–4.....	52
Figure 4-4: A) SDS-PAGE and Western blots of linear gradient purification of the virus expression in <i>Tnms42</i> cells (Figure 4-3) B) gp64 Western blot and C) HIV-1 p24 Western blot. M: molecular weight marker; S: supernatant; FT: flow-through; W: wash; P1 – P4: pooled peaks 1 – 4; CIP: cleaning-in-place	53
Figure 4-5: Chromatogram of the linear gradient of the <i>Tnms42</i> HIV-1 gag H1 VLP expression using a QA monolith. The loading material was 100 mL of clarified, nuclease treated and 0.8 μm filtered cell culture supernatant. Bars represent the area under the curve of the light scattering intensity (grey) at-line measurements. FT: flow-through; W: wash; P1-P4: pooled fractions for peaks 1–4.....	54
Figure 4-6: A) SDS-PAGE and Western blots of linear gradient purification of the <i>Tnms42</i> HIV-1 gag H1 VLP expression (Figure 4-5) B) gp64 Western blot and C) HIV-1 p24 Western blot. M: molecular weight marker; S: supernatant; FT: flow-through; W: wash; P1 – P4: pooled peaks 1 – 4; CIP: cleaning-in-place.....	55
Figure 4-7: Overlay of the normalized area under the curve of the light scattering signal for the mock fermentation, virus expression and HIV-1 gag H1 VLPs production.	56
Figure 4-8: Fractal dimension analysis of the MALS raw data of the linear gradient elution (left). Colored lines give the raw data; grey lines represent the fitted data of the respective runs: A) Mock fermentation B) Virus expression C) eVLP expression. On the right, the course of the fractal dimension of the respective expression runs is shown. The y-axis ($D_{1,2}$) indicates the fractal	

dimension, while the x-axis is the time course over the elution of the chromatography run The present data suggests a tendency from spherical shapes to elongated structures.	57
Figure 4-9: Analysis of λ (left) and fractal dimension D_2/D_1 (right) over the course of the elution of the respective runs are shown: A) Mock fermentation B) Virus expression C) eVLP expression. A value of $\lambda < 1$ indicates, that hollow, thin walled objects are eluting.	58
Figure 4-10: Chromatogram of the linear gradient purification of HIV-1 gag H1 VLPs using a QA monolith. The loading material was 50 mL clarified and nuclease treated supernatant and was filtered by 0.8 μm prior to loading. FT: flow-through; W: wash; P1 – P3: pooled peaks 1 – 3.....	60
Figure 4-11: A) SDS-PAGE and Western blots of linear gradient purification (Figure 4-10) B) haemagglutinin H1 and C) HIV-1 p24. M: molecular weight marker; S: supernatant; FT: flow-through; W: wash; FE: pooled Elution peaks; P1 – P3: pooled peaks 1 – 3.....	60
Figure 4-12: Chromatogram of the step gradient purification of HIV-1 gag H1 VLPs using a QA monolith. The loading material was 100 mL clarified and nuclease treated supernatant and was filtered by 0.8 μm prior to loading. FT: flow-through; W: wash; P1 – P4: pooled peaks 1 – 4; 2M: Regeneration step 2 M NaCl	64
Figure 4-13: Western blots of the step gradient purification (Figure 4-12). A) HIV-gag p24 of B) haemagglutinin H1 C) Baculovirus envelope protein gp64 D) Viral capsid protein vp39. M: molecular weight marker; S: supernatant; FT: flow-through; W: wash; P1 – P4: pooled peaks 1 – 4; 2M: Regeneration 2 M NaCl	65
Figure 4-14: Exemplary TEM pictures from step gradient purification of the <i>Tnms42</i> cell culture supernatant. A) VLP from P1 B) Baculovirus from P2 C) Baculovirus in P4.....	67
Figure 4-15: Linear gradient purification chromatogram of 100 mL filtered, cell free HEK293 supernatant containing HIV-1 Gag-GFP VLPs. Column is a 1 mL QA monolith. The at-line MALS-FI measurements are displayed as overlay. Bars show the area under the curve of the light scattering intensity (grey) and fluorescence (green). FT: flow-through; W: wash; P1-P5: pooled fractions for peaks 1–5 (adapted from [150]).	70
Figure 4-16: (A) SDS-PAGE and (B) Western blot scans of the linear gradient purification of HIV-Gag-GFP. Abbreviations: M: molecular weight marker; S: cell culture supernatant; L: loading material; FT: flow-through; W: wash; P1-P5: pooled fractions for peaks 1–5 (adapted from [150]).	72
Figure 4-17: Chromatogram of the step gradient purification of HIV-1 Gag-GFP VLP using a QA monolith. The loading material was 100 mL of clarified and 0.8 μm filtered HEK 293 cell culture supernatant. FT: flow-through; W: wash; P1-P4: pooled fractions for peaks 1–4 (adapted from [150]).	73
Figure 4-18: Electron microscopy micrographs of A) loading material (L) and pooled peaks B) P2 and C) P3 from step gradient purification (Figure 4-18 A) (adapted from [150]).	75

Figure 4-19: Analysis of the fractions P1-P4 from the step gradient purification (Figure 4-17 A) by analytical size exclusion chromatography coupled to MALS and fluorescence detectors (SEC-MALS-FL). A) P1; B) P2; C) P3; D) P4 (adapted from [150]).	76
---	----

Table Directory

Table 1-1: Summary of the Virus-like Particles used in this work.....	20
Table 1-2: Short summary of the expression systems described in this chapter. Adapted from [52].	22
Table 1-3: Summary of the analytical methods used in this work for measuring identity, quantity and particle morphology of the given analyte. NTA: Nanoparticle tracking analysis, MALS: Multi-angle light scattering, TCID ₅₀ : Tissue culture infection Dose 50%, TEM: Transmission electron-microscope, SAXS: small-angle X-ray scattering	31
Table 1-4: Decision matrix for VLP identification (simplified).....	32
Table 3-1: Summary and overview of the final purification methods of the different VLPs used in this thesis. All values are given for the CIMultus QA 1 mL column and mobile phases A (50 mM HEPES, pH 7.2) and B (50 mM HEPES, 2000 mM NaCl, pH 7.2)	41
Table 4-1: Summary and mass balance for total protein and dsDNA of the linear gradient purification of the mock fermentation cell culture supernatant (Figure 4-1) with the quantification of infective baculovirus (TCID ₅₀). S: supernatant; FT: flow-through; W: wash; P1 – P4: pooled peaks 1 – 4; CIP: cleaning-in-place	50
Table 4-2: Summary and mass balance for total protein and dsDNA of the linear gradient purification of the virus expression in <i>Tnms42</i> cells (Figure 4-3) with the quantification of infective baculovirus (TCID ₅₀). S: supernatant; FT: flow-through; W: wash; P1 – P4: pooled peaks 1 – 4; CIP: cleaning-in-place	52
Table 4-3: Summary and mass balance for total protein and dsDNA of the linear gradient purification of the <i>Tnms42</i> HIV-1 gag H1 VLP expression (Figure 4-5), with the quantification of infective baculovirus (TCID ₅₀). S: supernatant; FT: flow-through; W: wash; P1 – P4: pooled peaks 1 – 4; CIP: cleaning-in-place	55
Table 4-4: Summary and the mass balance for total protein and dsDNA of the linear gradient purification of HIV-1 gag H1 VLPs (Figure 4-10). S: supernatant; FT: flow-through; W: wash; FE: pooled Elution peaks; P1 – P3: pooled peaks 1 – 3; CIP: cleaning-in-place	61
Table 4-5: Particle mass balance for all and selected particles (d: 100 – 200 nm) and mean particle sizes from NTA of the linear gradient purification fractions of HIV-1 gag H1 VLPs (Figure 4-10). S: supernatant; FT: flow-through; W: wash; FE: pooled Elution peaks; P1 – P3: pooled peaks 1 – 3; CIP: cleaning-in-place; Same superscript letters (A/B) indicate significant size difference	62
Table 4-6: Summary and mass balance for total protein and dsDNA of the step gradient purification of HIV-1 gag H1 VLPs. S: supernatant; FT: flow-through; W: wash; P1 – P4: pooled peaks 1 – 4; 2M: Regeneration step 2 M NaCl; CIP: cleaning-in-place.....	65
Table 4-7: Particle and infective baculovirus mass balance for step gradient purification of HIV-1 gag H1 VLPs with log ₁₀ virus reduction factors and mean particle sizes for the process samples from NTA and TCID ₅₀ . S: supernatant; FT: flow-through; W: wash; P1 – P4: pooled peaks 1 – 4; 2M:	

Regeneration step 2 M NaCl; CIP: cleaning-in-place; Same superscript letters (A/B) indicate significant size difference; Form factor 2: spherical particle; Form factor 1: rod-shaped particle	66
Table 4-8: Total protein and dsDNA mass balance of the purification of HIV-1 Gag-GFP VLPs using a linear gradient elution (Figure 1). S: supernatant; L: loading material; FT: flow-through; W: wash; P1-P5: peaks 1-5 (adapted from [150]).	71
Table 4-9: Total protein and dsDNA analysis of the HIV-1 Gag-GFP VLPs purification using a step gradient elution (Figure 4-17). L: loading material; FT: flow-through; W: wash; P1-P4: peaks 1-4; CIP: cleaning-in-place (adapted from [150]).	74
Table 4-10: Table 2. Particles (diameter: 100–200 nm), total protein and dsDNA mass balance of the purification of HIV-1 Gag-GFP VLPs using a step gradient elution (Figure 3). L: loading material; FT: flow-through; W: wash; P1-P4: peaks 1-4; CIP: cleaning-in-place (adapted from [150]).	74

1 Introduction and Theoretical Background

This chapter gives an introduction into the topic of this doctoral thesis and conveys the needed theoretical background along with a review of the current literature.

1.1 Brief Summary on the History and Development of Vaccination

Since the first documented vaccination in the late 18th century by Edward Jenner [1] the research and technology behind vaccines and their production has made a tremendous progress. It has led to a wide range of available vaccines for veterinary or human application. The first scientifically reported vaccination was performed by Edward Jenner. He inoculated a boy named James Phipps with matter taken from fresh cowpox lesions of the dairymaid Sarah Nelms [2]. Today, we know the principle behind this process was an immunization using live viruses. Jenner's work however laid the groundwork, which ultimately led to the total eradication of smallpox. The WHO declared the world free of smallpox in 1980, 200 years after Jenner described the principle of vaccination [3]. Since the works of Louis Pasteur around 1880 we know that it is possible to use attenuated, or inactivated organisms produced in laboratory environment to effectively immunize against the respective diseases [4]. Inspired by Pasteur's work, Wright and Pfeiffer's research led to the first typhoid vaccine in 1896 by using inactivated *salmonella typhi* bacteria, which are known to trigger the typhoid fever [5].

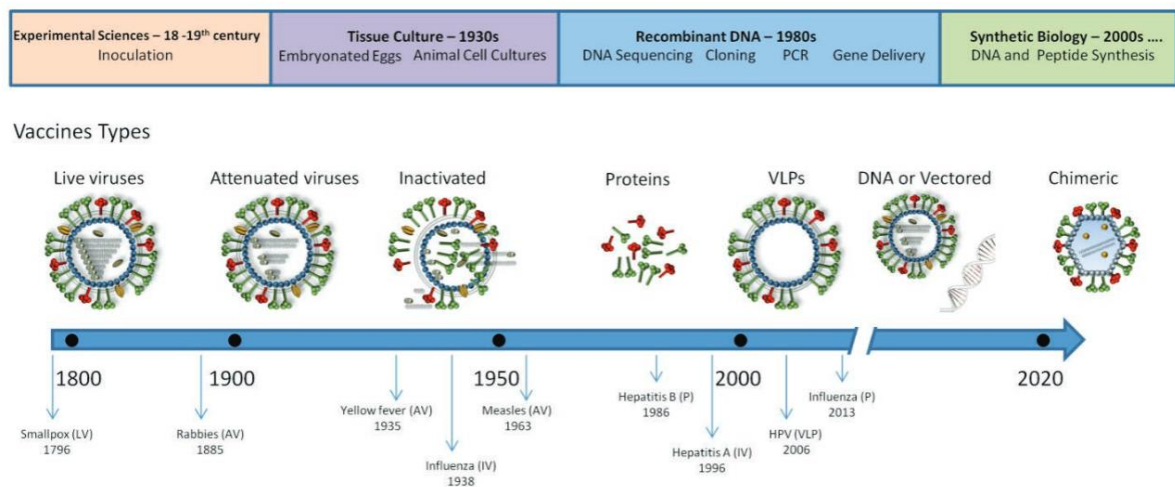


Figure 1-1: Schematic overview over the evolution of vaccine design with the advancements in technology adapted from [6]. In the 18 – 19th century inoculation techniques were used and later developing into tissue- and cell-culture techniques in the middle of the 20th century. After the pioneering work in the field of recombinant DNA and PCR sequencing recombinant vaccines could be developed. Since the 2000s the era of synthetic biology has further advanced and with genetic engineering, a high amount of different vaccine designs are in development.

A further important discovery was that not only whole inactivated organisms could induce an immunization process, but also purified components like polysaccharides, proteins or toxoids of the respective pathogens. Noteworthy examples for this are the diphtheria or tetanus vaccine from 1923 and 1926 respectively. It was shown that purified toxoids were capable of inducing an immunization and therefore could be used as a vaccine [7]. Purified polysaccharides were also used as vaccines

against bacterial induced meningitis or pneumonia from pathogenic strains of meningococcus (1969), or pneumococcus (1974) respectively [8]. One of the major drawbacks however, was the fact that many of the early vaccines could cause real virus or bacterial outbreaks in the patient after the administration. Well-known are outbreaks of foot-and-mouth disease in cloven-hooved animals triggered by vaccines with incorrectly inactivated viruses. Also documented are maladies triggered by escaped viruses from research or manufacturing facilities [9]. Kleid et al. discovered that it was possible to produce a vaccine from a single key protein of the respective pathogen virus, which led to the first genetically engineered vaccine. By overexpressing the capsid protein VP₃ of foot-and-mouth disease virus A₁₂ in *E. coli* it was now possible to vaccinate and protect cloven-hooved livestock from this virus. This led to an additional finding: It was possible to imitate an intact virion with artificially produced particles that had the ability to stimulate humoral and cellular immune responses. These particles were called Virus-Like Particles (VLPs). The first VLP vaccine was based on the hepatitis B virus surface antigen (HBsAg) in 1979 [10]. The hepatitis B virus itself is an enveloped virus built from three envelope proteins. These proteins have properties to self-assemble and form sub-viral particles commonly called HBsAg particles during an infection. The first generation HBsAg vaccine particles were purified from patients' sera. However, with major advances in recombinant protein expression, as well as safety concerns for blood isolates from chronic hepatitis B carriers, more efficient and safer strategies had to be developed. The success to fully sequence the nucleotide sequence of the hepatitis B virus and identifying the genes coding for the HBsAg proteins led to the second-generation hepatitis B vaccines. These were recombinantly produced in *E. coli*, expressing the viral envelope proteins to form a VLP [10]–[12]. Recent and prominent examples for VLP based vaccines are Cervarix® and Gardasil® stimulating immunization against the human papillomavirus (hpv) infections and other infections associated with causing cervical cancer along with other diseases [13].

1.2 Virus-Like Particles

VLPs mimic the virus of interest in its structure and conformation except its genetic material. They are self-assembling, highly repetitive bio-nanoparticles built from viral structure proteins. Their size mainly depends on the type of mimicked virus but ranges between 30 and 200 nm. In general, VLPs can be separated into two major groups: unenveloped and enveloped VLPs. Particles from the first group are exclusively built from viral proteins, while enveloped VLPs contain viral proteins and are additionally coated with a host-cell derived membrane [14]–[16]. The high diversity of VLPs derives from the countless conformational possibilities of the building blocks. VLPs can self-assemble from a single, two- or several viral proteins. Common conformations are highly ordered single, double or triple layers with or without a host-cell derived envelope (Figure 1-2).

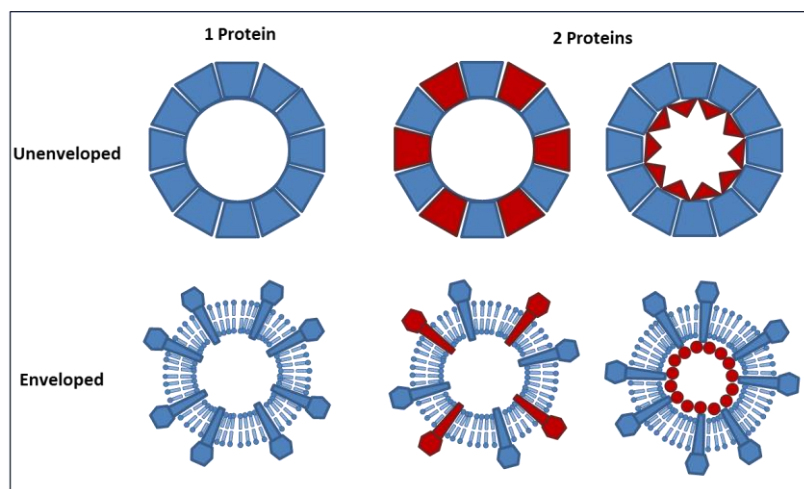


Figure 1-2: Possible conformational assemblies of enveloped and unenveloped VLPs built from one or two structural proteins.

Another key fact of VLPs is the absence of viral genomic material. This means that VLPs are lacking the tools required for reproduction via host infection (e.g. the viral life cycle). This property makes them safe candidates for vaccination, as they lack their infectious abilities compared to native viral particles. Due to the presentation of their respective antigens VLPs are capable to stimulate the cellular and humoral immune system with high efficiency in humans [6], [14], [17], [18]. Other VLP functions are drug delivery vectors [19], [20], gene therapy [21], or cancer treatment [22]. Due to their non-infectivity, they also pose no threat during production and can be handled safely during administration or as well as in research facilities without the high safety measures the original infectious virus would need.

1.2.1 VLP assembly & Budding-Process of HIVLPs

All VLPs used in this work share the same matrix protein Pr55_{gag} from the human immunodeficiency virus type 1 (HIV-1). This virus is categorized as a *Lentivirus* and belongs to the family of *Retroviridae* with the subfamily *Orthoretrovirinae* [23]. The HIV-1 gag gene encodes the structural polyprotein Pr55_{gag} and consists of different subdomains: The major structural protein p17 (MA), p24 capsid (CA), p7 nucleocapsid (NC), p6 linker protein (LI), along with small spacer peptides p2 and p1 (Figure 1-3 A).

After translation, the Pr55_{gag} is synthesized in the cytoplasm and subsequently transported to the plasma membrane of the host cell. During the cytosolic transport, the gag proteins start to self-assemble into intermediate structures and accumulates at the cytosolic side of the plasma membrane in dense patches. The formation of gag protein complexes leads to a plasma membrane curvature that leads to the formation of buds and finally to the release of matured VLPs (Figure 1-3 B) with approximately gag 2500 monomers per VLP and an approximately size of 100 – 150 nm [24]. During bud formation it is possible that producer cell-derived proteins or DNA/RNA are selectively or by chance incorporated into the VLPs [25]–[29].

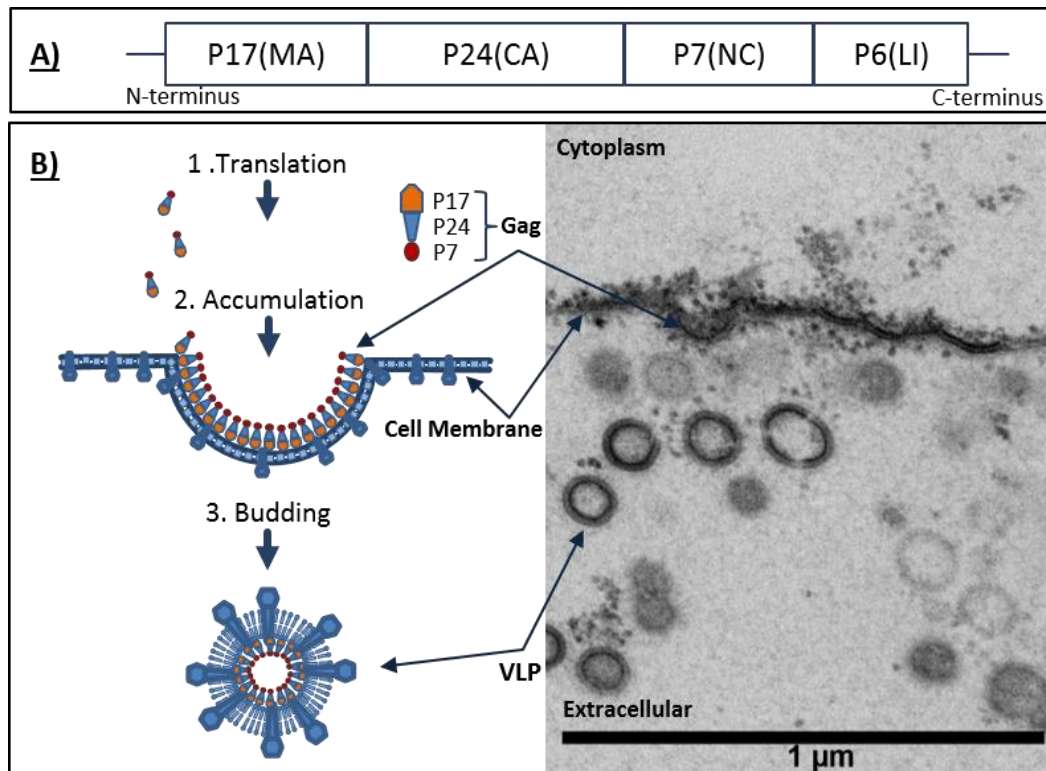


Figure 1-3: A) Schematic overview over the gag polyprotein gene and its monomers. B) Summary of the VLP formation and budding process, illustrated in three steps. After translation and expression of the gag polyprotein gene the native gag proteins accumulate at the plasma membrane of the host cell, which finally leads to a bud formation and release of an assembled enveloped VLP into the extracellular space. Gag proteins are on the inner surface of the VLP with a host cell derived membrane as outer layer. On the right side, a cryo-TEM picture shows the budding process in a *Tnms42* cell expressing HIV-1 gag H1 VLPs.

In this work, three different VLPs were used as model system (HIV-1 gag H1, HIV-1 gag, HIV-1 gag-GFP). Each of these VLPs is expressed in a different expression system. Table 1-1 summarizes the utilized VLPs and their origin.

Table 1-1: Summary of the Virus-like Particles used in this work.

VLP	Host	Expression-Type	Reference
HIV-1 gag H1	<i>Tnms42</i>	Recombinant baculovirus infection	-
HIV-1 gag	CHO	Transfection	[30]
HIV-1 gag-GFP	HEK 293	Step transfection	[31]

1.2.2 Distinction of VLPs to other extracellular vesicles

It is known for a long time that cells release extracellular vesicles (EVs). The first described vesicles were apoptotic bodies by Karl Vogt and a decade later by Rudolf Virchow [32]–[34]. The invention of ultracentrifuges and electron microscopes led to the discovery, that not only dying cells can secrete vesicles during apoptosis, but also healthy cells release vesicles, or particles into the extracellular space [20], [35], [36]. The scientific community united this heterogeneous population of membrane vesicles under the term of extracellular vesicles to combat the often-overlapping definitions of the different EV subtypes based on their origin, or biogenesis. Today, EVs are divided into four classes [37], [38]:

- 1) Apoptotic bodies: released as blebs during programmed cell death
- 2) Exosomes: formed in the endosomal network and released after fusion with multi-vesicular bodies via the plasma membrane
- 3) Microvesicles / Ectosomes: Direct budding from the plasma membrane
- 4) Outer membrane vesicles: formed by budding of the outer membrane of gram-negative bacteria

Microvesicles bud directly from the plasma membrane, while exosomes are secreted via exocytosis from multivesicular bodies. Each of these vesicle types have different tasks *in vivo*, as they transport and carry different cargoes that range from proteins, nucleic acids to lipids [39]. These cargo substances are mainly used for intercellular communication. The recipient cells can directly interact with the membrane proteins of the EV or absorb the vesicle to interact with the cargo molecules. This characteristic makes EVs along VLPs to potential candidates for therapeutic applications as a natural, *in vivo* drug delivery system [19], [20], [40]. Due to similar origins of EVs, it is apparent that they share a matching characteristic. During formation and secretion, the EVs take a portion of the originator cells plasma membrane with them. The same order of events happens during the budding process of enveloped VLPs during the spontaneous budding, where parts of the host cells plasma membrane are used as an envelope. Recent studies have also shown that EVs are co-expressed during the manufacturing process of viruses or enveloped VLPs [39]–[42]. This results in a special challenge, not only for the design of purification process, because separation of EVs and VLPs is required, but also on the analytical basis, to differentiate between product and host cell related impurity. The literature reports sizes for exosomes in the range between 50–150 nm and buoyant densities of 1.1 – 1.19 g/mL. Microvesicles range between 50–500 nm in diameter with buoyant densities of 1.6 g/mL. Apoptotic bodies are the largest extracellular vesicles with diameter ranges between 1- 5 μm and a relatively high buoyant density of 1.24 – 1.28 g/mL. HIV-1 gag VLPs have a size range between 100–200 nm in diameter and a density of 1.15 – 1.18 g/mL [43]–[46].

A clear distinction between EVs and eVLPs in the lab is difficult to achieve, due to strong similarities in the biogenesis of these particles (or vesicles), as well as their shared host cell membrane and therefore strong biochemical similarities of protein or lipid composition on their surface. Further the similar sizes or densities lead to an added challenge during separation and analytics.

1.3 Manufacturing of VLPs

Virus like particles are produced by recombinant protein expression in biotechnological processes. These processes are separated into the upstream processing (USP), where the protein building blocks are produced during the fermentation and the downstream processing (DSP), where the molecule or particle of interest is purified using a range of separation techniques to obtain the purified product.

VLPs have been successfully produced in numerous expression systems. The most important today are bacteria, yeast, mammalian and insect cell lines and recombinant plants. In early development stages, the selection of the best-suited expression system is greatly influenced by the conformational complexity of the VLP, the required post-translational modifications (PTM), or the proteins' structural complexity. This complexity again, is dictated by conditions needed during protein folding. In addition to the biological requirements, the technological factors for production also need to be considered. In later development stages, or market supply phases, factors like process robustness and production costs shift to become the key factors [6], [14], [17], [31], [47]–[52]. Table 1-2 gives a fast overview on VLP production and summarizes the expression systems with their respective advantages and disadvantages.

Table 1-2: Short summary of the expression systems described in this chapter. Adapted from [52].

Expression System	Advantage	Drawback
Bacteria	Less expensive, easy & fast expression, genetic stability, high-density fermentation, easy scale-up	No PTM, poor immunogenicity, host cell-derived contaminants, only simple proteins
Yeast	Less expensive, easy & rapid expression, easy scale-up, most protein folding and PTMs	High-mannose PTM, protein secretion may be problematic,
Plants	Rapid expression, highly scalable, less expensive, no mammalian pathogens, support most eukaryotic-type PTMs	Low yields, challenging DSP, regulatory issues
Mammalian	Support all protein folding along with complex mammalian-type PTMs, highest flexibility & complexity of VLPs	High cost, difficult scale-up, time-intensive USP, low yields, vulnerable to mammalian pathogens
Insect Cells	Moderately rapid expression supports most protein folding and eukaryotic PTMs, high flexibility and complexity of VLPs, no mammalian pathogens	High cost, difficult scale-up, not all PTMs, contamination with Baculovirus

Bacterial and **yeast** expression systems are cost-efficient and have excellent scale-up possibilities. They are well suited to produce unenveloped VLPs, assembled from one or two structural proteins, as both systems can produce in high density fermentation while containing a high expression-level. Disadvantages are limitations in protein folding as well as the lack of mammalian-like posttranslational modifications (PTM) in bacteria or in the case of yeast, with strong limitations. The PTMs however are important for the immunogenicity of VLPs usage as vaccine. Other problems arise during the purification process, as host-cell derived impurities like endo- or exotoxins need to be separated from the VLPs to meet the high regulatory requirements for vaccines. By now, there are some yeast-produced VLP vaccines, the most prominent being Gardasil®, that have been approved by regulatory agencies for human use [17], [53]–[56].

Another expression system capable of producing VLPs are **transgenic plants**. Here, the gene of interest is introduced to the plant genome using recombinant *Agrobacterium tumefaciens*. The most commonly used plants are *Nicotiana tabacum* or *Arabidopsis thaliana*. They are infected by exposition with agrobacterium carrying the gene of interest. This infection leads to a nuclear integration of the gene into the host genome and subsequently to expression of the desired protein [57]. Plant expression systems are safe during production and combine excellent scalability with a high production flexibility. Another advantage is that plants can perform mammalian-like PTMs and have a short development time from gene to protein production. The main drawback however, are still the low yields combined with challenging downstream process for plant produced materials, due to the high amounts of cell debris and other host cell-derived impurities [50].

Mammalian cells tend to have lower yields compared to other expression systems, like bacteria or yeasts, but their ability to perform PTMs with highest complexities combined with the capability to fold highly complicated proteins can make them the expression system of choice. The most important producer cell line today was extracted from Chinese hamster ovarie cells (CHO) [58]. Because of their non-human origin, their main asset is the lowered contamination risk for human-derived viruses [59]. CHO cell lines are well known for their capabilities to produce recombinant proteins, but also have been used to produce hantavirus-like particles that induced a specific immune response in mice along with many other VLP productions in development [60]–[63]. Another widely used producer line is HEK293. This cell line originated from human embryonic kidney cells and has been tested for the production of several VLPs like influenza, rabies or HIV [31], [64], [65]. Now, there are two ways to manufacture recombinant products in mammalian cells. The conventional method is to generate a stable cell line where the gene of interest (GOI) is integrated into the host genome. This process can take up to 6 months that starts with a cell line transfection followed by clone selection to identify the high producers [64]. The other option is a production using transient transfection using polyethyleneimine (PEI) in combination with recombinant plasmid DNA. In this case VLPs can be harvested approximately 48 to 72 h post transfection [31]. A major drawback when producing in mammalian cells is that they naturally secrete vesicles such as microvesicles and exosomes together with the desired VLPs. This makes the purification process very costly and

challenging, since enveloped VLPs and extracellular vesicles share the same host cell-derived membrane layer, making these particles very similar in their physico-chemical properties [30], [61].

Another infection-driven expression system is the **Baculovirus Expression Vector System (BEVS)**. Here a recombinant Baculovirus is used to infect a stable insect cell line. It was introduced in 1983 to produce human beta interferon in insect cells [66]. By now, BEVS has been used to produce a wide array different recombinant proteins [67] and also has been successfully used to produce VLPs like HIV, Chikungunya or porcine parvovirus-like particles [68]–[70]. For production two insect cell lines are commonly used Sf9 (*Spodoptera frugiperda*) and High Five cells (*Trichoplusia ni*). One of the main advantages of BEVS is that Baculovirus engineering is a fast and simple method, which can even be used to produce VLPs from viruses with high mutation rates like influenza [47]. Further, the Baculovirus insect cell system (B/IC) allows for product titers similar to bacterial or yeast expression systems, combined with lower production costs compared to mammalian producer lines like CHO or HEK293, which is also capable of complex protein folding and PTMs like glycosylation and phosphorylation [71], [72]. The main disadvantage of BEVS is that due to the virus infection of the host cell, enveloped Baculovirus (BV) are produced simultaneously during the VLP production. These coproduced BVs represent the main impurity for VLP purification which consequently turns the purification into an expensive and challenging process step [48].

1.4 Purification of VLPs

The aim of downstream processing is a purified, biologically active and quality-consistent product, which is generated by depleting host-cell related impurities or culture media components. The purification of enveloped VLPs is a challenging task [73], [74]. Due to the similarity of enveloped VLPs to host cell related EVs, a well-considered sequence of different separation steps are required for a product with high purity [61], [73], [75]. Figure 1-4 gives an overview of the typical steps of a purification process (middle) and the potential techniques (left). Each step aims to deplete a certain kind of impurity (right). For products with extracellular expression, like enveloped VLPs, the producer cells and crude impurities need to be separated during the clarification step by either centrifugation or filtration techniques. The aim during the capture step is to separate major impurities from the product, as well as to concentrate the product by drastically reducing the process volume. Different techniques have been used as a capture step including precipitation/flocculation or filtration techniques. Another highly scalable unit operation is preparative chromatography, where different resin types and ligand chemistries have been developed and successfully used. During the intermediate purification step, the product is further purified, by reducing host cell derived impurities like DNA/RNA or proteins. The final polishing step aims to deplete residual impurities like DNA/RNA, proteins and defective particles along with a possible buffer exchange. Techniques used during polishing range from filtration and size-exclusion chromatography steps.

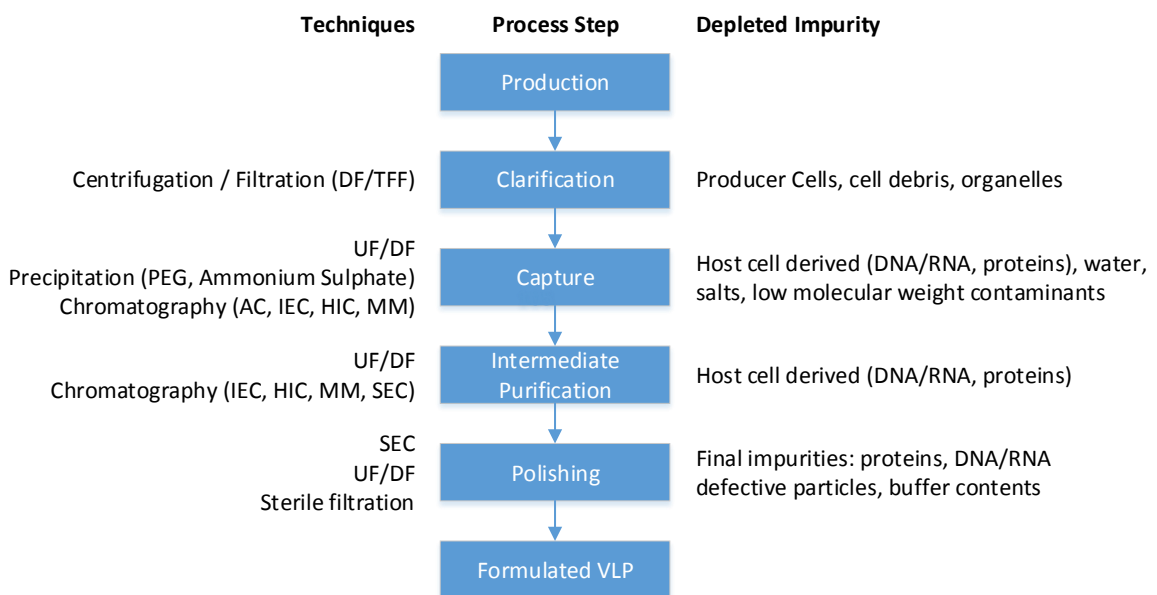


Figure 1-4: Schematic flow chart for manufacturing of secreted VLPs. After the initial production and clarification, the typical three stage purification strategy is used. The purification starts with a capture step followed by the intermediate purification and final polishing. On the left side, the potential purification techniques are shown for each step. The right side of the process shows the depleted impurities for each step. DF: depth filtration; TFF: tangential flow filtration; UF/DF: ultrafiltration / diafiltration; PEG: polyethylene glycol; AC: affinity chromatography; IEC: ion exchange chromatography; HIC, hydrophobic interaction chromatography; MM, mixed mode chromatography; SEC, size-exclusion chromatography

An alternative method often used is density gradient ultracentrifugation. Here, large molecules or bio-nanoparticles are separated by their different sedimentation velocity in a high-density medium like sucrose or caesium chloride. Different particle populations are enriched along the gradient according to their characteristic density. The main advantage of this method is that it combines a concentration and purification step. It was reported, that even the separation of hollow and filled particles with a reasonable resolution was possible [61], [76], [77]. A large drawback however, is that the method is laborious and is poorly scalable. Additionally, further purification is needed, as the gradient media needs to be separated from the product.

In contrast to the poor scalability of the density gradient centrifugation stands **chromatography**. It is highly scalable and one of the most intensively used unit operations in bio-separation processes. Chromatography has demonstrated its value not only for the purification of peptides or proteins but also viruses and VLPs [30], [61], [75], [77], [78]. The separation principle relies on physicochemical interactions between solutes in the mobile phase and the surface chemistry of the stationary phase (chromatography resin). The type of interaction mainly depends on the ligand chemistry of the used chromatography resin, which will be discussed later. Common chromatography matrices for bio-nanoparticle purification are packed beds (of porous beads), membrane adsorbers and monoliths. Schematic examples of these different chromatography stationary phases are shown in Figure 1-5.

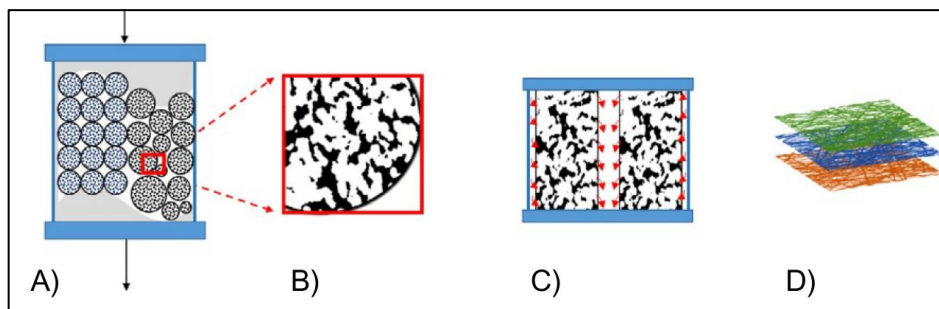


Figure 1-5: Schematic examples of chromatography stationary phases: A) Column with packed bed B) Chromatography Resin bead particle C) Monolith column with radial flow and continuous flow channel network D) Stacked membrane adsorber sheets. (adapted from: [79])

The beads for **packed beds** can be of spherical or non-spherical shape and typically consist of either polymeric or inorganic materials like silica or hydroxyapatite. Polymeric resins can be divided into natural polymers like agarose, cellulose or dextran and synthetic polymers. Here, the beads are produced from poly-acrylamide or poly-methacrylate. Important to note is, that pore sizes of the chromatography resin material play a major role during the interaction of the bead and the product of interest, as adsorption and desorption are mainly diffusion controlled processes and therefore limited by diffusion velocities into the pores. The high porosity of $\sim 40\%$ creates a very high surface area for product binding within the beads. For the purification of peptides or proteins the pore sizes range between 10 and 100 nm to allow an unhindered diffusion into the porous media. For the purification of large proteins or oligomers beads are designed with macro pores to allow better diffusion into the bead with sizes up to 400 nm [79], [80]. Bio-nanoparticles with sizes of 20 – 300 nm would theoretically be able to diffuse into macro pores. However, in comparison to biomolecules

they show up to 100-fold lower diffusion velocities [77], which would result in either long and ineffective processing times or a drastic loss in dynamic binding capacity at increased flow rates.

Monoliths and membrane adsorbers are allocated to the group of convective chromatography media. These two types of material combine high flow rates and high dynamic binding capacities, even for large biomolecules or particles [81]–[83]. The product of interest is transported to the ligand by convective flow and the mass transport is based on convection and not diffusion. In difference to monoliths, membrane adsorbers are either cast as long sheets or extruded hollow fibers and then later packed into cartridges as stacked sheets or hollow fiber modules. Most commonly used materials are poly-ethersulfone, regenerated cellulose and poly-vinylidene fluoride and later coupled with a ligand of choice. As monoliths, membrane adsorbers use convective flow to bring the solute to the ligand for interaction, reducing the mass transfer resistance while maintaining low pressure drops at higher flow rates [79], [84]–[86]. The binding capacity for small proteins is lower to conventional chromatographic resins per unit volume, as total surface area is usually higher in resin beads due to their high porosity. However, this relationship changes when regarding proteins with a molecular weight (MW) larger than 250 kDa or particles, as they cannot enter smaller pores or are strongly limited by their diffusion velocity. Membrane adsorbers have shown to work well for the purification of viruses and VLPs in the literature [87]–[90]. Drawbacks for membrane adsorbers are a lower resolution, as the breakthrough of the product of interest suffers from broadening effects. A further drawback is the difficulty in the utilization of step gradients during processing [77]. The scale-up of membrane adsorbers can be done to a certain size by increasing the cartridge size to increase the surface area. However, for large scale production a setup of parallel operated adsorbers becomes necessary.

In comparison to conventional resin beads, monoliths are produced *in situ* by a polymerization process that creates a continuous homogeneous block with network of flow channels with open pores. This results in very high porosity of up to 90%, allowing high flow rates with low pressure drops and high binding capacity for the efficient separation of large biomolecules or bio-nanoparticles at high productivity [30], [61], [78], [91], [92]. Typical materials for monolith columns are poly-methacrylate, poly-acrylamide and poly-styrene-divinylbenzene, or silica-based columns and are commercially available. The polymerization reaction is a highly exothermal process. Several parameters like temperature, pressure and cross-linker concentration need to be controlled very closely to ensure a homogeneous distribution of channels and pores [93]. The diameter of the interconnected channels is typically 1 – 2 μm with pores sizes of up to 6 μm , allowing a high convective flow, while maintaining a low pressure drop resulting in high adsorption kinetics for large biomolecules or bio-nanoparticles [94], [95]. A large advantage is that the breakthrough curves are independent of molecule size, its feed concentration or applied flow rates, which also results in a flow rate independent resolution [96]–[98]. The flow distribution within a monolith column can be either an axial flow through the monolith or a radial flow, as depicted in Figure 1-5 C), and depends on its geometrical design [99]. Different ligands for chromatographic separation can easily be coupled to the polymer network [100]–[102]. Due to the high ligand density on the surface area,

impurities like host cell DNA, tend to irreversibly bind to the column when using strong anion exchange ligands. Other reported problems are flow dependent entrapment of large particles. Particles or large molecules can be trapped in narrow channels or small pores. When the upstream diffusion is higher than the downstream convective flow this effect can be reversed, but ultimately leads to pressure increase or loss of binding capacity [103]. Another reported property is that the monolith bed is not fully rigid. High flow rates or pressure drops can lead to a structural change and a compression leading to increased process pressures after several process cycles, especially when working with crude feed stocks [104]. Another major drawback is, that currently monoliths cannot be prepared in sizes that would allow large scale production, as columns currently do not exceed volumes of 8 L [105].

As mentioned before, the chromatographic stationary phases can be coupled to a wide array of different ligands to make use of diverse physicochemical interactions between the solute and the stationary phase. The most common chromatography surface chemistries used for bio-nanoparticle purification are:

- Affinity chromatography (AC)
- Ion-exchange chromatography (IEC)
 - Anion-exchange chromatography (AIE) & Cation-exchange Chromatography (CIE)
- Hydrophobic-interaction chromatography (HIC)
- Mixed-mode chromatography (MMC)
- Size-exclusion chromatography (SEC) (not in monoliths)

Affinity chromatography is an extremely powerful chromatography technique, as it exploits the highly selective interaction between the ligand and solute in the mobile phase. Originally it was developed as a pure antibody-antigen, lectin-glycoprotein or enzyme-substrate interaction (=biospecific ligands). By now, the term affinity also refers to interactions due to the binding to specific groups on the protein or particle of interest (=pseudo-specific ligands) [80]. The biggest advantage of affinity ligands is their selectivity for its target structure. Usually AC is used as capture step, where only target molecules binds to the column and all impurities not carrying the binding site for the ligand pass the column without any interaction, leading to a high purity of the eluate. Drawbacks of this technique are the high cost for the resin, as expensive binding site screening needs to be performed or a tag needs to be introduced and later cleaved and separated from the product [79], [80].

Today, **ion-exchange chromatography** is the most commonly used chromatography technique for the purification of biomolecules and nearly every industrial purification process contains at least one IEC step [18], [80]. The technique is based on the interaction principle between two counter-charged molecules; here the ligand and the product of interest. IEC can be performed in two different modes: In cation exchange chromatography the ligand is negatively charged and binds only molecules with a positive net charge. In anion exchange chromatography only molecules with a negative net charge will bind to the positively charged ligand. The strength of this interaction can be increased by keeping

the ionic strength of the mobile phase as low as possible as charges on the product of interest are balanced by the counter-ions within the mobile phase and on the stationary phase. Upon binding, the counter-ions on the functional group on the resin are exchanged with the product. Elution is commonly achieved by changing the characteristics of the mobile phase. This can be accomplished by either increasing the ionic strength and therefore eluting the protein due to ionic competition or by changing the pH and therefore the net charge of the product itself and lowering the binding strength [106], [107].

Hydrophobic-interaction chromatography was first described by Shepard and Tiselius in 1949 as “salting out chromatography” [108] before the term HIC was characterized by Hjerten [109]. Today it is a widely used technique. In comparison to other chromatographic techniques, the hydrophobic ligand does not involve a direct interaction with the product of interest. The binding principle is based on hydrophobic interactions forced by high ionic strength in the mobile phase. By the addition of kosmotropic salts the solvate layer around the molecule/particle is taken away and the product of interest is “forced” out of solution. Binding occurs, when the energy to keep the molecule solvated is higher than the hydrophobic attraction. Then, the hydrophobic patches of the molecule interact with the ligand. Desorption (elution) works by lowering the ionic strength of the mobile phase, allowing the product to shift again into a solvated stage and desorb from the column. A major drawback however is that adding high salt concentrations to the product may lead to aggregation and ultimately loss of product [30], [80], [110].

To combat this problem, **mixed-mode chromatography** resins were developed as “salt tolerant ion exchangers”. One prominent example is hydroxyapatite chromatography and is in use since the 1950s [111]. Mixed-mode resins combine more than one type of physico-chemical interaction that contributes to the retention of the target molecule. Often IEC and HIC ligands are combined, as these different ligand-types can work well at different ionic strengths and offer a good optimization potential. Another unique example is the combination of SEC and IEC by creating a porous bead, where only the inner core is functionalized with salt-tolerant AIEC ligands. Drawbacks of these systems is that an extensive process optimization is needed to make full usage of the mixed interaction system [112].

In **size-exclusion chromatography** molecules and particles are separated by their size and or shape. SEC resins have no typical functionalized groups to interact with the solutes in the mobile phase and are intentional as inert as possible. The separation efficiency is solely based on the pore size of the resin, as large molecules or particles physically cannot enter the pores and pass the column faster than smaller solutes. Smaller solutes are slowed because they will enter the pores by diffusion and travel through the resin beads. As a result, solutes in the mobile phase are gradually separated by their size with the largest molecules eluting first. Commonly used materials for SEC are cross-linked poly-acrylamide or poly-methacrylate, silica or cross-linked dextran or agarose. In preparative scale SEC is usually used in two different situations: (1) Buffer exchange or group separation where a large size difference is needed between product and impurity, or (2) fractionation, where very similar sizes or protein variants need to be separated. However, SEC suffers from a low sample capacity (4-20% of

CV) and dilution effects ($\sim 1.1 - 1.2$) [79]. Another drawback is the meager pressure resistance of the resins, resulting in low process velocities and reducing the overall productivity. Despite these downsides however, SEC is often applied as a final purification / polishing step for bio-separation, as in later stages of the purification stream, the product is usually in a small volume and concentrated state [73], [76], [77].

1.5 Methodology of VLP Analytics

This chapter gives a short outline over the analytical methods used during process development and characterization of bio-nanoparticles. The biogenesis of enveloped viruses, VLPs or EVs results in bio-nanoparticles sharing the same plasma membrane envelope taken from their host, or originator cell [45], [113]. This circumstance creates a great challenge to analytical methods and the possibility to accurately identify or quantify the particle of interest. In many cases analytics are the bottleneck in research or development for enveloped VLPs. Often, the information from several different orthogonal methods is needed for a conclusive analytical result. In Table 1-3 a summary of the used analytical methods is given to emphasize this statement.

Table 1-3: Summary of the analytical methods used in this work for measuring identity, quantity and particle morphology of the given analyte. NTA: Nanoparticle tracking analysis, MALS: Multi-angle light scattering, TCID₅₀: Tissue culture infection Dose 50%, TEM: Transmission electron-microscope, SAXS: small-angle X-ray scattering

Trait	Analytical Method	Analyte
Identity	Western-Blot (WB)	Viral protein markers
	SDS-PAGE / coomassie	Total protein (Host cell / viral)
Quantity	Bradford assay	Total protein (Host cell / viral)
	PicoGreen® assay	dsDNA (Host cell / viral)
	NTA	Assembled VLP / Virus / Particle-like structures
	MALS	Assembled VLP / Virus / Particle-like structures
	TCID ₅₀	Baculovirus
Morphology & Size	(Cryo-)TEM	Assembled VLP / Virus / Particle-like structures
	NTA	Assembled VLP / Virus / Particle-like structures
	SAXS	Assembled VLP / Virus / Particle-like structures

As mentioned earlier, results from different orthogonal methods need to be put together for a conclusive result. Currently, no single available method can identify a specific bio-particle in the sample. Nanoparticle tracking analysis (NTA) or multi-angle light scattering (MALS) gives information on particle concentration, size and the particle-size distribution of the sample, but cannot distinguish between different types of particles, let alone identify them. For a reliable particle identification, another method is needed to identify the particle. In this work particles were indirectly identified by verifying the presence of specific VLP indicator proteins via Western blots. Here, the presence of the matrix protein HIV-1 gag or the integral membrane protein influenza haemagglutinin (H1) were needed. Only when both methods point in the same direction, VLP presence can be assumed. Table 1-4 shows a simplified decision matrix when only taking 2 methods are taken into account for particle identification. A sample containing the correct matrix proteins and/or antigens, but presence of particles according to NTA or TEM cannot not be verified, it hints to complications in VLP assembly or the budding process. In the reversed case, where particles are present, but no positive western blot for antigen or matrix-protein could be achieved, the data strongly points to the presence of

extracellular particles. However, in the case of a shared host cell membrane this verification is not sufficient, as from experience, extracellular vesicles will also carry at least the H1 and some traces of HIV-1 gag in their lipid bilayer envelope. Here, the significance of orthogonal methods comes into play. Extracellular vesicles tend to be smaller than the VLPs generated by the gag polyprotein and the combination of these analytical methods will supposedly allow a reliable identification.

Table 1-4: Decision matrix for VLP identification (simplified)

Specific Protein (WB)	Particles (NTA/MALS)	Conclusion
Yes	No	Incorrect protein expression, faulty budding process
No	Yes	Extracellular particles from host, sample impurity
Yes	Yes	Presence of VLP can be assumed with further testing

Quantification of VLPs or viruses on protein level works well with common techniques like Bradford assay [114], sodium dodecyl sulfate polyacrylamide gel electrophoresis (SDS-PAGE) and semi-quantitative with Western blot [115]. If quantification on a particle level is needed the available methods decrease. Here, NTA and MALS coupled to SEC were used [116]. In general, the analytical methods can either be separated into their information they deliver (Table 1-3) or in accordance to their fundamental functionality of the method like physicochemical or biological assays. The biological assays used in this work were the Bradford assay for the determination of total protein concentration and PicoGreen® assay for the quantification of and double stranded (ds) DNA. These kits were used according to the manufacturer's instructions. Presence of specific proteins was verified using Western blots, which were developed for HIV-1 gag, influenza haemagglutinin H1, or gp64 and vp39, major envelope or capsid proteins of baculovirus. Quantification of infective baculovirus was performed by tissue culture infection dose 50% (TCID₅₀) [117]. The respective description of each method can be found in chapter 3 "Material and Methods".

The physicochemical assays used in this work for bio-nanoparticles analysis were nanoparticle tracking analysis (NTA), multi-angle light scattering (MALS), small angle X-ray scattering (SAX) and transmission electron microscopic photographs.

Nanoparticle tracking analysis provides particle concentration, size and particle-size distribution of polydisperse liquid samples. The theory behind the measurement is built on two physical laws. Particles in suspension move with Brownian motion according to their size. When hit by a light source these particles will scatter the light. The scattered light is proportional to their size and depends on their respective refractive index. During the NTA measurement the focused laser beam (405 nm wavelength) passes through the sample in the flow cell. The scattered light is captured in a video clip by a CCD camera, which is mounted on a light microscope with a 20-fold magnification. After the measurement, the recorded video is analyzed by the NanoSight particle tracking software, where an algorithm tracks the movement of each illuminated particle from frame to frame. In Figure

1-6 a schematic illustration of the NTA principle is shown. The calculation of particle size is based on the Stokes-Einstein equation (1):

$$\frac{(x,y)^2}{4} = \frac{T K_b}{3\pi\eta d_h} \quad (1)$$

$\frac{(x,y)^2}{4}$ = Particle mean square displacement, T = temperature,

K_b = Boltzmann's Constant, η = viscosity, d_h = hydrodynamic diameter

The particle mean square displacement is directly proportional to relation of the product of the Boltzmann's constant K_b and temperature T and indirectly proportional to the product of solvent viscosity μ and the particle hydrodynamic diameter d_h . It describes the motion of particles per time [$m^2 s^{-1}$] and is determined by the software, tracking particles in x and y dimension [118].

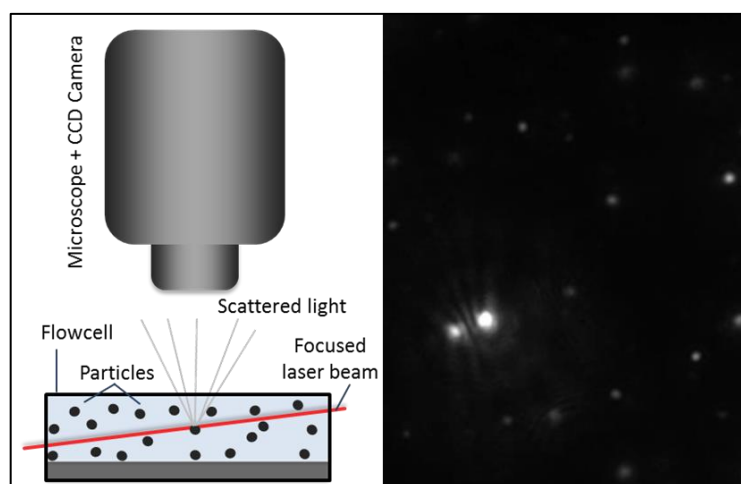


Figure 1-6: Left: Schematic drawing of the measurement principle of NTA. The laser light of the focused laser beam is scattered as it passes through the measuring chamber. Right: The illuminated particles are filmed in a video clip and later analyzed by the tracking software.

The particle size can be calculated, since the particle mean square displacement is measured during particle tracking as a diffusion distance. Temperature during measurement and sample viscosity (aqueous buffer systems) are known. NTA can measure particles to a minimal size of 30 nm and theoretically up to 2 μm in diameter. The particle concentration is calculated from the amount tracked particles in the measuring chamber and related to the known volume [119]–[121]. Further, the NanoSight is equipped with a fluorescence filter that allows measurements of photobleaching resistant fluorophores, to selectively measure specific particles with a fluorescent-tags, marker or an intrinsic fluorescence. Because of its two-dimensional tracking principle however, the method is not fully reliable for non-spherical structures such as rod-shaped particles like the baculovirus. During measurement a rod-shaped particle will diffuse from the focusing plane by a spinning motion leading to large differences in the surface area that is able to scatter the light. This results in a blinking pattern that the algorithm cannot properly track or count as particle during analysis.

Multi-angle light scattering (MALS) is one of the most commonly used methods to characterize or quantify bio-nanoparticles [14]. The detectors are built with a light source generating polarized light, a flow cell and a setup of up to 18 aligned detectors at fixed angles around the flow cell. These detectors measure the excess Rayleigh ratios of the intensity of the scattered light, when the polarized light impinges on a particle in solution [122], [123]. This principle and an exemplary detector setup is shown in Figure 1-7 A). The polarized laser beam passes through the flow cell and the oscillating electric field of the light induces an oscillating dipole, that again radiates light in an oscillating fashion. The intensity and angular dependence of the radiated light is dependent on the magnitude of induced dipole within the particle and therefore proportional to the particle size and quantity.

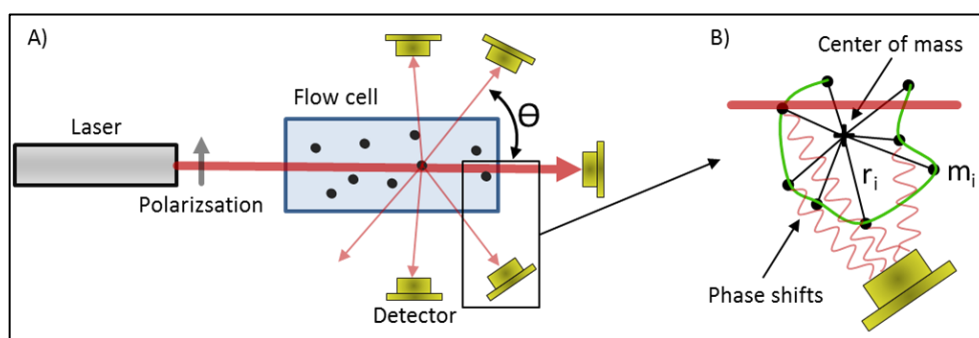


Figure 1-7: The principle of a Multi-angle light scattering detector. A) Detector setup with a laser light source providing polarized light and a flow cell. Particles scatter the light which is collected at fixed detectors at specific angles around the flow cell. B) Calculation principle of the root mean square radius (RMS) or radius of gyration (r_g): The distance r_i from the center of mass to the isotropic scattering center is needed to calculate the root mean square radius (RMS).

Particle quantity is calculated from the differential scattering intensities of the particles in solution (Eq. (2)). This is a function of the radius of the scattering particle and its refractive index, where N is the particle quantity, k is an optical constant that depends on the refractive index of the sample matrix,

$$N = \frac{k^2 R(\theta)}{i_1(\theta)} \quad (2)$$

N = particle quantity, k = optical constant, $R(\theta)$ = Rayleigh ratio,

$i_1(\theta)$ = single particle differential scattering intensity

$R(\theta)$ the Rayleigh ratio at the scattering angle θ and $i_1(\theta)$ the single particle differential scattering intensity [122], [124]. The single particle differential scattering intensity is obtained by applying the Rayleigh-Gans-Debye (RGD) approximation. RGD is applicable when the total phase shift of the incident light passes through the particle or molecule is negligible and the refractive indices of particle and sample matrix are very similar [122], [125].

Particle size is given by the root mean square radius (rms) or also known as radius of gyration (r_g), which is a measure of the particle's size weighted by the mass distribution about its center of mass. It is calculated from the slope at $\Theta = 0$ with the following equation (Eq. (3)).

$$\langle r_g^2 \rangle = \frac{\sum r_i^2 m_i}{M} \quad (3)$$

$\langle r_g^2 \rangle$ = root mean square radius, m_i = isotropic scattering center,

r_i^2 = distance between center of mass to isotropic scattering center, M = total mass

The radius of gyration is a function of the relationship between the sum of the distances r_i to the isotropic scattering centers m_i to the total mass M of the particle [122], [125], [126]. Figure 1-7 B) shows a graphical illustration of the calculation principle of the r_g .

MALS detectors can be used in batch mode, or in-line with an HPLC. This technique is called SEC-MALS, where the sample components are separated with the help of a SEC-column and then analyzed in the MALS detector and have been successfully used in VLP applications [116], [127]–[129].

In **Small angle X-ray scattering** (SAXS) sample are exposed to X-rays with a specific wavelength. Subsequently the scattering pattern of the X-rays is analyzed. This technique attracted a lot of attention in the biological community due to its broad spectrum of possible applications [130]–[132]. A great feature of SAXS is that there are nearly no limits in the sample composition. It can be used *in situ*, in static or dynamic experiments on liquid, gaseous or solid samples [133]. A simplified illustration of the experimental setup and measurement principle is given in Figure 1-8 A). Upon contact with the sample, the X-rays will scatter elastically in small angles ($\sim 0 - 5$ degrees), which produces a spatially averaged intensity distribution [133]–[136].

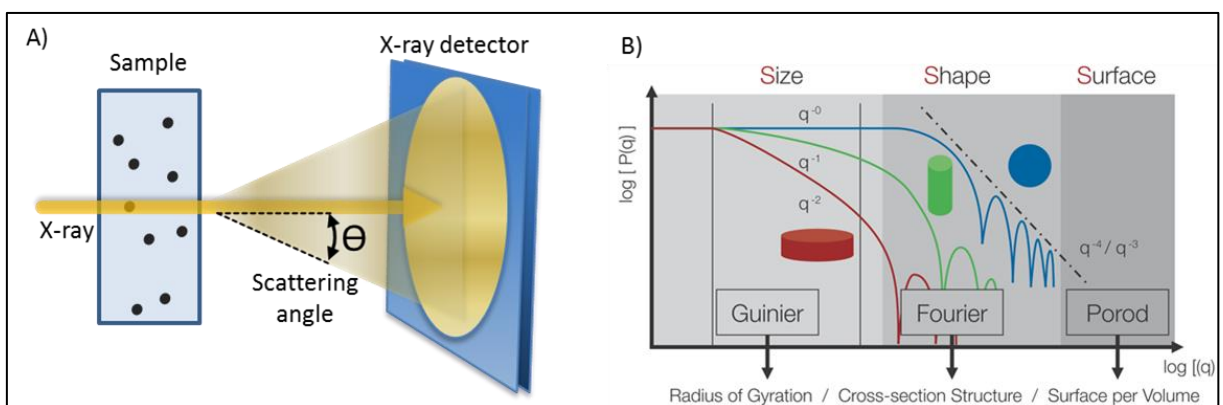


Figure 1-8: Illustration of the measuring principle of small angle X-ray scattering. A) Experimental setup for light scattering experiment. The X-ray beam passes the sample chamber and is scattered by particles. The X-ray detector measures the intensity as well as the position. B) Different sample properties can be extracted from the three regions of a SAXS profile (Guinier, Fourier and Porod) in a double logarithmic plot, depending on slope and shape of the curve [134].

From this scattering curve of SAXS profile different properties of the sample like pore size, surface to volume ratios, structures or even form factors can be extracted [134]. The SAXS profile has three distinct domains: Guinier, Fourier and Porod (see Figure 1-8 B)). The Guinier region allows extraction of the radius of gyration r_g by fitting a line to the natural log of the intensity plot as a function of the squared scattering vector q^2 [134], [136], [137]. Information on particle shape and form factor can be extracted by an indirect Fourier transformation within the Fourier region resulting in the pair distribution function [134], [136]–[138]. The Porod region allows extraction of information on surface to volume ratio or specific surface estimations for compact particles [134], [135], [139].

In this work a new concept to analyze MALS raw data is described. The concept postulated by Wyatt et al. [122], [140], [141] was adapted with notations taken from SAXS-theory and is described in chapter 3.10 on page 44.

2 Aim of this Work

The objective of this work was to develop purification protocols for enveloped VLPs and viruses. The purification strategy should exceed the current state of technology and should aim to be fast, simple and straightforwardly scalable.

Enveloped virus-like particles are considered promising candidates for next generation vaccines or immunotherapy. However, their purification remains a challenge because of a limited amount of suitable purification methods for preparative and analytical scale. Also, their size and structural similarity to host cell derived impurities like extracellular vesicles, or other bio-nanoparticles adds to this difficult task. The same applies for virus production, as many processes use more than 50 years old technologies, where inoculated hen eggs are used for virus propagation. Today, cell culture systems like the BV/IC or HEK293 are substantial components of recombinant expression systems for either proteins, or bio-nanoparticles. Different *Trichoplusia ni* cell lines have been recognized as good performers in their ability to secrete heterologous proteins at high yields [142]. Furthermore, it has been reported that convective chromatography media are very promising for the downstream processing of viruses and VLPs [30], [61], [78]. A major disadvantage for process development of bio-nanoparticles is that existing analytical tools for quantification are complex and laborious and new technologies and methods need to be developed.

Consequently, the following objectives were formulated for this doctoral thesis:

- Development of purification protocol for a direct capture and purification of HIV-1 gag H1 virus-like particles produced in a baculovirus insect cell system with a high product quality and purity.
- Development of a purification protocol for HIV-1 gag-gfp VLPs produced in HEK293 cell culture with a high product quality and purity.
- Develop new innovative approaches for analytical methods for VLPs or particles for in-process control, quantification or particle characterization.

3 Materials and Methods

This chapter summarizes the used materials and applied operational techniques to create this work.

3.1 Chemicals

The chemicals used for all experiments were acquired from Merck (Darmstadt, Germany) or Sigma Aldrich (St. Louis, MO, USA) unless otherwise stated.

3.2 Production of VLPs

3.2.1 Production of HIV-1 Gag-GFP VLP Supernatants in HEK-293 Cell Culture

3.2.1.1 Cell Culture Conditions

The HEK-293 cell line (HEK293SF-3F6, NRC, Montreal, Canada) was kindly provided by Dr. Amine Kamen from McGill University (McGill, Montreal, Canada). It is a serum free suspension cell line cultured in 20 mL of Freestyle 293[®] medium (Invitrogen, Carlsbad, CA, USA) and was supplemented with 0.9X of an in-house developed lipid mixture for optimal cell growth [31]. Further supplements were 19.8 mg/L of r-insulin (Novo Nordisk Pharmatek, Køge, Denmark), 1.6 mg/L of r-transferrin (Merck Millipore, Kankakee, IL, USA) and 0.1% Pluronic[®] (Invitrogen, Carlsbad, USA). The cell culture was shaken in an incubator at 37°C in a humidity controlled atmosphere of 5% CO₂ in air on an orbital shaker (Stuart, Stone, UK) at 130 rpm.

3.2.1.2 Plasmid

In this work a pGag-eGFP plasmid coding for a Rev-independent HIV-1 Gag protein which was fused to an enhanced GFP was used. Here, the Gag sequence from pCMV55M1-10 was cloned into into the pEGFP-N1 plasmid (Clontech, Takara Bio, Mountain View, CA, USA) [143]. Preparation and purification of the plasmids was performed as described in [144].

3.2.1.3 Transfection of HEK-293 Cells and VLP Production

Transient transfection was used for the HEK-293 cells using 25 kDa linear polyethylenimine (PEI) (PolySciences, Warrington, FO, USA) and an absolute DNA concentration of 1 µg/mL. Plasmid DNA was diluted in unused cell culture medium (10% of the total culture volume) after 10 s of vortexing. Subsequently PEI is added in a 1:2 (w/w) DNA:PEI ratio incubated for 15 min at RT for PEI/DNA complex formation. The PEI/DNA complexes were added to the cells during a medium exchange as stated in [31]. Three days post transfection (72 h) the cells were harvested by centrifugation at 4000 g for 30 min at RT for optimal VLP yield as stated in [145] and stored at 4°C until purification.

3.2.2 Production of HIV-1 Gag H1 VLP Supernatants in *Tnms42* Insect Cell Culture

3.2.2.1 Cell Line, Media and Culture Conditions

Spodoptera frugiperda Sf9 cells (ATCC CRL-1711) and the alphanodavirus-free Tn5B1-4 (High Five) derivative *Tnms42* cell line (obtained as a kind gift from Gary W. Blissard) were cultivated in HyClone SFM4 insect cell medium (GE Healthcare, Little Chalfont, UK). As supplement 0.1% Pluronic F68 (Sigma-Aldrich, St. Louis, Missouri, USA) was added. T-flasks were used to grow adherent cultures. When switching the cells to suspension cultures, 500-ml shaker flasks at a cell density between 5E+5 and 3E+6 cells/ml were used. The cells were cultured at 100 rpm and 27°C.

3.2.2.2 Recombinant Baculovirus Vectors

Recombinant BVs encoding the haemagglutinin H1 from Influenza A/California/04/2009 and the HIV-1 Gag matrix protein were produced as follows. The nucleotide sequence encoding the hemagglutinin (GenBank accession no. JF915184) including a T4 foldon trimerization domain, the C-terminal transmembrane- and endodomains was chemically synthesized by IDT (Leuven, Belgium). The fragment was cloned into the acceptor vector pACEBac-1 (EMBL, Grenoble, France) after PCR amplification. This resulted in pACEBac-1-H1 vector. The HIV-1 Gag gene was acquired from the full human immunodeficiency virus type 1 (HXB2) genome (GenBank accession no. K03455.1). The gene sequence was chemically synthesized by IDT (Leuven, Belgium) and amplified by PCR and then ligated into the pIDC donor vector (EMBL, Grenoble, France) resulting in pIDC-Gag.

Using Cre-LoxP recombination the acceptor-donor fusions of pACEBac-1-H1 and pIDC-Gag were combined. The fused H1-gag construct was implanted into the MultiBac genome via Tn7 transposition using DH10MultiBacY cells (EMBL, Grenoble, France). Recombinant BV stock was generated by transfection of Sf9 cells with the bacmid H1Gag-YFP. The FuGENE HD transfection reagent (Promega, Madison, Wisconsin, USA) was used according to the manufacturer's instructions. The viral seed stock was harvested by centrifugation for 10 min at 3000 x g (HERAEUS Megafuge16, Thermo Scientific, Waltham, Massachusetts, USA) four days post-infection (pi). Virus titer of the seeding stock was determined by plaque assay.

3.2.2.3 Expression of HIV-1 Gag H1 VLPs

BTI-Tn5B1-4 / *Tnms42* (*Trichoplusia ni*) or Hi5 cells were co-infected with rBV expressing HA (SF, PR or HIR) and or GFP (negative control) at a multiplicity of infection (MOI) of 10 and a cell density of 1.9×10^6 cells/ml in 500 ml shaker flasks. Cells were harvested 72 h post infection and separated from supernatant by low speed centrifugation for 10 min at 2000 g at room temperature. The baculovirus seeding stocks and cell culture supernatants used for these studies were kindly provided by Mrs. Krisztina Koczka, PhD and Mrs. Dipl.-Ing. Miriam Klausberger, PhD.

3.2.3 Production of HIV-1 Gag VLPs in CHO Cell Culture

3.2.3.1 Expression of HIV-1 gag VLPs

The HIV-1 gag VLP containing supernatants used for these studies were kindly provided by Icosagen (Tartumaa, Estonia). Further details on the production cell line as well as expression vector can be found in [61]

3.2.3.2 Purification of HIV-1 gag VLPs

The HIV-1 gag VLPs from CHO cell culture were used as VLP standard for several experiments and were purified as previously described by [61]. Samples of the pooled elution peaks were further purified by an endonuclease treatment. After dsDNA digestion the samples were dialyzed using Slide-A-Lyzer™ dialysis devices with a MWCO of 10.000 using the manufacturers recommendations. The dialysis buffer volume was 200-fold greater than the sample volume. The first two buffer exchanges (50 mM HEPES buffer at pH 7.2) were performed after 2 h at room temperature. The final dialysis step was performed at 4°C overnight.

3.2.4 Endonuclease treatment

Prior to the chromatographic purification, clarified cell culture supernatant was treated with Benzonase purity grade II (Merck KgA, Darmstadt Germany) with a final concentration of 150 U/mL at 37°C. The enzymatic reaction was stopped by 5 mM EDTA after 2 hours.

3.3 Liquid Chromatography

3.3.1 Preparative Scale Chromatography Equipment

For the chromatographic experiments an ÄKTA explorer 100 with a P-960 sample-pump and Frac-950 fraction collector or Äkta pure 25 M2 with a sample pump S9 and fraction collector F9-C (GE Healthcare, Uppsala, Sweden) were used. During the purification runs pH, conductivity and UV absorbance at 280 and 260 nm wavelength were monitored. Unicorn software 5.10 or Unicorn 6.4.1 was used for method programming, control and data acquisition.

3.3.2 Preparative Scale Chromatography

For the HIV-1 gag H1 and HIV-1 gag-GFP VLPs a chromatographic purification method was developed. Centrifuged cell culture supernatant was filtrated using 0.8 µm syringe filters (Millex AA filter, Millipore Bedford, MA, USA). Column equilibration in linear or step gradient elution was performed with a 50 mM HEPES, pH 7.2 buffer (mobile phase A) and 5 – 6% of 50 mM HEPES, 2000 mM NaCl pH

7.2 (mobile phase B) resulting in final sodium chloride concentration of 120 mM for equilibration. The filtrated culture supernatant was then loaded on 1 mL radial flow monoliths CIMmultus QA (BIA Separations, Ajdovščina, Slovenia). The column was washed with same buffer conditions used during column equilibration after loading for 30 bed volumes in linear gradient elution and reduced to 15 column volumes (CV) in step gradient elution. The load volume was adapted for each experiment and set between 50 and 100 CV. Linear gradients were conducted from 0-75% of mobile phase B in 50 bed volumes with a 10 CV hold step and a regeneration step at 100% B with a 10 to 15 CV hold time. Step gradient elution for HIV-1 gag H1 VLPs was set to 18 – 30 – 37 – 50 % B mobile phase B with a holding volume of 15 CV each. HIV-1 gag-GFP VLPs step gradient elution was set to 15 – 26 – 50 – 100% B with 15 CV hold steps each. The regeneration phase of the column was performed at 100% B, while the sanitization was performed with 60 bed volumes of 1 M NaOH. Flow rates were kept at 1 mL/min for all experiments. Elution fractions of 1 mL were collected into tubes or directly collected into 96-well plates. Fractions were pooled according to the chromatogram of the individual experiments and fraction analytics. The Flow through fractions during sample application, column wash and column sanitization were also collected.

Table 3-1: Summary and overview of the final purification methods of the different VLPs used in this thesis. All values are given for the CIMultus QA 1 mL column and mobile phases A (50 mM HEPES, pH 7.2) and B (50 mM HEPES, 2000 mM NaCl, pH 7.2)

VLP	Host	Elution	Equilibration	Wash	Gradient	Regeneration
HIV-1 gag H1	<i>Tnms42</i>	Lin. gradient	5% B for 15 CV	5% B for 15 CV	5 – 75% in 50 CV 75 – 100% B in 10 CV	100% B 10 CV
HIV-1 gag H1	<i>Tnms42</i>	Step gradient	6% B for 15 CV	6% B for 15 CV	18 – 30 – 37 – 50 % B 15 CV each	100% B 15 CV
HIV-1 gag	CHO	Step gradient	17.5% B for 15 CV	17.5% for 20 CV	0 – 25 – 45% B 15 CV each	100% B 30 CV
HIV-1 gag-GFP	HEK 293	Lin. gradient	6% B for 15 CV	6% B for 15 CV	6 – 50% B in 50 CV 10 CV hold 50% B	100% B 10 CV
HIV-1 gag-GFP	HEK 293	Step gradient	6% B for 15 CV	6% B for 15 CV	15 – 26 – 50 – 100% B 15 CV each	100% B 10 CV

3.3.3 High-Performance Liquid Chromatography (HPLC) Equipment

SEC-HPLC experiments were performed using an Ultimate 3000 system (Thermo Fisher, Waltham, MA, USA). The HPLC system was equipped with a quaternary pump LPG-3400SD, WPS-3000TSL analytical autosampler, DAD 3000 UV-detector and FLD 3100 fluorescence detector. Chromeleon 7 software (Thermo Fisher Scientific, Waltham, MA, USA) was used for method programming, control and data acquisition. The flow rate was kept at 0.3 mL/min for all experiments as described in [116]. A TSKgel G5000PWXL (300.0 mm × 7.8 mm i.d.) column in combination with a TSKgel PWXL guard

column (40.0 mm × 6.0 mm i.d.) (Tosoh Bioscience, Stuttgart, Germany) was used. MALS signals were acquired with a DAWN HELEOS 18-angle detector (Wyatt, Santa Barbara, CA, USA) and differential refractive index detector Optilab rEX (Wyatt, Santa Barbara, CA, USA) with the Astra 5.3.4 software (Wyatt, Santa Barbara, CA, USA) for programming and measuring. Data analysis and evaluation were performed in Astra 6.1.2 using the number density method and a sphere model fit and a particle refractive index of 1.46 adapted from [146].

3.3.4 At-line Multi Angle Light Scattering as Fraction Analytics

The HPLC-Setup from chapter 3.3.3 was also used for at-line elution fraction analytics tool. This was achieved by bypassing the HPLC column and subsequently reducing analysis time from 30 min (with column) to 1.5 min (without column). Elution fractions from the preparative scale linear gradient purification runs of the HIV-1 Gag-GFP VLPs were injected using the LPG-3400SD quaternary pump and the WPS-3000TSL autosampler. The DAD 3000 UV-detector (set to 280 nm), FLD 3100 fluorescence detector (excitation 480 nm / emission 505 nm) and DAWN HELEOS 18-angle MALS detector were connected in series. For each injection, the area under curve (AUC) was calculated from light scattering and fluorescence signals using Chromeleon 7 software (Thermo Fisher Scientific, Waltham, MA, USA) and subsequently plotted over the course of the linear gradient purification as overlays of the chromatograms.

3.4 Protein Concentration and dsDNA Content

Bradford assay was used to measure protein concentration. For the calibration curve diluted (TE-buffer) bovine serum albumin (BSA) standards were used in the range of 50 – 200 µg/mL. As protein dye reagent Coomassie blue G-250 (Bio-Rad Laboratories, Hercules, CA, USA) was used. Double stranded DNA (dsDNA) was quantified using the Quant-iT™ PicoGreen® dsDNA kit (Life technologies, Waltham, MA, USA). Both assays were carried out in a 96-well plate format and executed using the respective manufacturer's instructions.

3.5 Sodium Dodecyl Sulfate-Polyacrylamide Gel Electrophoresis (SDS-PAGE)

Precast NuPAGE Bis/Tris gels 4-12% (Invitrogen, Carlsbad, CA, USA) were used in a MES-SDS buffer system. The manufacturer's instructions were slightly adapted: Samples were either applied in "Same Volume" or "Same Protein Concentration" across the gel. In "Same Volume" application 40 µL of sample were mixed with 20 µL 4x LDS sample buffer and 2M DTT was added to a final concentration of 1% v/v. Samples incubation was at 95°C for 20 min. "Same Protein Concentration" samples were individually diluted with deionized water to obtain same protein concentrations and treated as stated above. As a protein marker SeeBlue® Plus2 Pre-stained Protein Standard (Invitrogen, Carlsbad, CA, USA) was used. Coomassie Brilliant Blue G-250 based on EZBlue™ Gel Staining Reagent (Sigma Aldrich, St. Louis, MO, USA) was used for protein staining.

3.6 Western Blot Analysis

SDS-PAGE gels were blotted using 0.2 μm nitrocellulose membranes and Trans-Blot[®] turbo system (Bio-Rad, USA). Protein blocking was achieved by overnight incubation in PBS with 3% BSA and 0.1% w/v Tween-20. The **GP64 detection** was achieved by incubation with primary antibody anti-ACV5 antibody, mouse monoclonal (Abcam, London, UK) diluted 1:1500 in PBS with 1% BSA for 2 h followed by a secondary antibody incubation with anti-mouse IgG conjugated with alkaline phosphatase (Sigma Aldrich, St. Louis, MO, USA), diluted 1:1000 in PBS with 1% w/v BSA for 1 h. **Detection of H1** was done by incubation with primary antibody Influenza A virus H1N1 HA polyclonal antibody IgG (produced in rabbit) diluted 1:2000 in PBS with 1% w/v BSA for 2 h followed by a secondary antibody incubation with anti-rabbit IgG conjugated with alkaline phosphatase (Sigma Aldrich, St. Louis, MO, USA), diluted 1:2000 in PBS with 1% w/v BSA for 1 h. **HIV-1 p24** was detected by incubating the primary mouse monoclonal antibody against the HIV-1 p24 protein (diluted 1:1000 in PBS with 1% w/v BSA) (Icosagen AS, Tartumaa, Estonia) for 2 h, followed by secondary antibody incubation with anti-mouse IgG conjugated with alkaline phosphatase (Sigma Aldrich, St. Louis, MO, USA), diluted 1:1000 in PBS-T with 1% w/v BSA for 1 h. The coloring reaction was induced by adding 10 mL premixed BCIP[®]/NBT solution (Sigma Aldrich, St. Louis, MO, USA). After 5 min incubation the blots were scanned.

3.7 Tissue Culture Infective Dose (TCID₅₀)

Fractions of the purification were analyzed by TCID₅₀ to determine the content of infectious baculovirus. Briefly, Sf9 cells were seeded into sterile, tissue culture-treated 96-well microplates (Corning Inc., Corning, NY) at 20,000 cells/well in a total volume of 100 μL . Samples were serially 5-fold diluted in medium including antibiotics (dilution range 2.0×10^{-02} – 2.56×10^{-07}) in duplicates. 15 μL of each virus dilution was added to wells of a row yielding 12 replicates per virus dilution. Plates were incubated for 5 days at 27°C and the infection status was determined on basis of the expression a YFP reporter in infected cells. The viral titer in TCID₅₀/mL was calculated using the method of Reed & Muench [147] and was converted into pfu/mL by the Poisson distribution-derived factor 0.69. The data of the TCID₅₀ assays was kindly provided by Mrs. Dipl.-Ing. Miriam Klausberger, PhD.

3.8 Nanoparticle tracking analysis (NTA)

Particle size distribution and sample concentration were determined using NTA. The measurements were performed on a NanoSight NS300 (Malvern Instruments Ltd., Worcestershire, UK) using a blue laser (488 nm), neutral density filter and fluorescence filter (500 nm). Samples were serially diluted to achieve a range of 20 to 80 particles per video frame in the flow cell using particle-free water or 50 mM HEPES buffer pH 7.2 (0.1 μm filtrated). Each sample was measured in 3 different dilutions in triplicates of 60 s videos. This procedure results in 9 videos per measured sample. Prior to the measurement the camera level was manually adjusted to values between 14 and 16. Subsequently the videos were analyzed using the NanoSight software version 3.2 with the lowest possible detection threshold which then was kept constant over the measurements. Particle concentration was calculated for “all particles” and for particles with diameters ranging between 100-200 nm.

3.9 Transmission Electron Microscopy (TEM)

The samples were incubated for 1 min on 400-mesh copper grids, coated with Pioloform film and shaded with carbon. After fixation with 2.5% glutaraldehyde solution for 15 min and three wash steps with water samples were stained with 1% uranyl acetate solution for 30 seconds followed by air drying step. The negatively stained specimens were analysed in a Tecnai G2 200 kV transmission electron microscope (FEI, Eindhoven, The Netherlands), operating at 80 keV.

3.10 Fractal Dimension Analysis and Calculation from MALS Data

The MALS measurements were analyzed adapting the concept introduced by Wyatt [122], [140], [141]. The equations given by Wyatt were adapted and combined with parts from the SAXS theory. Wyatt conceptually describes MALS as a scattering technique where the range of the wave vector is dependent of the refractive index, as stated in the following equation (Eq. (4)):

$$P(\theta) = 1/(N + 1)^2 \sum_{i,j} (\sin(Qr_{ij})) / (Qr_{ij}) \quad (4)$$

$P(\theta)$ = Form factor in dependence of the scattering angle θ , N = amount of identical scattering mass points, r_{ij} = pair distances from the mass points i, j

Here two conceptual computation methods are described:

3.10.1 Conceptual MALS Computation using Characteristic Tailing of Scattering Curves

By changing Eq. (4) to the following notion (Eq. (5)) we avoid counting the scattering pairs more than once:

$$P(\theta) = 2/(N(N - 1)) \sum_{i,j'} \sin(Qr_{ij}) / (Qr_{ij}) \quad (5)$$

The scattering wave vectors Q were computed as described in Eq. (6):

$$Q = 4\pi n_0 / \lambda_0 \sin(\theta) \quad (6)$$

n_0 = is the refractive index, λ_0 = wavelength of the light source

Equation Eq. (6) can be rewritten and can be described similar to SAXS theory [148], which leads to Equation Eq. (7):

$$P(\theta) = \int_0^\infty dr p^1(r) \sin(Qr) / (Qr), \text{ where } \int_0^\infty dr p^1(r) = 1 \quad (7)$$

The numerical computation of the MALS scattering data does not lead to reliable results due to strong background noise when approaching scattering pairs with distances above a ≈ 100 nm. This problem was resolved by changing the notation to the following:

$$p(r - a) = \int_0^\infty \delta(r' - a) p(r - r') dr \quad (8)$$

The equation (8) can be interpret as follows. Each object of considerable large size can be disseminated into characteristic entities that separated by a characteristic distance, a. Here $p(r-a)$ is the:

$$\mathcal{F}(p(r - a))[Q] = \exp(iQa) \mathcal{F}(p(r))[Q] \quad (9)$$

Next, the lack of data points, if compared to SAXS, hindered to compute pair density $p(r)$ at high quality but we approximated it by its characteristic tailing $p(r)$:

$$p(r) = \frac{r^{D_1} - r^{D_2}}{\frac{1}{D_1 + 1} - \frac{1}{D_2 + 1}} \quad (10)$$

A hollow sphere can be approximated as: $p(r) \approx r^{D'_1} - r^{D'_2}$

A graphical description how the fractal bodies are built from the equation (8) is shown in Figure 3-1.

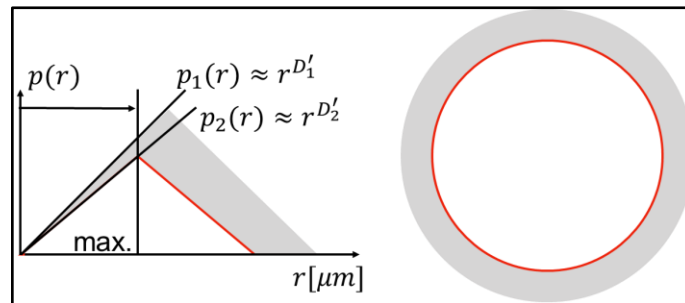


Figure 3-1: Graphical description, how the fractal bodies are built from the equation $p(r)$ to compute the possible pair densities of particles representing hollow spheres.

$$\mathcal{F}(p(r))[Q] = \frac{Q^{D_1} - Q^{D_2}}{\frac{1}{D_1 + 1} - \frac{1}{D_2 + 1}} \quad (11)$$

To estimate the scattering intensity $I(Q)$ the following equation was used (Eq. (12)):

$$I(Q) = \frac{Q^{D_1} - Q^{D_2}}{\frac{1}{D_1 + 1} - \frac{1}{D_2 + 1}} \quad (12)$$

$I(Q)$ = Scattering intensity of an object. In the present work the scattering intensity is interpreted as power law: Q^{D_x} . We assume hollow objects, thus we subtract from the Fourier transform of the pair density of a hypothetically fully filled object the Fourier transform of the pair density of its potential core. D_1 = Fractal dimension of the particles hull. D_2 = Fractal dimension of the particles core

The two summands of Eq. (12) represent a hollow body. In our case, these hollow bodies represent the expected bio-nanoparticles ranging from the sizes of small extracellular vesicles up to VLPs or viruses. When computing the theoretical scattering curve for a hollow sphere particle, a curve is obtained as shown in Figure 3-2. The thickness of the outer shell of the hollow particle was assumed to be 10 nm, which equates to the typical thickness of biological membranes [149].

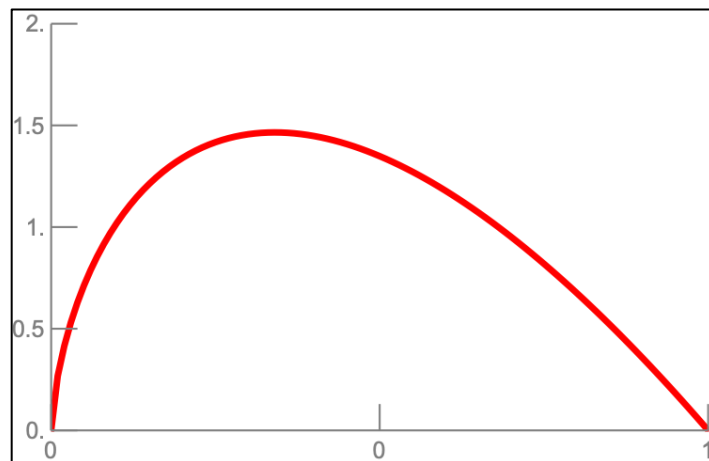


Figure 3-2: Theoretical scattering curve for a spherical hollow particle.

3.10.2 Conceptual MALS Computation using Truncated Forms of Pair Densities

Another concept (concept II) to compute the raw light scattering data is to use truncated forms of fractal pair densities. For large fractal objects or spheres, $p(r)$ can be written as:

$$p(r) \approx \exp(-ar)/r^{D-1} \quad (13)$$

In this case, we also assume that a fractal object can be built as described in Figure 3-1 (page 45); Then $p(r)$ corresponds to the following equation:

$$p(r) \approx C(\exp(-a_1r)/r^{D_1-1} - \lambda \exp(-a_2r)/r^{D_2-1}) \quad (14)$$

The scattering intensity $I(Q)$ is described as the subtraction of the original scattering intensity I_o and the residual scattering intensity I_i :

$$I(Q) = I_o(Q) - I_i(Q) \quad (15)$$

The improvement of Eq. 13 is twofold. First, the parameter a no longer reassembles a distance but a correlation length. Second, we can compute an analytical expression of the Fourier Transformation. It is given in Eq. 16

$$I_{a,D}(Q) \propto \sqrt{\frac{2}{\pi}} / a^D \Gamma(D-1) \frac{\left(a \sin \left(D \tan^{-1} \left(\frac{Q}{a} \right) \right) - Q \cos \left(D \tan^{-1} \left(\frac{Q}{a} \right) \right) \right)}{Q \left(\frac{Q^2}{a^2} + 1 \right)^{D/2}} \quad (16)$$

As given in Figure 3-1 we discriminate between an outer and an inner volume of a fractal object. The hollow object is then built by the difference of the two pair densities. We neglect interactions of the shell with the inner volume. This results in the following Fourier transformation given in Eq. (17)

$$I(Q) = C(I_{a_1,D_1}(Q) - \lambda I_{a_2,D_2}(Q)) \quad (17)$$

4 Results and Discussion

This chapter is separated into two subchapters that recapitulate the major subjects that have been addressed in this doctoral thesis.

Chapter 4.1 (page 49) describes the development of a purification protocol for HIV-1 gag H1 VLPs produced in BEVS. It begins with a comparison of different expression levels (chapter 4.1.1 - 4.1.1.4, page 49 - 56) using a conceptual MALS computation technique, followed by a classic method development resulting in a purification protocol for a step salt gradient (chapter 4.1.3, page 64) using a strong AEX monolith column.

Chapter 4.2 (page 70) describes the development for a purification protocol for a HIV-1 gag-GFP VLP expressed in a HEK293 cell line and summarizes the contributions (development of the at-line MALS analysis protocol with MALS-SEC control, the development of the purification protocol for the HIV-1 gag-GFP VLPs) to the following publication of Pereira et al. 2019 [150]. This also includes conducting the experiments, collecting and interpreting data, creating graphs and tables including writing parts of the publication.

4.1 Purification Method Development for HIV-1 gag H1 VLPs Expressed in BVES

The baculovirus expression system has been shown to effectively produce different eVLPs [68]–[70]. However, a reoccurring impurity is the baculovirus due to the functionality of the expression system. When expressing eVLPs, the BV is considered an impurity and needs to be separated from the product of interest within the purification process.

4.1.1 Characterization of Expression Levels of *Tnms42*

The aim of this experiment was to understand the attribution of the different expression stages to the total particle load within the respective supernatant. For this, each supernatant was clarified by centrifugation (800 rpm for 10 min) and treated with nuclease enzymes to digest free, non-incorporated dsDNA and subsequently filtrated with a 0.8 µm syringe filter. The treated supernatants were then loaded into a unused 1 mL QA monolith column and purified using a linear salt gradient from 100 mM NaCl to 2000 mM NaCl in 48 CV. Flow rates were kept at 1 mL/min and fractions of 1 (0.5 mL during Elution) were collected and analyzed with at-line MALS to obtain the light scattering intensity, which is directly proportional to particle size and particle quantity [123], [140], [141]. The raw light scattering data from the MALS detector were analyzed using the two different computation concepts described in chapter 3.10. The idea was to differentiate the expression stages (Mock, virus expression and VLP expression) on a particle basis to improve the quality of the eVLP purification. Supporting analytics were Bradford and PicoGreen® assays, along SDS-PAGE and Western blots. The first experiment (chapter 4.1.1.1) was performed with conditioned media (or mock fermentation) of the *Tnms42* cell line and harvested 3 days after passaging. Here the expected particle load are extracellular vesicles. The second experiment (chapter 4.1.1.2) is a supernatant harvested 3 days post infection with a recombinant baculovirus carrying a gene for producing yellow fluorescent protein. The expected particle load in this supernatant is BV and EVs. Experiment three (chapter 4.1.1.3) shows the expression of the HIV-1 gag H1 VLPs in the linear gradient, where EVs, BVs and eVLPs are expected.

4.1.1.1 *Tnms42* Mock Fermentation in Linear Gradient

During the loading phase (L/FT) strong UV signals can be seen in the chromatogram (Figure 4-1). As expected, the signal drops during the wash, where weakly or unbound species are flushed from the column. During the elution 3 distinctive, but not base-line separated peaks were identified and pooled as indicated in the chromatogram. For each elution fraction, the total light scattering signal was measured by MALS and integrated to receive the area under the curve. This is represented in the bar graph overlay (grey) in the chromatogram. As the intensity of the scattered light is directly proportional to the particle size and quantity [123], this method gives a fast insight into particle distribution over the course of the elution. Interesting to note is that the UV signals 280 and 260 nm are not fully representative for particle detection. In this chromatogram for example, the high UV signals of P1 do not translate to a high light scattering intensity. Here, the highest light scattering

intensity was found on P3. Further we saw, that the UV 214 nm signal can give additional information to the UV 280 or 260 nm but is not sufficient as a single indicator wavelength for particle elution.

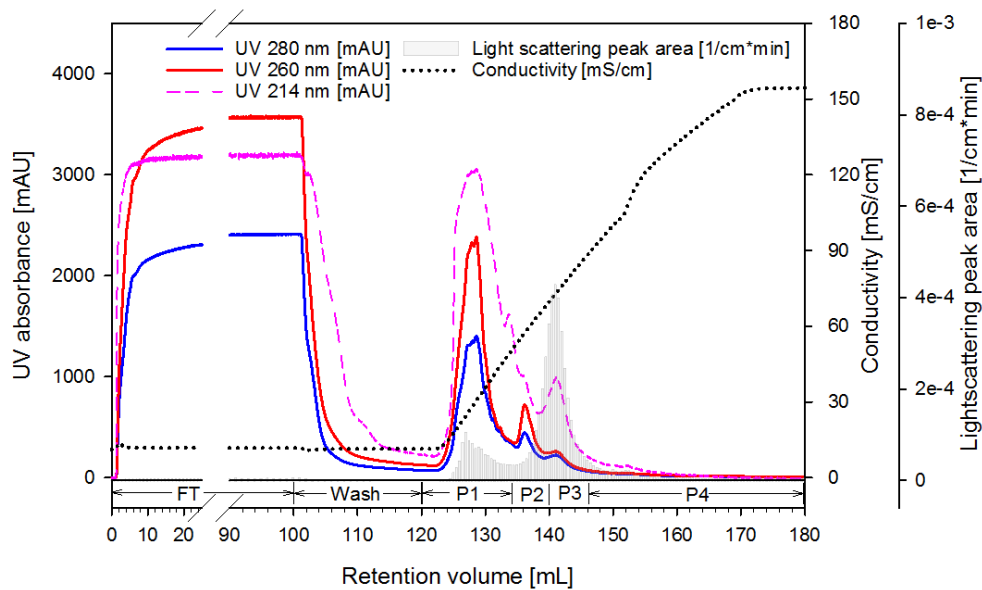


Figure 4-1: Chromatogram of the linear gradient of the *Tnms42* mock fermentation using a QA monolith. The loading material was 100 mL of clarified, nuclease treated and 0.8 µm filtered cell culture supernatant. Bars represent the area under the curve of the light scattering intensity (grey) at-line measurements. FT: flow-through; W: wash; P1-P4: pooled fractions for peaks 1–4

According to Bradford assay, the majority of protein was found in the FT fraction (94.9%). In the W 2.4% of the protein were flushed from the column. In P1 4.5% of the total protein was found which also can be seen in the high UV peak in the chromatogram. Only small amounts of protein were detected in P2, while P3 and P4 could not be quantified, as the protein concentration was below the lower limit of quantification for this assay. Comparable to the distribution of the protein, the majority of dsDNA was found in the FT fraction (73.7%) and was not bound to the column due to the high conductivity of the loading material (11.8 mS/cm). Only low amounts of dsDNA (1.1%) were found in the W fraction. During elution, the biggest portion of dsDNA was eluted in P2 with 38.1%. P1 and P3 showed similar amounts of dsDNA (9.3% and 9.5% respectively). The TCID₅₀ assay was performed as control and was, as expected, negative for all samples.

Table 4-1: Summary and mass balance for total protein and dsDNA of the linear gradient purification of the mock fermentation cell culture supernatant (Figure 4-1) with the quantification of infective baculovirus (TCID₅₀). S: supernatant; FT: flow-through; W: wash; P1 – P4: pooled peaks 1 – 4; CIP: cleaning-in-place

Sample	Volume [mL]	Total protein [µg/mL]	Total protein %	dsDNA [ng/mL]	dsDNA %	Infective baculovirus TCID ₅₀ [pfu/mL]	%
L	100	952.4	100	173.3	100	0.00	-
FT	100	904.0	94.9	127.8	73.7	0.00	-
W	20	116.0	2.4	9.4	1.1	0.00	-
P1	12	358.9	4.5	135.0	9.3	0.00	-
P2	7	101.2	0.7	944.3	38.1	0.00	-
P3	9.5	<LLOQ	-	173.8	9.5	0.00	-

P4	34.5	<LLOQ	-	<LLOQ	-	0.00	-
CIP	10	124.0	1.3	8.3	0.5	0.00	-
Recovery			103.9		132.3		

<LLOQ: lower than lower limit of quantification

The high protein concentration found in Bradford assay for the loading material L and the flow-through FT can also be seen in a strong protein bands in the SDS-PAGE in their respective lanes (Figure 4-2 A)). Further, the protein bands in P1 are clearly visible but in lower concentration in comparison to the loading material, which shows the high depletion of proteins during the loading phase as the majority of protein passes through the column without binding. Peaks 3 and 4 did not show any protein bands in the Coomassie staining, verifying the low protein concentration found in the Bradford assay. The Western blots of the indicator proteins for baculovirus (gp64, Figure 4-2 B)) and eVLPs (HIV-1 gag p24, Figure 4-2 C)) were negative for all samples. This was expected because the conditioned media should not contain any building blocks for baculovirus or matrix proteins for VLP formation.

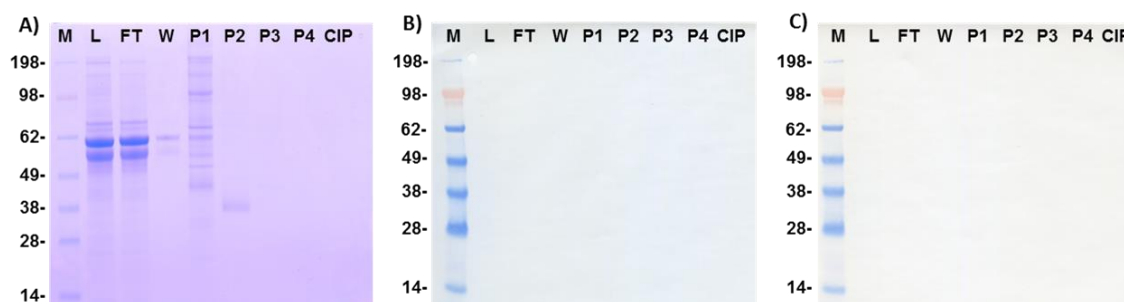


Figure 4-2: A) SDS-PAGE and Western blots of linear gradient purification of the mock fermentation supernatant (Figure 4-1) B) gp64 Western blot and C) HIV-1 p24 Western blot. M: molecular weight marker; S: supernatant; FT: flow-through; W: wash; P1 – P4: pooled peaks 1 – 4; CIP: cleaning-in-place

The comparison of the normalized light scattering areas of the three expression stages and subsequent fractal dimension analysis is given in chapter 4.1.1.4 on page 56.

4.1.1.2 *Tnms42* Virus Expression in Linear Gradient

The chromatogram of the virus expression shows high UV absorption signals during the loading phase (L/FT), which drop during the wash (Figure 4-3). Comparable to the mock fermentation (Figure 4-1), three peaks were identified and pooled according to the chromatogram with the information from the three UV signals (280, 260 and 214 nm). Each elution fraction was measured by MALS to obtain the total light scattering signal, which was integrated to receive the area under the curve. This is represented in the bar graph overlay (grey) in the chromatogram. As the intensity of the scattered light is directly proportional to the particle size and quantity [123], this method gives a fast insight into particle distribution over the course of the elution. Interesting to note is that the UV signals 280 and 260 nm are not fully representative for particle detection, as in this chromatogram light scattering peaks do not fully overlay with the UV signals.

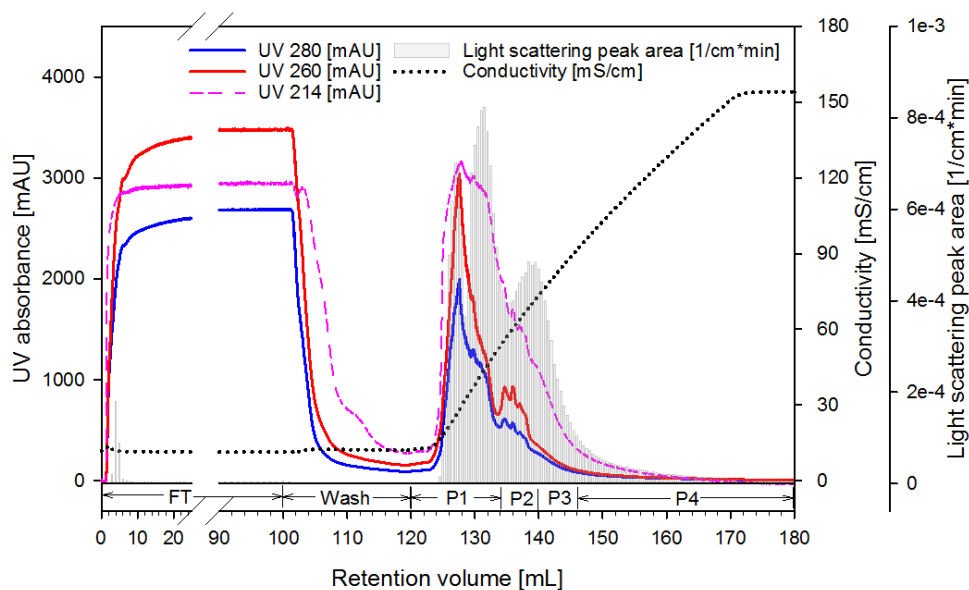


Figure 4-3: Chromatogram of the linear gradient of the virus expression in *Tnms42* cells using a QA monolith. The loading material was 100 mL of clarified, nuclease treated and 0.8 μm filtered cell culture supernatant. Bars represent the area under the curve of the light scattering intensity (grey) at-line measurements. FT: flow-through; W: wash; P1-P4: pooled fractions for peaks 1–4

The pooled fractions were analyzed by Bradford and PicoGreen[®] assay (Table 4-2). High protein (85.5%) and dsDNA (55.2%) load were detected in the FT fraction and did not bind to the column owed to the high conductivity of the loading material (11.44 mS/cm). Very low amounts of protein (1.8%) and dsDNA (1.5%) were flushed from the column during the wash phase, indicating good binding properties of the column, as no isocratic elution was detected. The amount of eluted protein decreases over the course of the elution. In P1 6.5%, in P2 only 3.3% and in P3 0.5% of the total protein were detected. P4 was below the lower limit of quantification of the assay and could not be quantified. The highest amount of dsDNA in the elution peaks was found in P3 with 49.9% and P2 with 19.9%. In P4 only 8.6% of the total dsDNA were detected. The lowest amount of dsDNA was found in P1 with 4.1% of the dsDNA regarding the loading material.

Table 4-2: Summary and mass balance for total protein and dsDNA of the linear gradient purification of the virus expression in *Tnms42* cells (Figure 4-3) with the quantification of infective baculovirus (TCID₅₀). S: supernatant; FT: flow-through; W: wash; P1 – P4: pooled peaks 1 – 4; CIP: cleaning-in-place

Sample	Volume [mL]	Total protein [$\mu\text{g/mL}$]	Total protein %	dsDNA [ng/mL]	dsDNA %	Infective baculovirus TCID ₅₀ [pfu/mL]	Infective baculovirus %
L	100	1129.0	100	991.7	100	1.77×10^7	100
FT	100	969.2	85.8	547.4	55.2	3.33×10^2	0.00
W	20	103.9	1.8	74.5	1.5	4.67×10^2	0.00
P1	9.5	707.5	6.0	426.5	4.1	n.a.	0.00
P2	6.	612.6	3.3	3297.1	19.9	2.63×10^8	89.2
P3	12.5	48.7	0.5	3957.5	49.9	n.a.	0.00
P4	35	<LLOQ	-	244.0	8.6	1.98×10^5	0.4
CIP	10	413.2	3.6	56.6	0.6	<LLOQ	0.00
Recovery			101.1		139.8		89.5

<LLOQ: lower than lower limit of quantification; n.a.: not analyzable

TCID₅₀ was carried out to see the distribution of the infective BV during course of the elution (Table 4-2). The samples of P1 and P3 could not be analyzed. The assay was repeated three times with the same result of the *sf9* cells disintegrating. However, no viral activity could be found, because the BVs used for the TCID₅₀ assay carry gene for yellow fluorescent protein (YFP). This YFP is used as a positive control of the assay and is present after successful infection. It was suspected that an unknown impurity in the sample lead to cell lysis. But based on the other analytics and other purification runs the absence of BVs was ruled out due to the presence of gp64 bands in the Western blot and the distribution of BV in the VLP expression run (Table 4-3). According to TCID₅₀ 89.2% of the total infective BV were recovered in P2. In P4 only a residual fraction of BV was recovered (0.4%) according to TCID₅₀. These values agree with the Western blot targeting the gp64 BV protein (Figure 4-4 B)). A strong band can be seen for the loading material. No gp64 was found in the FT or W fractions. Strong gp64 bands were detected in the elution peaks 1 – 3, the strongest one in P3. P4 only shows a very faint band for gp64. The WB against the HIV-1 gag p24 was negative for all samples (Figure 4-4 C)). This is an expected result, as the BV used for infection did not carry any gene coding for the gag polyprotein. The SDS-PAGE gel showed high protein load for the L and FT, as seen in the total protein values seen in the Bradford assay and chromatogram (Figure 4-3, Table 4-2 and Figure 4-4 A)). The higher protein load in P2 and P3 is also clearly visible in the respective bands of the SDS-PAGE gel scan. The very low protein concentrations in P3 and P4 from the Bradford assay are verified by the lack of protein bands in the gel scan.

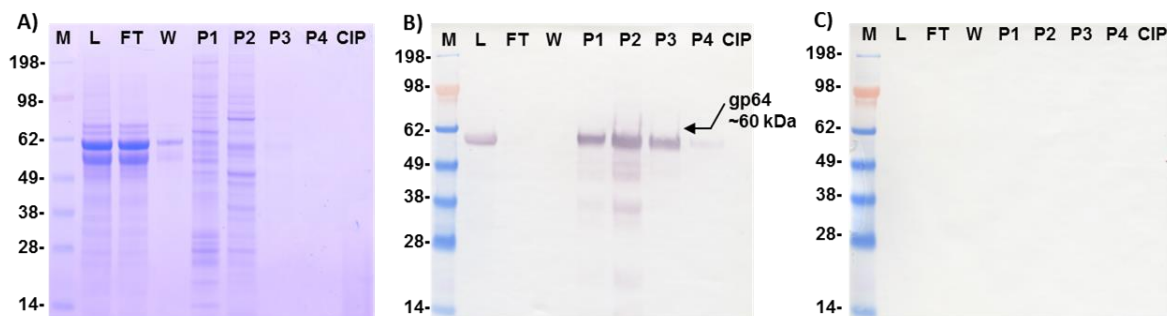


Figure 4-4: A) SDS-PAGE and Western blots of linear gradient purification of the virus expression in *Tnms42* cells (Figure 4-3) B) gp64 Western blot and C) HIV-1 p24 Western blot. M: molecular weight marker; S: supernatant; FT: flow-through; W: wash; P1 – P4: pooled peaks 1 – 4; CIP: cleaning-in-place

The comparison of the normalized light scattering areas of the three expression stages and subsequent fractal dimension analysis is given in chapter 4.1.1.4 on page 56.

4.1.1.3 *Tnms42* VLP Expression in Linear Gradient

The chromatogram for the HIV-1 gag H1 VLP expression (Figure 4-5) shows high UV absorption values for the loading phase (L/FT). During the wash an elution peak is visible, which might indicate an isocratic or early elution of bound material. However no significant protein or dsDNA content was measured in the fraction analytics (Table 4-3). Here, only 1.4% of the total protein or dsDNA were eluted. The TCID₅₀ signal in the W fraction was below the lower limit of quantification of the method. The chromatogram shows various peaks in the UV signals. Fractions were pooled according to the chromatogram with the help of the UV signals 280, 260 and 214 nm.

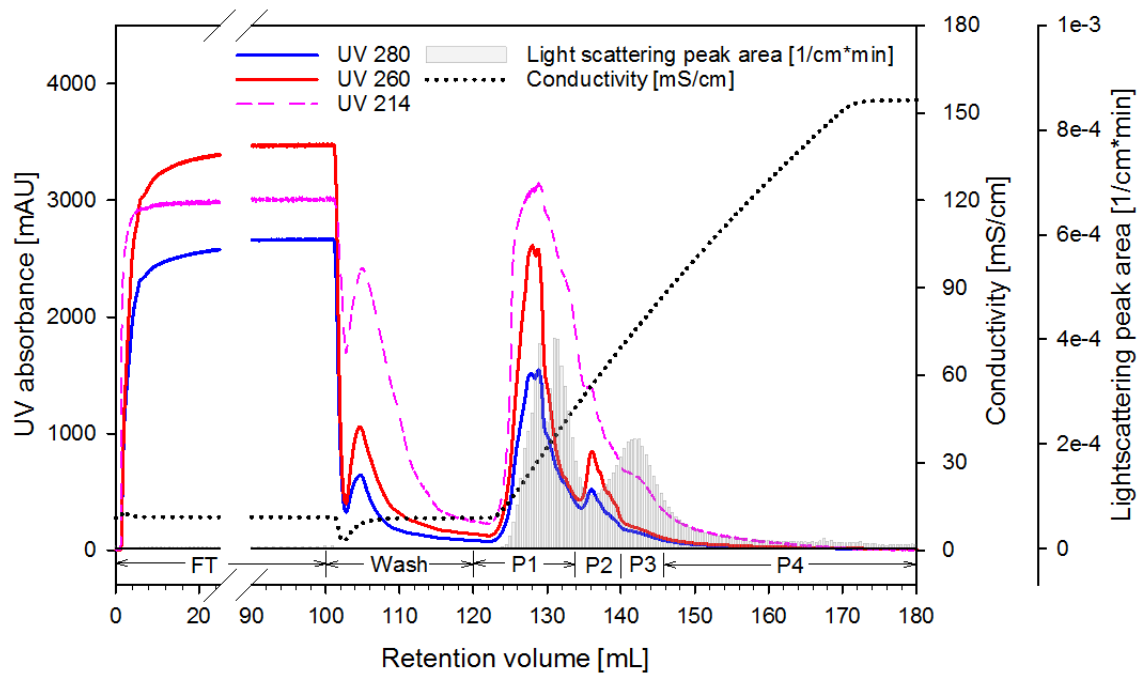


Figure 4-5: Chromatogram of the linear gradient of the *Tnms42* HIV-1 gag H1 VLP expression using a QA monolith. The loading material was 100 mL of clarified, nuclease treated and 0.8 μ m filtered cell culture supernatant. Bars represent the area under the curve of the light scattering intensity (grey) at-line measurements. FT: flow-through; W: wash; P1-P4: pooled fractions for peaks 1–4

As in the previously described experiments the FT fraction showed a large portion of the total protein (89.7%) and total dsDNA (73.9%). In the elution peaks, the majority of the protein load elutes in the beginning of the linear gradient. In P1 4.5%, in P2 2.1% and in P3 0.4% of the total protein were found. In P4 the protein signal was below the lower limit of quantification. This was verified by SDS-PAGE, where protein bands are clearly visible for the samples L and FT. The high protein amount during elution is visualized by the Coomassie staining in P1 and P2 (Figure 4-6 A)). The majority of the bound dsDNA elutes in P3, where 54.5% of the total dsDNA were found. In P4 11.4% and in P3 9.5% of the total dsDNA could be recovered. In P1 only a small portion of 2.8% were detected. According to the TCID₅₀ no infective BV could be found in the FT and W fraction. The highest amount of infective BV was found in P2, where 13.5% in regard to the loading material were found. In P3 7.5% and P4 0.1% BV were found. In P1 3.9% BV were detected. The total recovery of BV was only 25%.

Table 4-3: Summary and mass balance for total protein and dsDNA of the linear gradient purification of the *Tnms42* HIV-1 gag H1 VLP expression (Figure 4-5), with the quantification of infective baculovirus (TCID₅₀). S: supernatant; FT: flow-through; W: wash; P1 – P4: pooled peaks 1 – 4; CIP: cleaning-in-place

Sample	Volume [mL]	Total protein [µg/mL]	Total protein %	dsDNA [ng/mL]	dsDNA %	Infective baculovirus TCID ₅₀	
						[pfu/mL]	%
L	100	971	100	543.8	100	3.20 x 10 ⁶	100
FT	100	870.7	89.7	401.7	73.9	<LLOQ	-
W	20	67.1	1.4	37.7	1.4	<LLOQ	-
P1	10	441.1	4.5	153.5	2.8	1.25 x 10 ⁶	3.9
P2	6.0	333.2	2.1	859.1	9.5	7.22 x 10 ⁶	13.5
P3	14	25.9	0.4	2115.7	54.5	1.72 x 10 ⁶	7.5
P4	66	<LLOQ	-	187	11.3	2.94 x 10 ³	0.1
CIP	10	254.6	2.6	27.3	0.5	<LLOQ	-
Recovery			100.6		153.9		25.0

<LLOQ: lower than lower limit of quantification

The WBs for the respective indicator proteins for baculovirus (gp64) and the matrix protein HIV-1 gag of the expressed VLPs are shown in Figure 4-6 B) and C). The presence of the baculovirus capsid protein gp64 could be confirmed, as strong bands were found in lanes L, P1, P2 and P3. Only a faint band can be seen in P4. The band in P2 is slightly stronger than the bands in P1 and P3 for gp64. The WB against the gag polyprotein was also positive. Here, the loading material showed a band for the full-size polyprotein at ~55 kDa. Further, the elution Peaks P1, P2 and P3 showed a positive gag band. Like the gp64 WB, the P2 lane shows the strongest band for HIV-1 gag matrix protein. Lane P3 shows only a faint band, which indicates that species containing the gag protein elute earlier than species containing the gp64.

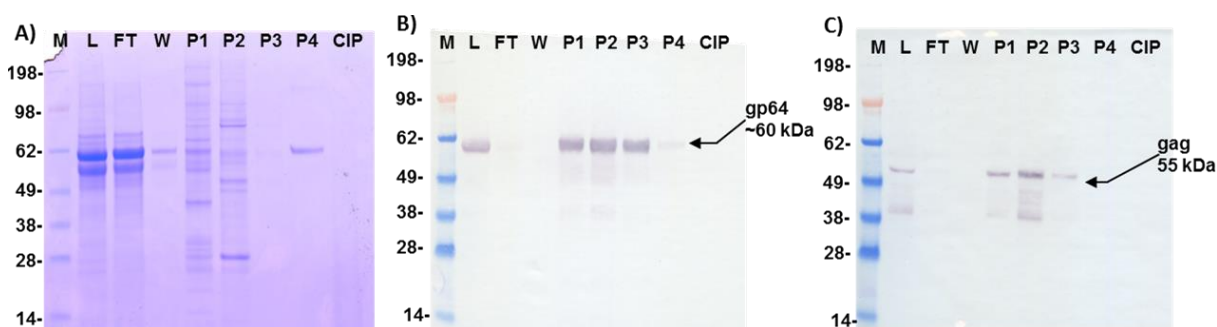


Figure 4-6: A) SDS-PAGE and Western blots of linear gradient purification of the *Tnms42* HIV-1 gag H1 VLP expression (Figure 4-5) B) gp64 Western blot and C) HIV-1 p24 Western blot. M: molecular weight marker; S: supernatant; FT: flow-through; W: wash; P1 – P4: pooled peaks 1 – 4; CIP: cleaning-in-place

The comparison of the normalized light scattering areas of the three expression stages and subsequent fractal dimension analysis is given in chapter 4.1.1.4 on page 56.

4.1.1.4 Normalized Light Scattering Area and Fractal Dimension Comparison

Figure 4-7 shows an overlay of the normalized integrated light scattering signals obtained from the linear gradient purifications of the mock fermentation, virus expression and HIV-gag-1 H1 VLP expression. For the mock fermentation supernatant, it is visible that the main light scattering signal peak elutes at 141 mL retention volume. A small peak is seen at 128 mL retention volume. When the same cell line is infected with recombinant baculovirus (virus expression run, red bars) the peak distribution shifts clearly. Now, a distinctive double-peak is visible in the early elution at 126 and 131 mL retention volume, followed by a broad peak shoulder from 137 to 139 mL. The next expression stage is the HIV-1 gag H1 VLP. Here the *Tnms42* cells were infected with a recombinant baculovirus carrying genes for the HIV-1 gag polyprotein that functions as a matrix protein and the haemagglutinin H1 functioning as an antigen. Here the peak pattern changes slightly in comparison to the virus expression. The overall peak area is smaller, but the peaks are separated more distinctively. A double peak can be identified in the early elution at 129 and 131 mL with another peak at 142 mL retention volume.

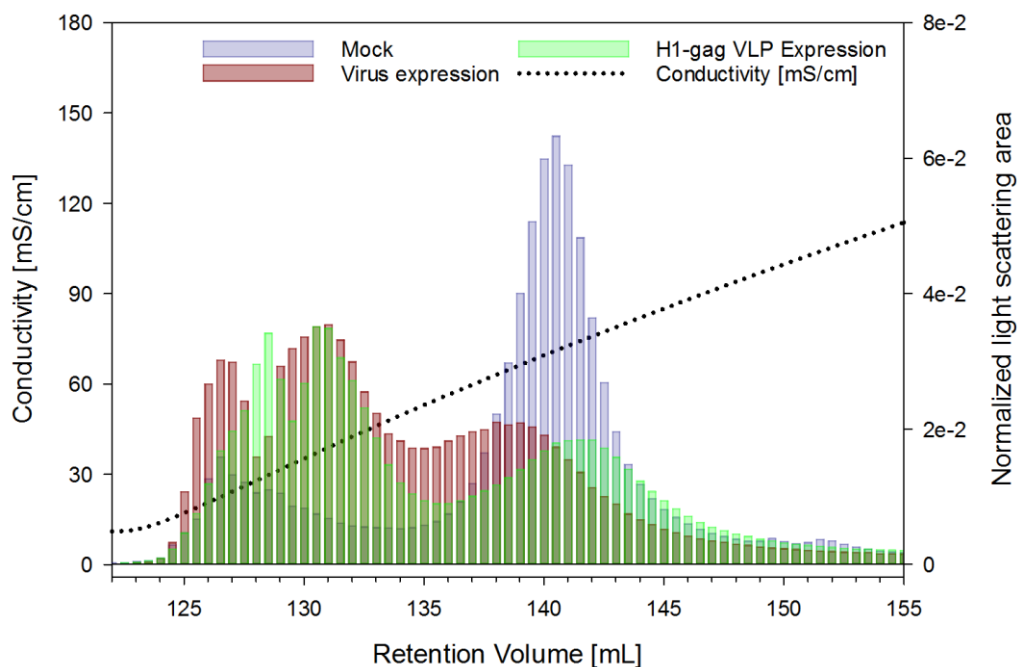


Figure 4-7: Overlay of the normalized area under the curve of the light scattering signal for the mock fermentation, virus expression and HIV-1 gag H1 VLPs production.

Small differences in the particle distribution and scattering area can be seen between the three different expression stages in Figure 4-7. However, no clear statement of the particle composition can be given based on this type of data evaluation. To increase the understanding of the elution behavior of the different particles present in the respective expression stages, two concepts for MALS data computation were established. The raw light scattering data was extracted and computed as described in chapters 3.10.1 and 3.10.2. The first conceptual method aims to compare the fractal dimensions of the eluting particles. The computed raw signals of the MALS detector for the elution of the respective runs are shown in Figure 4-8.

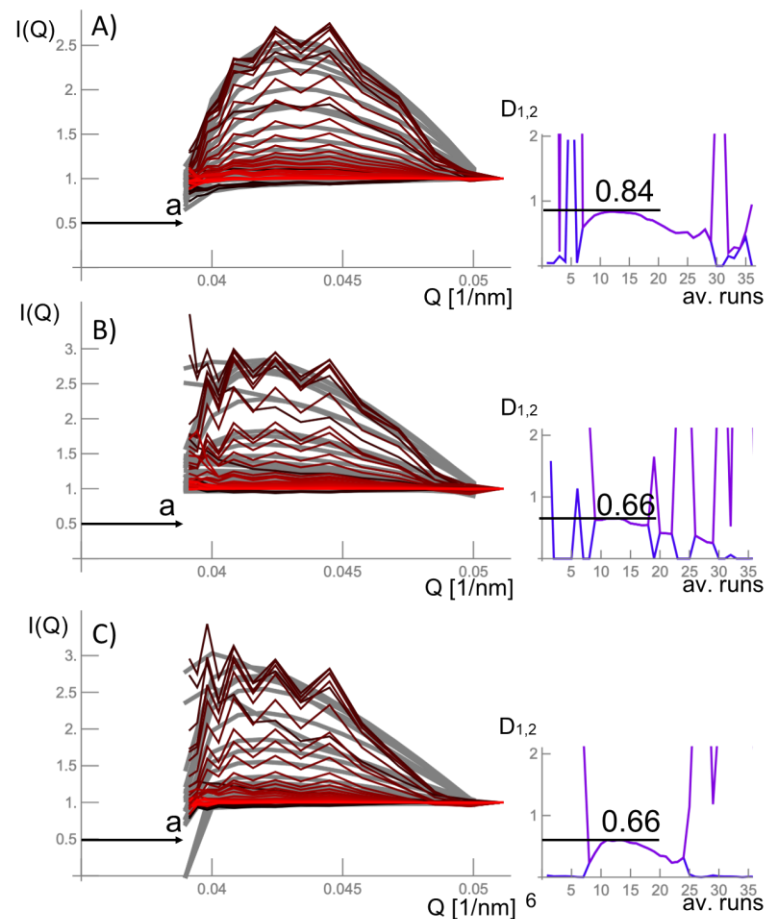


Figure 4-8: Fractal dimension analysis of the MALS raw data of the linear gradient elution (left). Colored lines give the raw data; grey lines represent the fitted data of the respective runs: A) Mock fermentation B) Virus expression C) eVLP expression. On the right, the course of the fractal dimension of the respective expression runs is shown. The y-axis ($D_{1,2}$) indicates the fractal dimension, while the x-axis is the time course over the elution of the chromatography run. The present data suggests a tendency from spherical shapes to elongated structures.

The course of the fitted curves (grey lines) in Figure 4-8 A) indicate the same behavior as the theoretical curve, for was calculated for hollow spheres (Figure 3-2, page 46) in the range between 0.045 – 0.05 1/nm. This observation is consistent with the expected particle load for the mock fermentation. Here, smaller particles with diameters of 30 – 80 nm are expected, as no virus particles or VLPs were expressed and smaller spherical sizes are characteristic for extra cellular vesicles [20], [44], [151]. When comparing the runs B) and C), where the particle load changes due to the addition of infective virus material the $D_{1,2}$ drops from 0.84 to 0.66 (Figure 4-8, left A)-C)). This change in the fractal dimensions indicates a clear tendency from spherical shapes to elongated bodies like the ovoid form of baculovirus. However, it is important to state, that, as expected, the fractal dimensions are quite similar between the runs of the virus expression (B)) and the eVLP expression (C)). Here it seems, that the high particle load in the samples leads to an overloading of the sample cell of the MALS detector. Further it is important to state that the natural particle size distribution of the investigated particles overlap to a certain degree, which makes the differentiation very challenging. In this case we can state that we could identify thin walled objects and that the course of the fractal dimensions suggests a change from spherical to elongated bodies. This observation however is

consistent to the findings of the other supporting analytical methods deployed for the respective purification runs in chapters 4.1.1.1 to 4.1.1.3.

The other conceptual method described in chapter 3.10.2 on page 47 uses the truncated forms of fractal pair densities to analyze the raw MALS data. This approach improves the resolution to predict the time when hollow particles such as small extracellular vesicles, viruses or VLPs are eluting. However, this approach reduces the sensitivity to calculate and differentiate the fractal dimensions of the eluting particles significantly. The computed data analysis for this method is shown in Figure 4-9. On the left side the term λ is shown over the course of the elution. A value of $\lambda < 1$ indicates, that hollow, thin walled objects are eluting. On the right side of Figure 4-9 the relation of D_2 to D_1 over the course of the elution is shown, which indicates the fractal dimension in this analysis.

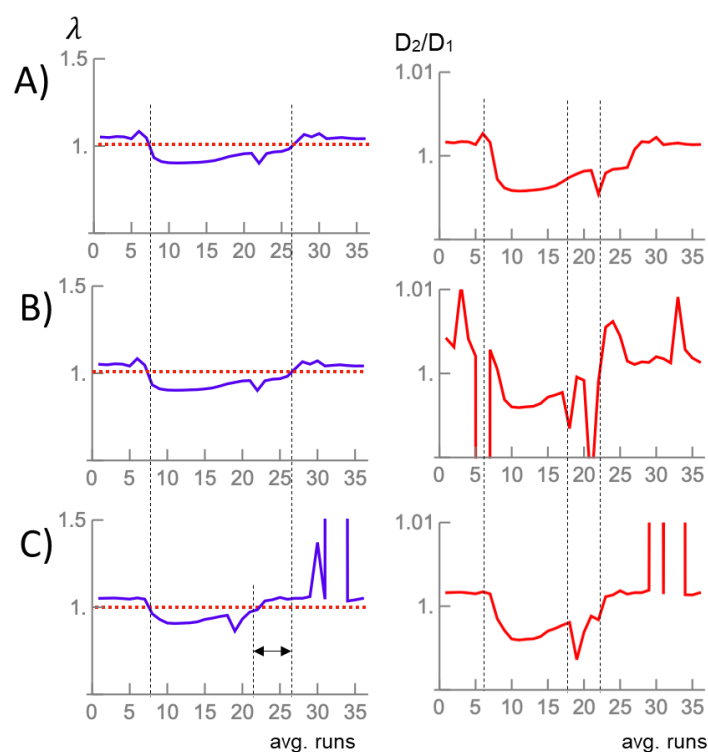


Figure 4-9: Analysis of λ (left) and fractal dimension D_2/D_1 (right) over the course of the elution of the respective runs are shown: A) Mock fermentation B) Virus expression C) eVLP expression. A value of $\lambda < 1$ indicates, that hollow, thin walled objects are eluting.

The time when the signal of λ drops below 1 is consistent over the three runs (A – C) in Figure 4-9. This might indicate that at the start of the elution the smallest particles are eluted from the column. The time span of hollow particles eluting during the course of the elution decreases. This could be explained by the addition of the recombinant virus in run C). Due to the infection cycle of the virus and production of eVLPs the particle size distribution of the budded particles narrows, as more defined particles (eVLPs) are synthesized. This leads to a sharper elution profile, as higher amounts of similar particles elute and thereby shortening the elution time span of hollow particles (indicated by the arrow). On the right side of Figure 4-9 the fractal dimension of the ratio between inner and outer shell over the course of the elution is shown. The ratio however does not significantly change from A), B), C) and is relatively constant around 1. This behavior can also be seen over the course of each

respective run, where the ratio is relatively constant in the middle part of the elution. Only in the early and late elution stages we observed differences and fluctuations. We concluded that the fluctuations originate from early eluting proteins which cause a light scattering signal, but are not thin walled particles. At the end of the elution we expected protein or other aggregates which could explain the fluctuations in the ratio D_2/D_1 at the end of the elution, which would also generate a light scattering signal and could therefore interfere with the particle analysis. Further, it was assumed that spherical particles in general, which are present in all samples over the three different expression stages may be the common cause, as these seem to be the most prominent object and therefore the most common “scatterer” in the respective samples. This in combination with the lower resolution compared to traditional SAXS methods and the slightly overlapping particle size distributions of extracellular vesicles and eVLPs an exact differentiation was not possible with this conceptual method. However, this method was able to indicate the exact timestamp, when thin walled objects eluted during the purification run. With the first conceptual method a clear tendency could be given, that the fractal dimension changes to elongated objects when baculovirus is present in the expression system. Unfortunately a clear differentiation between baculovirus and eVLPs could not be given using this method at this stage of method development.

4.1.2 Linear Gradient Purification of HIV-1 gag H1 VLPs

The HIV-1 gag H1 VLPs were produced in *Tnms42* insect cells and harvested three days after infection with recombinant baculovirus. For process development 50 mL cell culture supernatant was clarified by centrifugation (800 rpm for 15 min) and treated with nuclease to digest free extracellular, non-incorporated dsDNA and subsequently filtered using a 0.8 μm syringe filter. The loading material was loaded into a 1 mL QA monolith column. Elution was achieved by a linear gradient of 50 CV ranging from 100 – 1500 mM NaCl followed by a plateau phase of 10 CV with 2000 mM NaCl for regeneration. Cleaning-in-place was achieved by 60 CV of 1 M NaOH. Flow rates were kept constant at 1 mL/min and fractions of 1 mL were collected for process analytics.

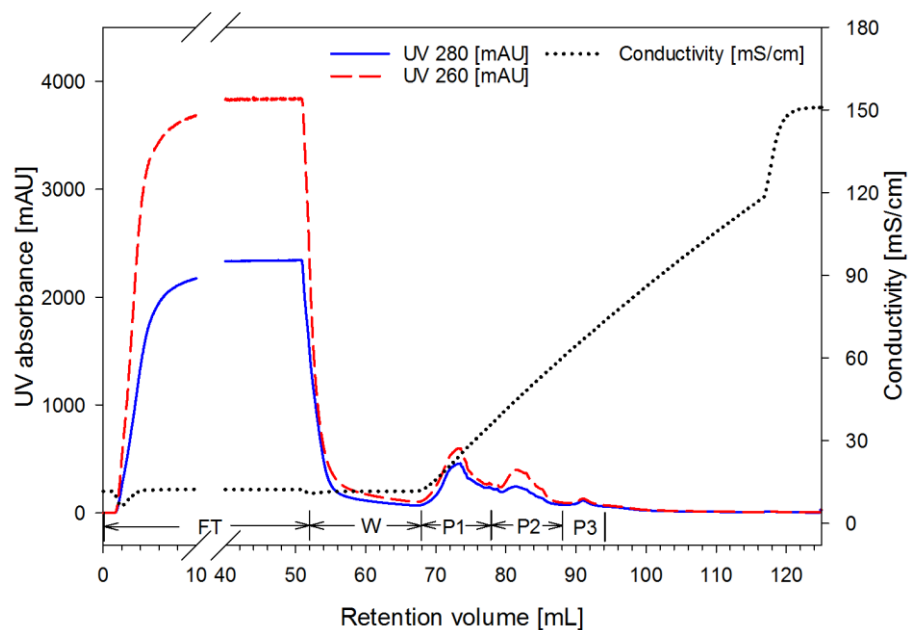


Figure 4-10: Chromatogram of the linear gradient purification of HIV-1 gag H1 VLPs using a QA monolith. The loading material was 50 mL clarified and nuclease treated supernatant and was filtered by 0.8 μm prior to loading. FT: flow-through; W: wash; P1 – P3: pooled peaks 1 – 3

During the loading phase, strong UV signals can be seen in the chromatogram (Figure 4-10) (L/FT). The UV signals drop significantly during the wash (W), as weakly or unbound species are flushed from the column. Between 70 and 96 mL retention volume, three distinctive, but not base-line separated, peaks were identified and pooled according to the chromatogram (P1 – P3).

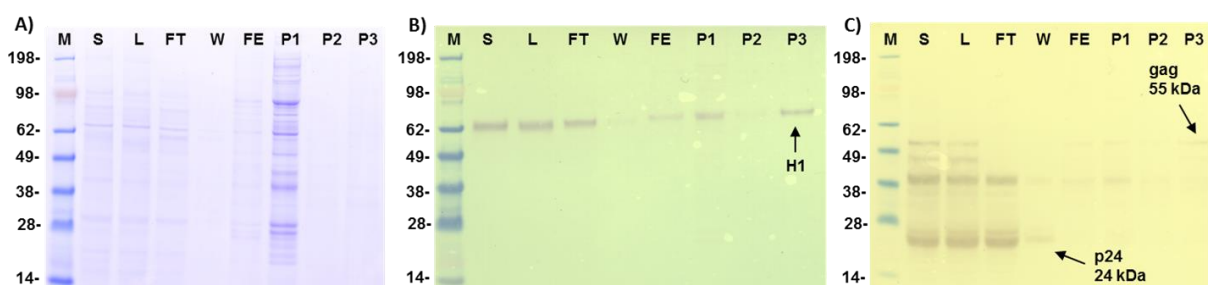


Figure 4-11: A) SDS-PAGE and Western blots of linear gradient purification (Figure 4-10) B) haemagglutinin H1 and C) HIV-1 p24. M: molecular weight marker; S: supernatant; FT: flow-through; W: wash; FE: pooled Elution peaks; P1 – P3: pooled peaks 1 – 3

In comparison to peaks 1 and 3, the UV 260 nm signal in peak 2 is significantly higher, indicating a high dsDNA load in the respective fractions. Heterocyclic rings of the nucleotides in DNA or RNA that absorb the UV light strongly at a wavelength of 260 nm. The expected high DNA load was confirmed by PicoGreen assay (Table 4-4). Here, 9.7% of the total dsDNA (in regard to the loading material) eluted in peak 2. Only smaller traces (<1%) of DNA could be found in the peaks 1 and 3. Due to the high conductivity of the loading material (12.25 mS/cm), the majority of protein (72.8%) and dsDNA (46.4%) did not bind to the column and was found in the flow-through fractions, which is also visible in the FT lane of the SDS-PAGE gel scan (Figure 4-11 A)). The digestion of the free dsDNA can be seen in the decrease in dsDNA concentration of samples S and L in Table 4-4. Approximately 52% of the total dsDNA was digested. Residual DNA was attributed to be incorporated in baculovirus or entrapped in VLPs [152], because Benzonase® cannot digest DNA inside of particles. The PicoGreen® assay however is able to detect dsDNA in particles such as VLPs or viruses as well as free dsDNA in solution [78]. In Peak 1 the highest protein concentration of 592.2 µg/mL was detected, which represents 7.7% of the total protein. Peaks 2 and 3 showed only low protein concentrations (<0.5%). Residual and strongly bound species that could not be eluted by concentrations of 2000 mM NaCl were desorbed during the CIP, where 11.5% of the total protein was eluted.

Table 4-4: Summary and the mass balance for total protein and dsDNA of the linear gradient purification of HIV-1 gag H1 VLPs (Figure 4-10). S: supernatant; FT: flow-through; W: wash; FE: pooled Elution peaks; P1 – P3: pooled peaks 1 – 3; CIP: cleaning-in-place

Sample	Volume [mL]	Total protein [µg/mL]	Total protein %	dsDNA [ng/mL]	dsDNA %
S	50	297.1	-	1690.8	-
L	50	306.1	100	893.4	100
FT	50	222.8	72.8%	414.4	46.4%
W	15	46.8	4.6%	51.1	1.7%
P1	2	592.2	7.7%	697.9	0.6%
P2	2	38.0	0.5%	154.4	9.7%
P3	1	24.5	0.2%	2234.4	0.4%
CIP	15	117.4	11.5%	222.2	0.0%
Recovery			97.3%		58.9%

The presence of the VLP indicator proteins HIV-1 gag and haemagglutinin H1 was confirmed by Western blot analysis of the process samples (Figure 4-11 B) and C)). H1 could be found in the supernatant and loading material. The FT showed a strong H1 band, which means that some of the haemagglutinin did not bind to the column. We concluded that this comes from free or misfolded H1 protein that was not incorporated into the VLPs or from fragmented VLPs. H1 was also found in peaks 1 and 3. The gag polyprotein was found in the supernatant and loading material. Only fragments and no full-size gag polyprotein (55 kDa) was found in the FT fraction. We assumed that these gag fragments (visible in SDS-PAGE bands S, L FT) originated either from misfolding, a faulty assembly process, denaturation or VLP fragmentation due to problems during the budding process. Fine bands of full-size gag can be seen in the elution peaks 1 and 3, hinting to a successful VLP expression, as both VLP indicator proteins are present in the respective elution peaks according to

Western blot analysis. Indicator proteins only confirm a successful expression, and their presence on a protein level. But also particle fragments, free or misfolded protein can give a positive analysis result [153]. When the particle of interest shares the host cell membrane with an impurity like the baculovirus more analytical methods need to be applied. After verifying the presence of indicator proteins for VLPs, the presence of particles needs to be verified by an orthogonal analytical method. For the particle quantification and characterization NTA was used. Here, particle concentration, particle size and size distribution were measured of all process samples (Table 4-5). In S and L high particle concentrations between ~ 5 and 9×10^{10} particles/mL were found. NTA is known to overestimate particle concentrations in samples with high background noise, such as supernatant or loading samples, where aggregated proteins, dsDNA complexes, host cell debris or other extracellular vesicles lead to high measurement variation [154]. This may lead to overcompensation when calculating recoveries or peak yields. Particle concentration in the FT and W fraction is very low in comparison to the loading material, as only 1.1% (FT) and 0.1% (W) of the total particles could be found in the respective sample. This indicates an effective particle binding during loading. The elution (P1 – P3) shows a low recovery of particles, as only 7.5% of the total particles could be attributed to these samples. Peak 1 showed the highest particle recovery of 3.5% along with Peak 3 (3.1%). In Peak 2 only 0.9% of the particles were found. During the CIP step, 9.1% of the total particles were flushed from the column indicating a strong particle binding. In addition, the particle data was filtered to only show the concentration of particles with a size range of a diameter of d : 100 – 200 nm. This changes the distribution of the recovered particles slightly. The biggest difference is in P1, as most of the particles were not counted in this size range which is explained by the mean particle size of the respective sample. In P1 the mean particle size is 96 nm. However, an overall trend can be seen within the values of the mean particle size. Smaller particles tend to elute with lower conductivity than larger particles. The particle size grows with increasing conductivity along the elution in peaks 1 – 3.

Table 4-5: Particle mass balance for all and selected particles (d : 100 – 200 nm) and mean particle sizes from NTA of the linear gradient purification fractions of HIV-1 gag H1 VLPs (Figure 4-10). S: supernatant; FT: flow-through; W: wash; FE: pooled Elution peaks; P1 – P3: pooled peaks 1 – 3; CIP: cleaning-in-place; Same superscript letters (A/B) indicate significant size difference

Sample	Volume [mL]	Particles (LS) all particles [particles/mL]	Particles (LS) all particles %	Particles (LS) d : 100 – 200 nm [particles/mL]	Particles (LS) d : 100 – 200 nm %	Mean particle diameter [nm]
S	50	5.81×10^{10}		3.22×10^{10}		130 ± 13
L	50	9.03×10^{10}	100	6.06×10^{10}	100	158 ± 10
FT	50	9.77×10^8	1.1	6.74×10^8	1.1	128 ± 12
W	15	1.97×10^8	0.1	1.30×10^8	0.1	147 ± 17
P1 ^A	2	7.84×10^{10}	3.5	2.16×10^{10}	1.4	^A 96 ± 6
P2 ^B	2	2.13×10^{10}	0.9	1.21×10^{10}	0.8	^B 113 ± 10
P3 ^{AB}	1	1.38×10^{11}	3.1	1.02×10^{11}	3.4	^{AB} 135 ± 6
CIP	15	2.74×10^{10}	9.1	1.33×10^{10}	6.6	122 ± 12
Recovery			17.7		13.4	

It was assumed that larger particles have a higher number of binding sites for ligand interaction and therefore need higher amounts of Cl⁻ ions to generate desorption conditions and subsequently to be eluted from the column [155]. The biggest particles were eluted in P3 with 135 nm.

With the present data we concluded, that the majority of the VLP elute in P1, as the presence of indicator proteins is given (positive H1 and p24 WB) and a high particle concentration was detected by NTA. The determined particle mean size of 96 ± 6 nm is also in accordance with values reported in the literature [156], [157]. The majority of DNA was eluted in P2, where also a lower particle concentration was detected. We concluded that the baculovirus is starting to be desorbed from the column as the reached conductivity values (45 mS/cm) in P2 are similar to reported values from the literature [78], [158]. Indicated by the significant bigger mean particle size of 135 ± 6 nm in P3 compared to P1, we concluded that the majority of BV elutes in P3 as the size is in accordance with reported values in the literature [159]. Using this information, we developed a scalable capture step using a step gradient elution. This is described in the next chapter.

4.1.3 Step Gradient Purification

The HIV-1 gag H1 VLPs were produced in *Tnms42* insect cells and harvested three days after infection with recombinant baculovirus. For the step gradient purification 100 mL cell culture supernatant was clarified by centrifugation (800 rpm for 15 min) and treated with nuclease to digest free dsDNA and filtered using a 0.8 μm syringe filter prior to loading. Elution was achieved by a step salt gradient consisting of 4 steps (360, 600, 740 and 1000 mM NaCl) for 15 CV, followed by a regeneration step with 100% mobile phase B (2000 mM NaCl) for 15 CV. Cleaning-in-place was achieved by 60 CV of 1 M NaOH. Flow rates kept constant at 1 mL/min and fractions of 1 mL were collected for process analytics.

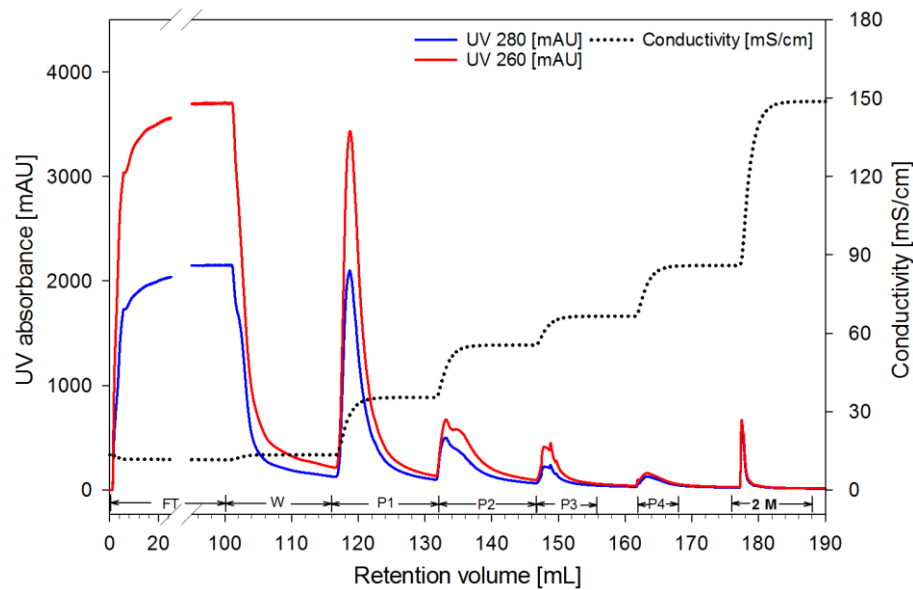


Figure 4-12: Chromatogram of the step gradient purification of HIV-1 gag H1 VLPs using a QA monolith. The loading material was 100 mL clarified and nuclease treated supernatant and was filtered by 0.8 μm prior to loading. FT: flow-through; W: wash; P1 – P4: pooled peaks 1 – 4; 2M: Regeneration step 2 M NaCl

The chromatogram shows high UV absorption signals during the L/FT phase, which immediately drops during the W phase, as weakly or unbound species are transported out of the column. The four steps of the gradient and regeneration phase produced 4 distinctive peaks that show a typical tailing behavior known from radial chromatography monoliths. This is a consequence of the non-constant flow velocities within the column, that are created by the change of the cross-sectional area along the column [160]. Comparable to the linear gradient purification (chapter 4.1.2), the majority of protein (65%) and dsDNA (60.5%) did not bind to the column and was found in the FT fraction (Table 4-6). Also, the reduction of ~46% of free dsDNA in the supernatant by the nuclease treatment is comparable to the values reached in the linear gradient. We assumed that the residual dsDNA is incorporated in infective baculovirus, extracellular vesicles or was entrapped within some VLPs during the formation and budding process [161], [162]. The highest protein concentration was found in P1 with 814. $\mu\text{g}/\text{mL}$, which represents 17.7% of total protein regarding the loading material. The remaining peaks show significantly lower protein levels (3.8, 0.2 and 0.5% respectively) The highest dsDNA percentage elutes in peaks 2 and 3 with 14.0 and 14.1% of the total dsDNA respectively. The

regeneration step (2M) eluted strongly bound species from the column, which represent 1.2% of the total protein and 2.2% of the total dsDNA.

Table 4-6: Summary and mass balance for total protein and dsDNA of the step gradient purification of HIV-1 gag H1 VLPs. S: supernatant; FT: flow-through; W: wash; P1 – P4: pooled peaks 1 – 4; 2M: Regeneration step 2 M NaCl; CIP: cleaning-in-place

Sample	Volume [mL]	Total protein [$\mu\text{g/mL}$]	Total protein %	dsDNA [ng/mL]	dsDNA %
S	100	333.5	-	1375.2	-
L	100	322.3	100	780.2	100
FT	100	209.5	65.0	472.4	60.5
W	15	32.9	1.5	47.6	0.9
P1	7	814.2	17.7	367.2	3.3
P2	7	172.8	3.8	1573.3	14.1
P3	7	9.0	0.2	1561.1	14.0
P4	7	22.4	0.5	376.8	3.4
2M	15	25.9	1.2	115.5	2.2
Recovery			89.8		98.5

Presence of the VLP indicator proteins was confirmed with Western blots against HIV-1 gag polyprotein (p24), acting as the required matrix protein for VLP formation and haemagglutinin (H1), representing the antigen structure for the model-vaccine VLP. Baculovirus presence was confirmed on protein level with positive Western blots against gp64 and vp39 (Figure 4-13 A – D)). The gp64 is an essential protein for infective BVs, as it is required for the fusion with the cell membrane of the host cell during infection [163], [164]. The vp39 is a major matrix protein for the nucleocapsid and is present in matured BVs.

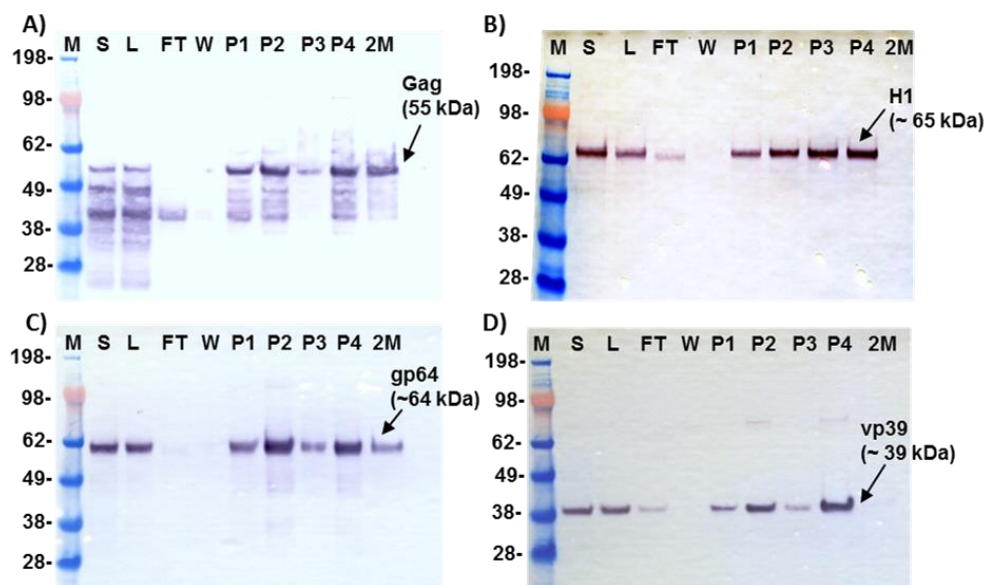


Figure 4-13: Western blots of the step gradient purification (Figure 4-12). A) HIV-gag p24 of B) haemagglutinin H1 C) Baculovirus envelope protein gp64 D) Viral capsid protein vp39. M: molecular weight marker; S: supernatant; FT: flow-through; W: wash; P1 – P4: pooled peaks 1 – 4; 2M: Regeneration 2 M NaCl

The WB against p24 (Figure 4-13 A)) shows bands for the full-size gag polyprotein in all fractions except FT and W. We concluded, that the binding to the column is very efficient and that misfolded or free gag did bind on the column. In the FT fraction a smearing at ~40 kDa is visible that was attributed either a gag fragment that did not bind to the column, or unspecific binding of the antibody other proteins that were blotted from the SDS-gel P3 shows the weakest band for gag. In general, the p24 antibody did show some smearing in the lanes. We attributed this to either disintegration of the gag polyprotein or to unspecific binding of the antibody that creates a color reaction from the secondary antibody used for the coloring reaction. P2 and P4 show the strongest bands in the Western blot for p24. Similar to the anti-gag WB, strong bands for H1 could be detected in all fractions except FT and W (Figure 4-13 B)). Again, a faint band can be seen in the FT, that was again attributed to misfolded, free, non-incorporated H1 or small membrane fragments that cannot bind to an AIEX-column under the used conditions due to charge differences. A trend can be seen, as the band thickness increases from P1 to P4 with increasing conductivity. No H1 could be detected in the 2M fraction.

The Western blot for gp64 revealed strong bands for S and L, indicating a high amount of expressed protein (Figure 4-13 C)). No gp64 was found in the WB for FT and W fractions. The elution fractions showed the strongest gp64 signal in peaks 2 and 4. Weakest bands were found in elution peak 3 and 1. The column regeneration (2M) also showed a clearly visible band of gp64. The second baculovirus marker protein vp39 was also found in all analyzed samples of the purification except W. Only a faint band was found in the FT fraction indicating some unbound or fragmented species. The strongest band was found in elution peak 4 with a 2nd strongest band in peak 2. Peak 1 showed a band with moderate thickness and only a faint band in peak 3. No vp39 was detected in the sample from the column regeneration step.

Table 4-7: Particle and infective baculovirus mass balance for step gradient purification of HIV-1 gag H1 VLPs with log₁₀ virus reduction factors and mean particle sizes for the process samples from NTA and TCID₅₀. S: supernatant; FT: flow-through; W: wash; P1 – P4: pooled peaks 1 – 4; 2M: Regeneration step 2 M NaCl; CIP: cleaning-in-place; Same superscript letters (A/B) indicate significant size difference; Form factor 2: spherical particle; Form factor 1: rod-shaped particle

Sample	Volume [mL]	Particle concentration d: 100 – 200 nm		Infective baculovirus TCID ₅₀		Log ₁₀ virus reduction factor	Mean particle diameter [nm]	Form factor SAXS
		[particles/mL]	%	[pfu/mL]	%			
S	100	3.81 x 10 ⁹	-	4.69 x 10 ⁶	-	-	139 ± 25	-
L	100	2.55 x 10 ⁹	100	6.05 x 10 ⁶	100	-	156 ± 9	-
FT	100	7.25 x 10 ⁷	2.8	< LLOQ	-	-	106 ± 5	-
W	15	2.63 x 10 ⁷	0.2	< LLOQ	-	-	134 ± 28	-
P1 ^A	7	5.37 x 10 ⁹	14.7	2.72 x 10 ⁵	0.3	2.5	^A 126 ± 1	1.5
P2 ^{AB}	7	3.91 x 10 ⁹	10.7	1.68 x 10 ⁷	19.5	0.7	^{AB} 137 ± 2	1.7
P3 ^A	7	8.78 x 10 ⁸	2.4	2.18 x 10 ⁶	2.5	1.6	^A 145 ± 8	1.5
P4 ^{AB}	7	4.99 x 10 ⁹	13.7	1.79 x 10 ⁷	20.8	0.7	^{AB} 160 ± 0.1	1.3
2M ^{AB}	15	9.50 x 10 ⁸	5.6	2.14 x 10 ⁷	5.3	1.3	^{AB} 197 ± 15	-
Recovery			50.2		48.4			

< LLOQ: lower than lower limit of quantification

For the particle mass balance and characterization NTA was used (Table 4-7). Here, supernatant and loading material showed 3.81×10^9 and 2.55×10^9 particles/mL, respectively. The FT fraction showed very low amounts of particles (2.8% of the total particles), that indicates good binding conditions for the particles. During the wash only 0.2% of the particles could be detected, which indicates an efficient particle capture with sufficient binding strength, as isocratic elution can be excluded due to low desorption of particles. Elution peaks 1 – 4 showed high amounts of particles in general. The highest number of particles was found in peak 1, representing 14.7% of the total particles in regard to the loading material with a mean particle size of 126 nm, which is significantly the smallest particle size found in the elution peaks. This is in good agreement with the expected particle size of the HIV-1 gag H1 VLPs. The 2nd highest number of particles was found in peak 4, representing 13.7% of the total particles. Here, the mean particle size is the biggest with 160 nm and is significantly bigger than all other peaks. In P2 eluted 10.7% of the total particles. Peak 3 showed the lowest number of eluted particles with 2.4% of total particles. During the column regeneration 5.6% of the total particles were eluted from the column. In total 50.2% of the particles (in regard to the loading material) were recovered, which is a similar value when comparing this to values reported in the literature [30], [31], [61], [165].

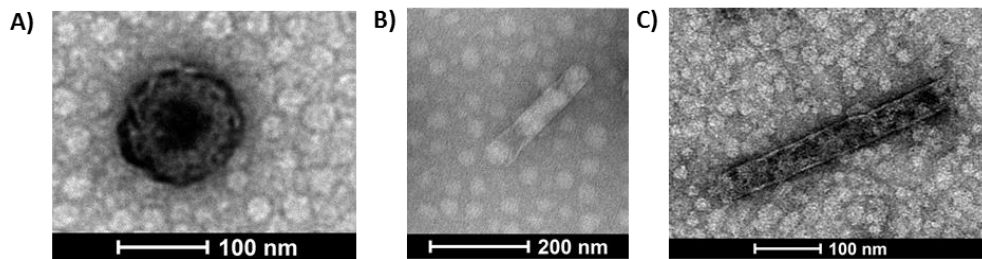


Figure 4-14: Exemplary TEM pictures from step gradient purification of the *Tnms42* cell culture supernatant. A) VLP from P1 B) Baculovirus from P2 C) Baculovirus in P4

The distribution of infective baculovirus was obtained with a TCID₅₀ and converted to pfu/mL [166] (Table 4-7). The loading material contained a virus load of 6.95×10^6 pfu/mL. No virus was detected in FT and W fractions indicating a very good binding of the BV to the column material. Baculovirus was primarily eluted in P2 (19.5%) and P4 (20.8), which corresponds to a conductivity of 55 and 85 mS/cm, respectively in the mobile phase during elution. Here the log₁₀ virus reduction factor of 0.7 is found for P2 and P4. Only 0.3% of the total BV was found in P1 which calculates to a log₁₀ virus reduction factor of 2.5. According to the EMA this virus reduction is categorized within the range of second highest reduction factor for one unit operation [167]. In P3 2.5% of the BV was eluted. The mean particle size of this peak also does not significantly vary from the measured mean particle size in P4. During column regeneration 5.3% of the BV was flushed from the column. In total 48.4% of the BV was recovered over the elution, which in comparison to the literature, is a good recovery [78], [158].

For further particle characterization the pooled peaks P1 – P4 were analyzed by SAXS and form factors (FF) were calculated as described and summarized by Boldon et al. in 2015 [132]. A homogeneous sample of spherical particles would give a form factor of 2, while a sample containing

only rod-shaped particles with the same lengths-to-height ratio would give a form factor of 1. When mixing the spherical and rod-shaped particles the overall form factor would change, as the sample is not homogeneous. The same principle applies when evaluating the calculated form factors from peaks 1 – 4. P1 and P3 showed an FF of 1.5 indicating a fair amount of rod-shaped and spherical particles. For P2 an FF of 1.7 was calculated, which would point to a larger portion of spherical than rod-shaped particles. The FF for P4 was calculated to 1.3, indicating the majority of particles to be rod-shaped. This is in good agreement with the findings of the TCID₅₀, where 20.8% of the infective BV was eluted. However, for P1 the FF was expected to point more to spherical particles, as nearly 15% of particles and only 0.3% of the total BV were detected in this Peak. According to the TCID₅₀ a portion of 15.5% of total BV was eluted in P2. The expected FF was a value lower than the calculated 1.7. When comparing the TCID₅₀ values from the peaks 1 – 4 it can be seen that there is an early eluting BV group in P2 (15.5% of BVs) and a late eluting group of BVs in P4 (20.8% of total BV). The mean particle size in these two peaks however is significantly different with 137 nm in P2 and 160 nm in P4. It was concluded that the size difference is responsible for the different elution properties, as in P2 species are eluted with 35 mS/cm and P4 elutes with 86 mS/cm. Further we hypothesized that the unexpected FFs are influenced by varying length-to-height ratios of the BVs and can therefore tend to be over- or underestimated.

After summarizing the collected data, we concluded the following explanation for the elution peaks. In the column regeneration with 2 M NaCl we see species eluting from the column with a mean particle size of 197 nm. This fraction shows some bands for p24 and gp64. We concluded that this regeneration pool consists of very large particles, or aggregated fragments of BV or VLP that bind strongly to the column. Large multiprotein gp64 aggregations forming liposome-like structures have been reported in the literature by Markovic et al. in 1998 [161] and the aggregation and loss of infectivity of BVs has also been reported [165], [166]. The elution of infective BV is separated into P2 and P4. We saw an early BV peak eluting at 35 mS/cm in P2 and a late eluting BV peak 4 at 86 mS/cm. This distribution of BV elution is mainly shown by the results of the TCID₅₀ and the presence of strong bands of the indicator proteins gp64 and vp39 in their respective lanes in the WBs. The particle size is in accordance with values reported in the literature [72], [163], [165], [167]. It was also described in the literature, that the BV and recombinant product share the same host cell membrane [113]. This explains why indicator proteins for VLPs (H1 and gp24 in Peaks 2 and 4) were found. P3 showed low amounts of particles and BV (each >2.5%). In this peak also a high portion of the total DNA was recovered (14% of the total dsDNA). Finally, we concluded, that the HIV-1 gag VLPs are eluted in P1. This is based on the positive WBs for the indicator proteins H1 and p24, the detection of particles with the correct mean particle size according to literature. It can also be stated in this regard, that the indicator proteins for BV were positive in P1, however a strong presence of BV does not agree with the other performed orthogonal assays as the mean particle size is too small for BV and the TCID₅₀ showed only very low residual amounts of BV. P1 showed a high number of particles with a low virus titer. This can be calculated to a log₁₀ virus reduction factor of 2.5. The majority of host cell protein (>83%) and host cell DNA (>96%) was depleted. From 100 mL cell culture supernatant it would be possible to create 450 doses from the pooled P1 within a process time of

under 2 h when assuming a particle load of 1×10^9 particles per dose. The WHO and FDA recommend a maximum of 10 ng dsDNA per vaccination dose [168], [169]. In our case the calculated dsDNA per vaccination dose would be 5.7 ng, which means that the developed capture step for HIV-1 gag VLPs is compliant with the recommendations set by FDA and the WHO in this regard. However, a full separation of BV from the product was not achieved. The residual amount of BV present in P1 needs to be separated or inactivated by a consecutive unit operation step with a higher \log_{10} virus reduction factor and higher selectivity or resolution for these two species to be fully compliant to the recommendations set by FDA or WHO.

4.2 Purification Method Development for HIV-1 Gag-GFP VLPs Expressed in HEK-293

The notion of these experiments was to accelerate the process development timeline for enveloped virus-like particle purification. This was achieved by establishing a high-throughput at-line MALS-FI analysis method capable of detecting the particles through the purification process combined with a semi-quantification. Strong anion-exchange monoliths are capable to join the capture and purification step, as crude loading material can be used. This is favorable in bio-separation processes of bio-nanoparticles such as eVLPs and exosomes [30], [168]. The first step was to characterize VLP elution using linear gradients, where the at-line particle detection method was used for particle detection. The data obtained from these experiments was used to develop an step elution process, that could be easily scaled-up.

4.2.1 Linear Gradient Purification of HIV-1 Gag-GFP VLPs

The cell free and clarified supernatants containing HIV-1 Gag-GFP VLPs were produced as described in chapter 3.2.1. For the chromatography experiments, 100 mL supernatant was loaded into the column. A linear salt gradient (100 - 1000 mM NaCl, 50 CV) was used for elution. Fractions of 1 mL were directly collected into 96 deep-well plates and subsequently analyzed using the newly developed at-line MALS-FI method (chapter 3.3.4). The light scattering and fluorescence peak areas were calculated for each elution fraction by computing the respective area under the curve (AUC) of the MALS and fluorescence signals. The chromatogram is shown in Figure 4-15. The MALS-FI data is shown in the grey and green bars as overlay (delay volume corrected).

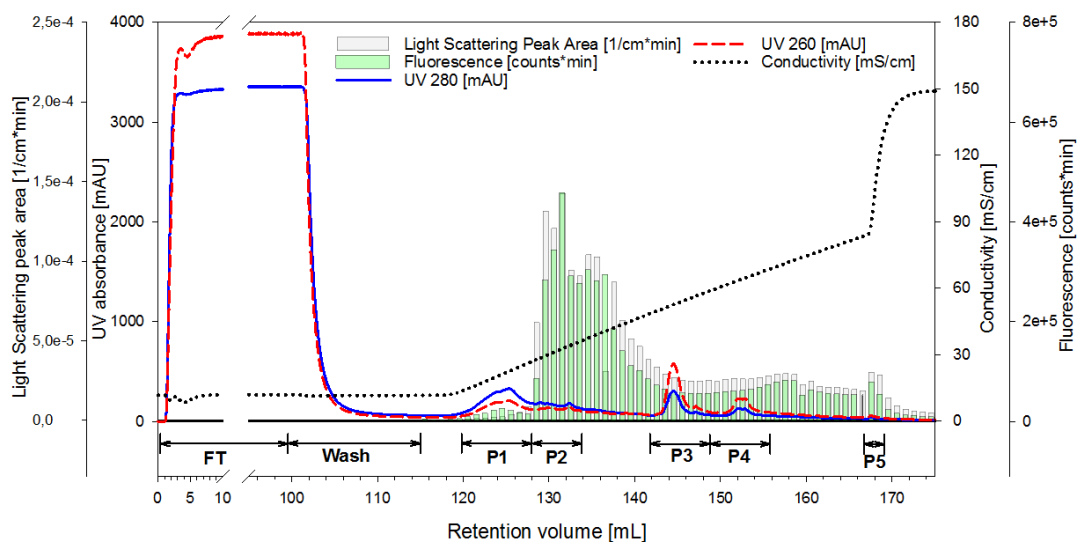


Figure 4-15: Linear gradient purification chromatogram of 100 mL HEK293 supernatant containing HIV-1 Gag-GFP VLPs. Column is a 1 mL QA monolith. The at-line MALS-FI measurements are displayed as overlay. Bars show the AUC of the light scattering (grey) and fluorescence (green) signal. Abbreviations: FT: flow-through; W: wash; P1-P5: pooled fractions for peaks 1–5 (adapted from [150]).

The chromatogram shows the course of the UV 280 and 260 signals and the linear salt gradient. For analytical purposes 5 distinctive peaks were pooled as indicated in the chromatogram (Figure 4-15). The course of the light scattering and fluorescence measurements show a strong signal increase between 130 – 142 mL retention volume (NaCl concentration 27 – 49 mS/cm) that flattens over the course of the elution. Literature states, that the light scattering intensity is directly proportional to the particle concentration [123], as the scattering intensity of particles is much higher than compared to proteins. This allows the conclusion that the majority of the VLPs elute in the range of 27 – 49 mS/cm, where the light scattering signal intensity is the highest. This is also in accordance with the fluorescence measurements, as the main structure protein HIV-1 gag of these VLPs was fused with an eGFP [169]. Further, the conclusion was made, that this method is not only able to identify the particle containing fractions but can also give a semi-quantitative prediction via the scattering intensity. When comparing the course of the UV signals (280 & 260 nm) with the course of the light scattering peak area and fluorescence intensities, it is striking that the UV signals do not give an accurate picture of the VLP elution. However, this at-line method allows for an accelerated process development, which surpasses the typical a major challenge during process- and analytical-development for bio-nanoparticles, as product titers are usually low in early development stages and recovery rates of particles are low.

Quantification of the total protein and dsDNA was achieved by Bradford and PicoGreen® assays respectively (Table 4-8). During the loading phase (0 – 100 mL retention volume) 43% of the protein left the column without binding and was pooled in the FT fraction. This can be explained by the relatively high conductivity of 11.8 mS/cm in the loading material. No protein could be detected in the wash fraction. At the start of the elution weakly bound protein is flushed from the column (P1). Similar results were observed when loading conditioned media, where non transfected cells were growing as a negative control (data not shown).

Table 4-8: Total protein and dsDNA mass balance for the HIV-1 Gag-GFP purification (Figure 4-15). Abbreviations: S: supernatant; L: loading material; FT: flow-through; W: wash; P1-P5: peaks 1-5 (adapted from [150]).

Sample	Volume [mL]	Total protein [µg/mL]	Total protein %	dsDNA [ng/mL]	dsDNA %
S	100	310.9	-	1387.5	-
L	100	313.1	100	1289.4	100
FT	100	134.9	43.1	37.5	2.9
W	15	< LLOQ	-	< LLOQ	-
P1	7	367.6	8.2	10.2	0.1
P2	5	275.1	4.4	310.5	1.2
P3	6	< LLOQ	-	51114.5	23.8
P4	6	< LLOQ	-	3129.6	14.6
P5	2	< LLOQ	-	1108.3	1.7
Recovery			55.7		44.3

< LLOQ: lower than lower limit of quantification

A different behavior can be observed with dsDNA binding. Here, only 3% of the initial DNA load was found in the FT fraction. The majority of the dsDNA was eluted at conductivities of 50 – 68 mS/cm in peaks 3 and 4 where only small amounts of proteins were found. This is also in accordance with the SDS-PAGE gel scans, where strong protein bands can be seen for the loading material, FT and Peaks 1 and 2 (Table 4-8 and Figure 4-16 A)).

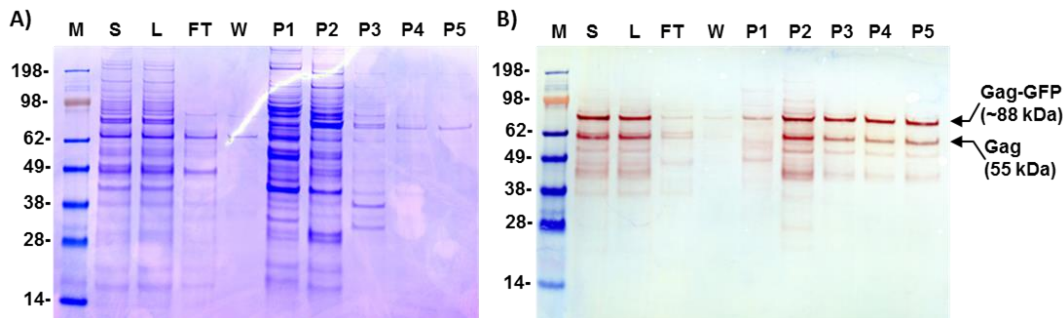


Figure 4-16: (A) SDS-PAGE and (B) Western blot scans of the HIV-Gag-GFP VLPs purification (Figure 4-15). Abbreviations: M: molecular weight marker; S: cell culture supernatant; L: loading material; FT: flow-through; W: wash; P1-P5: pooled fractions for peaks 1–5 (adapted from [150]).

To confirm the presence of the VLP matrix protein, a HIV-1 p24 western blot was implemented (Figure 4-16 B)). We observed a double band signal for the p24 WB. We concluded that the heavier p24 band accounts for the Gag-polyprotein fused with the eGFP at ~88 kDa, while the lighter p24 band is the assembled Gag with 55 kDa. Strong p24 signals for the gag protein (55 kDa) and the Gag-GFP (~88 kDa) can be seen for the supernatant and loading material. FT and wash did only show weak bands. Strong bands were found in the elution fractions. This WB confirmed the effective and strong binding of VLPs to the column (no VLPs in FT/W). This result is in accordance to the observations from the multi angle light scattering and fluorescence measurements, as the strongest p24 bands can be seen for P2. The MALS, fluorescence and WB measurements all indicate that the highest portion of the HIV-1 Gag-GFP VLPs elute in peak 2.

In comparison to the cell culture loading material (L) peak 2 shows a depletion of approx. 96% of the total protein and 99% of the total dsDNA. P3 and P4 still contain a high VLP load, but in that gradient region the dsDNA starts to co-elute, which accounts for ~24% and ~16% of the total dsDNA load. The co-elution of dsDNA and enveloped VLPs when working with anion exchange chromatography is known in the literature [30].

It can be summarized, that the at-line measurement of the light scattering and fluorescence signal allowed for a fast identification of the product fraction in the linear gradient and permits a fast transition to a step gradient elution.

4.2.2 Step Gradient Purification of HIV-1 Gag-GFP VLPs

As described earlier the step gradient elution profile was developed on the base of the results obtained from the linear gradient purification and the newly implemented at-line MALS-FI measurement. All factors like loading material preparation, column and buffer conditions (Equilibration, loading and regeneration) were kept constant. The step gradient elution was designed to maximize the recovery of the VLPs. From the linear gradient experiments we knew that the VLPs elute in the range of 27 – 49 mS/cm. In terms of purity we wanted to separate the VLPs from small protein and dsDNA impurities. This led to a step gradient with three plateaus of 15 CV each at 300, 520, and 1000 mS/cm (~15 – 26 – 50% B) that corresponds to 30, 49 and 86 mS/cm. For analytical characterization the fractions were pooled as indicated in the chromatogram (Figure 4-17).

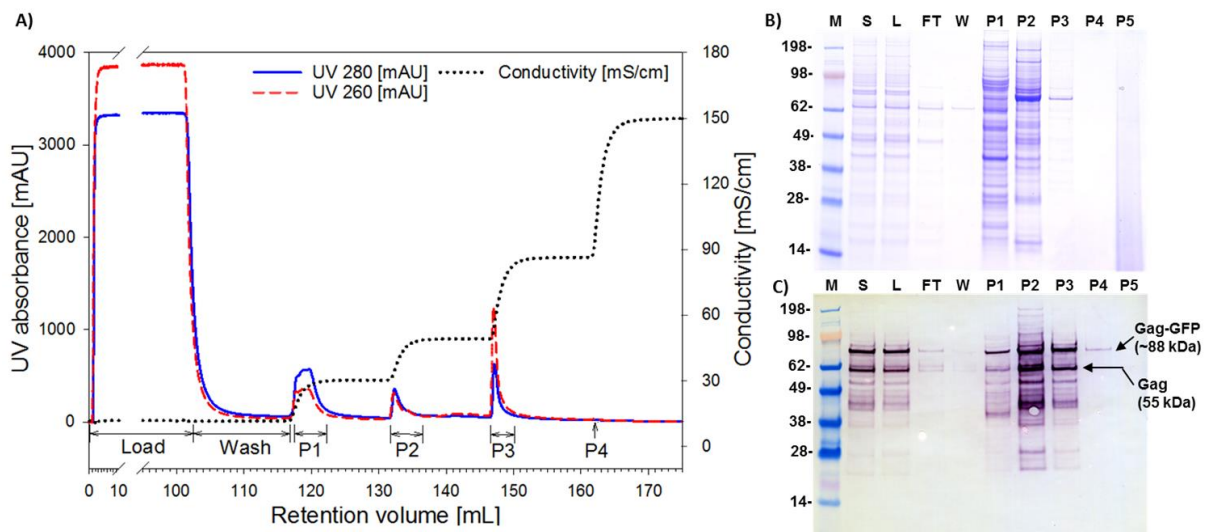


Figure 4-17: Chromatogram of the step gradient purification of HIV-1 Gag-GFP VLP using a QA monolith. The loading material was 100 mL of clarified and 0.8 μ m filtered HEK 293 cell culture supernatant. FT: flow-through; W: wash; P1-P4: pooled fractions for peaks 1–4 (adapted from [150]).

The chromatogram shows three distinctive peaks in the UV 280 and 260 nm signals. The fourth peak is difficult to see in Figure 4-17 A). The protein and dsDNA amounts were measured by Bradford and PicoGreen® assays (Table 4-9). SDS-Page gel scans are used for the visualization of protein distribution. The presence of the gag-protein was shown using a WB targeting the p24 protein building block (Figure 4-17 B and C). Further, TEM pictures were taken of the loading material, P2 and P3 (Figure 4-18). Additionally the pooled peaks were analyzed by NTA. Here, particle quantification and particle size distribution were measured in fluorescence and light scattering mode (Table 4-10).

In the FT fraction ~43% of the total protein was found, which passed the column without binding. These non-binding conditions for small proteins in the anion-exchange column are induced by the high conductivity in the cell culture supernatant (11.8 mS/cm). Lightly bound proteins were flushed from the column during the washing step (2.1%), or eluted in P1 at 30 mS/cm (~300 mM NaCl), which corresponds to 10.5% of the total protein load in regard to the loading material. The majority of dsDNA was eluted in P3 with 85.4% of the total dsDNA in regard to the loading material. In contrast

to the linear gradient purification a higher amount of dsDNA could be found in the FT and W fraction (8.8 and 21.6%).

The presence of the p24 was confirmed in peaks 1 – 3. However, only a very small amount of particles could be attributed to P1 (3-5%). This was measured by NTA in scattering and fluorescence mode. This is a first hint of the presence of fragmented VLP fragments, which is most likely to an incorrect assembly process.

Table 4-9: Total protein and dsDNA analysis of the HIV-1 Gag-GFP VLPs purification using a step gradient elution (Figure 4-17). Abbreviations: L: loading material; FT: flow-through; W: wash; P1-P4: peaks 1-4; CIP: cleaning-in-place (adapted from [150]).

Sample	Volume [mL]	Total protein [$\mu\text{g/mL}$]	Total protein %	dsDNA [ng/mL]	dsDNA %
L	100	297.8	100	448.0	100
FT	100	126.7	42.5	39.2	8.8
W	15	41.0	2.1	645.5	21.6
P1	5	632.2	10.6	91.5	1.0
P2	3	510.3	5.1	975.4	6.5
P3	3	62.4	0.6	12747.8	85.4
P4	1	< LLOQ	-	691.6	1.5
CIP	15	456.8	23.0	< LLOQ	-
Recovery			83.9		124.8

< LLOQ: lower than lower limit of quantification

The NTA did further confirm the effective binding of the VLPs, as no particles could be found in the W and FT fraction. As designed by the step gradient elution the majority of particles were found in peak 2 (17-50%), the main product fraction in the expected size range of 100 – 200 nm. The presence of the Gag-GFP fusion protein was demonstrated in the Western blot analysis. Only ~14% of the total fluorescent particles were found in P3, where 85% of the dsDNA eluted from the column.

Table 4-10: Summary of the NTA fraction analytics for particles in the diameter range: 100–200 nm. Abbreviations: L: loading material; FT: flow-through; W: wash; P1-P4: peaks 1-4; CIP: cleaning-in-place (adapted from [150]).

Sample	Volume [mL]	Particles (NTA) ^a d: 100 – 200 nm [particles/mL]	Particles (NTA) ^a d: 100 – 200 nm %	Particles (NTA) ^b d: 100– 200 nm [particles/mL]	Particles (NTA) ^b d: 100 – 200 nm %
L	100	2.4×10^{10}	100	2.7×10^9	100
FT	100	< LLOQ	-	< LLOQ	-
W	15	< LLOQ	-	< LLOQ	-
P1	5	2.2×10^{10}	4.5	1.5×10^9	2.8
P2	3	1.3×10^{11}	16.5	4.5×10^{10}	49.9
P3	3	2.7×10^{10}	3.3	1.2×10^{10}	13.6
P4	1	5.0×10^9	0.2	< LLOQ	-
CIP	15	n.d.	-	n.d.	-
Recovery			24.5		66.3

a: measured in light scattering mode, b: measured in fluorescence mode, < LLOQ: lower than lower limit of quantification, n.d.: not determined

The next analytical tool was the TEM. Here the loading material (L), P2 and P3 were analyzed for correctly assembled spherical structures. In Figure 4-18 we see spherical structures with a darker colored core surrounded by another darker ring. The outer ring matches the expected thickness of the lipid bilayer plus the inner layer of gag-polyprotein that functions as the VLP envelope. The dark core represents the hollow sphere, as the coloring agent (uranyl acetate) of the sample preparation enriches in the void areas of the spherical structure, which results in a darker contrast in the microscope picture.

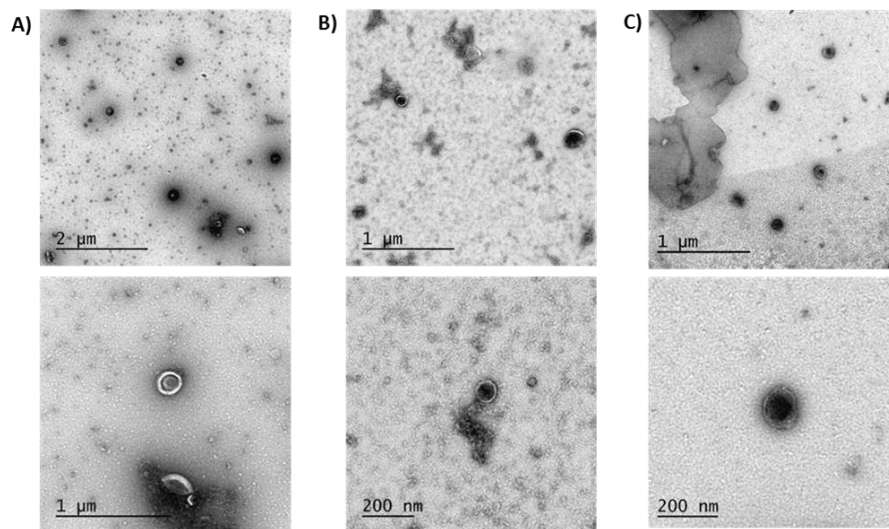


Figure 4-18: Electron microscopy micrographs of A) loading material (L) and pooled peaks B) P2 and C) P3 from step gradient purification (Figure 4-18 A) (adapted from [150]).

By this point the product fraction P2 was depleted of 94% of the dsDNA contamination and approx. 95% of the total protein in regard to the loading material. The presence of the p24 was confirmed by the WB analysis and the spherical structure and correct size were determined by NTA and TEM.

As an in-depth analysis SEC-MALS-FI was conducted of the peaks 1 – 4 of the step gradient elution ((Figure 4-19 A) – D)). Due to the pore size of 100 nm of the SEC column, it is able to separate correctly assembled HIV-1 Gag-GFP VLPs from small proteins like free Gag-GFP complexes or even VLP fragments smaller than the column pore size. The correctly assembled VLPs will elute in the void fraction of the column, while smaller compounds will interact with the column pores and will elute with a delay that is indirectly proportional to the compound size. The benefit of this method is to be able to distinguish the sample components between correctly assembled fluorescent VLPs and the smaller building components like, Gag-GFP or particle fragments, that would still be identified in the WB as VLP. The VLP standard (100 – 200 nm) were HIV-1 gag VLPs produced and purified as described by Steppert et al. [30]. The reference for free, unbound protein was a GFP standard (27 kDa). As expected the VLP standard eluted after approx. 20 min within the void volume of the respective SEC column. The GFP standard eluted after 35 min post injection (Data not shown).

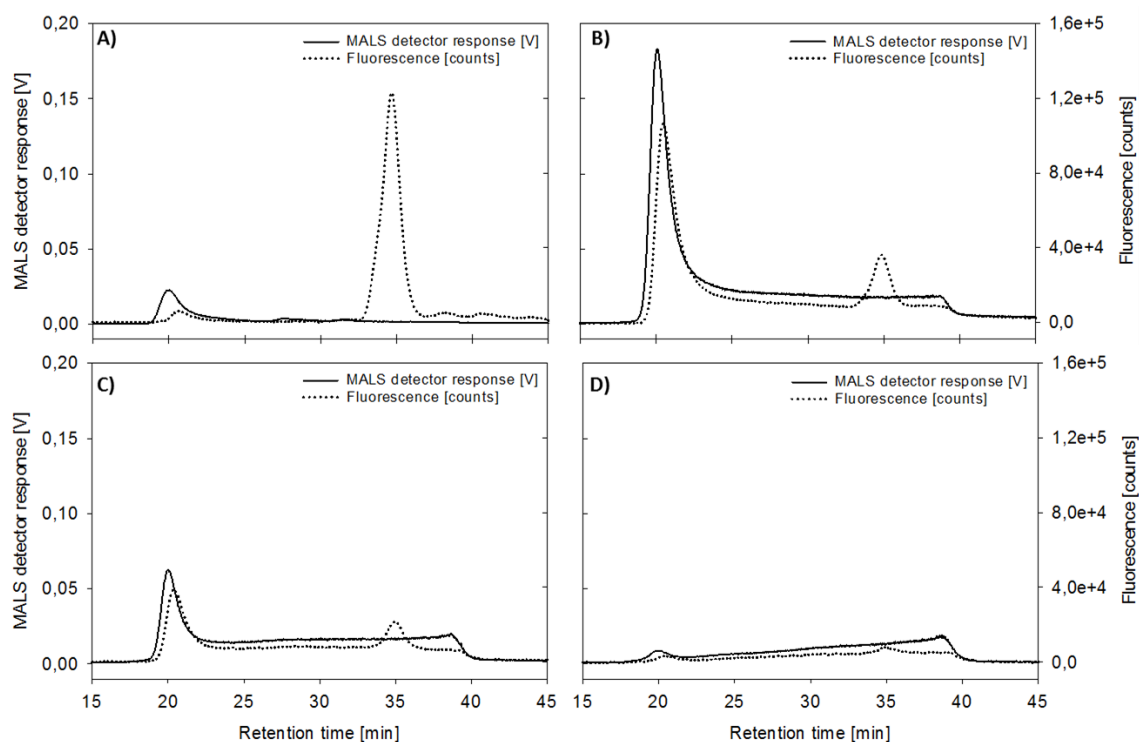


Figure 4-19: Analytical SEC of the pooled peaks P1-P4 of the step gradient purification (Figure 4-17 A). Shown are the overlays of the MALS and fluorescence detector signals (SEC-MALS-FL). A) P1; B) P2; C) P3; D) P4 (adapted from [150]).

The P1 showed only a minor light scattering peak at the 20 min mark and a very small fluorescence peak, where VLPs are expected to elute. However, a significant fluorescence peak can be seen at 35 min retention time, which confirms the presence of free Gag-GFP protein in P1. This result confirms the observation from the Western blot analysis, where the presence of incorrect assembled or fragmented VLPs along with Gag-GFP containing protein aggregates were suspected. P2 shows a mirrored picture (Figure 4-19 B)). Here we see a very high light scattering and fluorescence signal at the VLP elution time (20 min) while the 35 min peak only shows a fluorescence signal. This indicates that this sample still contains small amounts of product related impurities, like Gag-GFP, which co-eluted with the HIV-1 Gag-GFP VLPs. The same pattern can be seen in P3 (Figure 4-19 C)). This is somewhat expected, since the analytical array also confirmed the presence of fluorescent VLPs in this sample. However the intensity of the signals is significantly lower, which can be explained by the lower particle load in this peak confirmed by NTA (Table 4-10).

Further the geometric radii of the particles eluted in P2 and P3 were calculated from the MALS data. This calculation is based on the Rayleigh-Gans-Debye approximation. In P2 the geometric radius was calculated for the VLPs to 70 nm (= 140 nm diameter) and P3 69 nm (= 138 nm diameter). These results correspond well with the particle size calculated by the NTA (Table 4-10). Here, the hydrodynamic radius is calculated using the Stokes-Einstein equation and the diffusion constant. The hydrodynamic radii were calculated to 126 nm and 140 nm for peak 2 and peak 3 respectively.

We can conclude that the SEC-MALS-FL method confirmed the functionality and validity of the at-line measurement method as a valuable and robust analytical tool for DSP of bio-nanoparticles.

5 Summary and Conclusion

The Elution behavior of different expression levels of the BEVS (conditioned media, virus expression and VLP expression) was investigated with a linear gradient on a monolith AEX-column using MALS, WBs and total host cell protein and DNA assays. A new concept for MALS raw data analysis was developed, where the raw light scattering signal was used to calculate the fractal dimensions of the eluting fractions. This allowed a differentiation of the eluting particles. The fractal dimensions indicated a clear tendency from spherical shaped structures to elongated bodies during the course of elution. This finding is also in accordance with the results from other analytical methods like NTA, SDS and WBs.

Further, a purification protocol for the HIV-1 gag H1 VLPs produced with Tnms42 cells was developed. Here, a classical approach of process development was used. In the first instance a linear salt gradient protocol was developed where the whole range of available fraction analytics (Bradford assay for total protein, PicoGreen® for total dsDNA, SDS-PAGE and Western Blots to verify the presence and successful expression of specific indicator proteins (HIV-1 gag p24, haemagglutinin H1, gp64 and vp39), NTA for particle concentration, particle size and particle size distribution, SAXS for particle morphology and transmission electron microscopy for particle identification) was used. After identification of the critical process parameters and identifying the eluting species the protocol was then adapted to an easily scalable salt step gradient elution separating the VLP and Virus fraction to the best of the column's abilities. The chosen salt steps were developed as following: column equilibration with 6% B followed by elution with steps of 18 – 30 – 37 50% B for 15 CV each. The process uses simple buffer media (Media A: 50 mM HEPES, pH 7.2 for equilibration and media B: 50 mM HEPES, 2 M NaCl, pH 7.2 for elution). Due to the flow rate independent resolution of monolithic chromatography material, high flow rates of 1 CV/min could be used. With the accumulated data product peaks were characterized. The key process parameters are given at the end of this chapter.

Additionally, a purification protocol for fluorescent HIV-1 gag-gfp VLPs produced in a HEK293 cell line was developed. In parallel to the process development, a novel at-line particle monitoring method was developed. Furthermore, a MALS-FI method for the detection of the fluorescent VLPs was established to accelerate process development significantly. In the beginning a linear gradient purification protocol was developed, where the elution fractions were directly analyzed by a combination of MALS and fluorescence, resulting in a novel particle-monitoring method. This method allowed for a direct particle tracking during the elution and made a very fast transition to a scalable step gradient possible. The final purification protocol for the HIV-1 gag-gfp particles used the following steps: Equilibration with 6% B and elution with 15 – 26 – 50 – 100% B for 15 CV each. The product peaks were characterized using the process analytics mentioned earlier in this chapter. The summarized key process parameters are given in the concluding remarks at the end of this chapter.

The following conclusions can be made:

- Two fast, simple and easily scalable purification procedures for HIV-1 gag VLPs produced in BEVS and HEK293 cell cultures were developed:
 1. Purification of HIV-1 gag H1 VLPs expressed in BEVS:
 - Majority of host cell protein and DNA depleted
 - Presence of HIV-1 gag and H1 proteins confirmed by WB
 - 2.4 log reduction of BV in VLP Peak according to TCID₅₀
 - Presence of particles confirmed by TEM & NTA
 - Two subclasses of BV identified: early and late-eluting BV with different sizes (P2 & P4)
 - 450 vaccination doses (at 1 x 10⁹ particles/mL) and <6 ng/mL host cell DNA could be produced from 100 mL cell culture supernatant and per mL column material
 2. Purification of HIV-1 gag-gfp VLPs expressed in HEK293:
 - Majority of host cell protein and DNA depleted
 - Presence of HIV-1 gag protein confirmed by WB
 - Presence of fluorescent particles confirmed by NTA & SEC-FL-MALS
 - High particle recovery (>66%) and high product yield (~50%)
 - Fast and simple at-line process analytics developed for in-process control and accelerated process development
 - 390 vaccination doses (at 1 x 10⁹ particles/mL) and <8 ng/mL host cell DNA could be produced from 100 mL cell culture supernatant and per mL column material
- An at-line fraction analysis method for particles using MALS was developed and successfully deployed as a valuable addition for in-process control and greatly accelerated the purification process development for eVLPs.
- An SEC-MALS-FL method was established to analyze and characterize the fluorescent HIV-gag-gfp VLPs during the process development.
- Two conceptual approaches for MALS raw data analysis were developed and used for particle characterization. The calculation of the fractal dimensions gave valuable insights in particle morphology and could be deployed as an in-time fraction analysis tool to characterize particle morphologies during elution.

6 References

- [1] E. Jenner, *The origin of the vaccine inoculation*. DN Shury, 1801.
- [2] N. J. Willis, "Edward Jenner and the Eradication of Smallpox," *Scott. Med. J.*, vol. 42, no. 4, pp. 118–121, Aug. 1997, doi: 10.1177/003693309704200407.
- [3] H. Bazin and E. Jenner, *The eradication of smallpox*. Elsevier, 2000.
- [4] H. Bazin, "Pasteur and the birth of vaccines made in the laboratory," in *History of Vaccine Development*, Springer, 2011, pp. 33–45.
- [5] D. H. M. Groschel, R. B. Hornick, D. H. M. Gröschel, and R. B. Hornick, "Who Introduced Typhoid Vaccination: Almroth Wright or Richard Pfeiffer?," *Rev. Infect. Dis.*, vol. 3, no. 6, pp. 1251–1254, 1981, doi: 10.1093/clinids/3.6.1251.
- [6] A. F. Rodrigues, H. R. Soares, M. R. Guerreiro, P. M. Alves, and A. S. Coroadinha, "Viral vaccines and their manufacturing cell substrates: New trends and designs in modern vaccinology," *Biotechnol. J.*, vol. 10, no. 9, pp. 1329–1344, 2015, doi: 10.1002/biot.201400387.
- [7] F. J. Grundbacher, "Behring's discovery of diphtheria and tetanus antitoxins," *Immunol. Today*, vol. 13, no. 5, pp. 188–190, 1992, doi: 10.1016/0167-5699(92)90125-Q.
- [8] E. C. Gotschlich, I. Goldschneider, and M. S. Artenstein, "Human immunity to the meningococcus: V. The effect of immunization with meningococcal group C polysaccharide on the carrier state," *J. Exp. Med.*, vol. 129, no. 6, pp. 1385–1395, 1969.
- [9] D. G. Kleid *et al.*, "Cloned viral protein vaccine for foot-and-mouth disease: responses in cattle and swine," *Science (80-.)*, vol. 214, no. 4525, pp. 1125–1129, 1981.
- [10] C. J. Burrell, P. Mackay, P. J. Greenaway, P. H. Hofschneider, and K. Murray, "Expression in *Escherichia coli* of hepatitis B virus DNA sequences cloned in plasmid pBR322," *Nature*, vol. 279, no. 5708, p. 43, 1979.
- [11] F. Galibert, E. Mandart, F. Fitoussi, P. Tiollais, and P. Charnay, "Nucleotide sequence of the hepatitis B virus genome (subtype ayw) cloned in *E. coli*," *Nature*, vol. 281, no. 5733, p. 646, 1979.
- [12] P. Charnay, E. Mandart, A. Hampe, F. Fitoussi, P. Tiollais, and F. Galibert, "Localization on the viral genome and nucleotide sequence of the gene coding for the two major polypeptides of the hepatitis B surface antigen (HBs Ag)," *Nucleic Acids Res.*, vol. 7, no. 2, pp. 335–346, 1979.
- [13] B. Akgül, J. C. Cooke, and A. Storey, "HPV-associated skin disease," *J. Pathol. A J. Pathol. Soc. Gt. Britain Irel.*, vol. 208, no. 2, pp. 165–175, 2006.
- [14] L. H. L. Lua, N. K. Connors, F. Sainsbury, Y. P. Chuan, N. Wibowo, and A. P. J. Middelberg, "Bioengineering virus-like particles as vaccines," *Biotechnol. Bioeng.*, vol. 111, no. 3, pp. 425–440, Mar. 2014, doi: 10.1002/bit.25159.
- [15] L. A. Lee and Q. Wang, "Adaptations of nanoscale viruses and other protein cages for medical applications," *Nanomedicine Nanotechnology, Biol. Med.*, vol. 2, no. 3, pp. 137–149, Sep. 2006, doi: 10.1016/J.NANO.2006.07.009.
- [16] M. O. Mohsen, L. Zha, G. Cabral-Miranda, and M. F. Bachmann, "Major findings and recent advances in virus-like particle (VLP)-based vaccines," *Semin. Immunol.*, vol. 34, pp. 123–132,

- 2017, doi: 10.1016/j.smim.2017.08.014.
- [17] J. Fuenmayor, F. Gòdia, and L. Cervera, "Production of virus-like particles for vaccines," *N. Biotechnol.*, vol. 39, pp. 174–180, 2017, doi: 10.1016/j.nbt.2017.07.010.
- [18] A. Roldão, R. Leda, and M. Jt, "Virus-like particles in vaccine development. - PubMed - NCBI," vol. 9, no. 10, pp. 1149–1176, 2010.
- [19] C. N. Chao *et al.*, "Gene therapy for human glioblastoma using neurotropic JC virus-like particles as a gene delivery vector," *Sci. Rep.*, vol. 8, no. 1, pp. 1–11, 2018, doi: 10.1038/s41598-018-19825-w.
- [20] G. van Niel, G. D'Angelo, and G. Raposo, "Shedding light on the cell biology of extracellular vesicles," *Nat. Rev. Mol. Cell Biol.*, vol. 19, no. 4, p. 213, Jan. 2018, doi: 10.1038/nrm.2017.125.
- [21] M. F. Bachmann and P. Whitehead, "Active immunotherapy for chronic diseases," *Vaccine*, vol. 31, no. 14, pp. 1777–1784, 2013.
- [22] M. Zochowska *et al.*, "Virus-like particle-mediated intracellular delivery of mRNA cap analog with in vivo activity against hepatocellular carcinoma," *Nanomedicine Nanotechnology, Biol. Med.*, vol. 11, no. 1, pp. 67–76, 2015.
- [23] A. M. Q. King, E. Lefkowitz, M. J. Adams, and E. B. Carstens, *Virus taxonomy: ninth report of the International Committee on Taxonomy of Viruses*, vol. 9. Elsevier, 2011.
- [24] N. L. Goicochea, S. A. K. Datta, M. Ayaluru, C. Kao, A. Rein, and B. Dragnea, "Structure and stoichiometry of template-directed recombinant HIV-1 Gag particles," *J. Mol. Biol.*, vol. 410, no. 4, pp. 667–680, 2011.
- [25] M. Delchambre *et al.*, "The GAG precursor of simian immunodeficiency virus assembles into virus-like particles.," *EMBO J.*, vol. 8, no. 9, pp. 2653–2660, 1989.
- [26] V. Karacostas, K. Nagashima, M. A. Gonda, and B. Moss, "Human immunodeficiency virus-like particles produced by a vaccinia virus expression vector," *Proc. Natl. Acad. Sci.*, vol. 86, no. 22, pp. 8964–8967, 1989.
- [27] R. Wagner *et al.*, "Studies on processing, particle formation, and immunogenicity of the HIV-1gag gene product: a possible component of a HIV vaccine," *Arch. Virol.*, vol. 127, no. 1–4, pp. 117–137, 1992.
- [28] K. Mergener, M. Fäcke, R. Welker, V. Brinkmann, H. R. Gelderblom, and H.-G. Krüsslich, "Analysis of HIV particle formation using transient expression of subviral constructs in mammalian cells," *Virology*, vol. 186, no. 1, pp. 25–39, 1992.
- [29] J. W. Wills, R. C. Craven, and J. A. Achacoso, "Creation and expression of myristylated forms of Rous sarcoma virus gag protein in mammalian cells.," *J. Virol.*, vol. 63, no. 10, pp. 4331–4343, 1989.
- [30] P. Steppert *et al.*, "Separation of HIV-1 gag virus-like particles from vesicular particles impurities by hydroxyl-functionalized monoliths," *J. Sep. Sci.*, vol. 40, no. 4, pp. 979–990, 2017, doi: 10.1002/jssc.201600765.
- [31] L. Cervera, S. Gutiérrez-Granados, M. Martínez, J. Blanco, F. Gòdia, and M. M. Segura, "Generation of HIV-1 Gag VLPs by transient transfection of HEK 293 suspension cell cultures using an optimized animal-derived component free medium," *J. Biotechnol.*, vol. 166, no. 4,

- pp. 152–165, 2013, doi: 10.1016/j.jbiotec.2013.05.001.
- [32] A. Diamantis, E. Magiorkinis, G. H. Sakorafas, and G. Androutsos, “A brief history of apoptosis: from ancient to modern times,” *Oncol. Res. Treat.*, vol. 31, no. 12, pp. 702–706, 2008.
- [33] R. L. K. Virchow, *Cellular pathology: as based upon physiological and pathological histology. Twenty lectures delivered in the Pathological institute of Berlin during the months of February, March and April, 1858*. RM De Witt, 1860.
- [34] B. Alberts *et al.*, *Essential cell biology*. Garland Science, 2013.
- [35] M. Yáñez-Mó *et al.*, “Biological properties of extracellular vesicles and their physiological functions,” *J. Extracell. vesicles*, vol. 4, no. 1, p. 27066, 2015.
- [36] P. Wolf, “The nature and significance of platelet products in human plasma,” *Br. J. Haematol.*, vol. 13, no. 3, pp. 269–288, 1967.
- [37] S. J. Gould and G. Raposo, “As we wait: coping with an imperfect nomenclature for extracellular vesicles,” *J. Extracell. vesicles*, vol. 2, p. 10.3402/jev.v2i0.20389, Feb. 2013, doi: 10.3402/jev.v2i0.20389.
- [38] E. van der Pol, A. N. Böing, E. L. Gool, and R. Nieuwland, “Recent developments in the nomenclature, presence, isolation, detection and clinical impact of extracellular vesicles,” *J. Thromb. Haemost.*, vol. 14, no. 1, pp. 48–56, 2016, doi: 10.1111/jth.13190.
- [39] A. Arakelyan, W. Fitzgerald, S. Zicari, C. Vanpouille, and L. Margolis, “Extracellular vesicles carry HIV Env and facilitate HIV infection of human lymphoid tissue,” *Sci. Rep.*, vol. 7, no. 1, p. 1695, Dec. 2017, doi: 10.1038/s41598-017-01739-8.
- [40] P. Gluschankof, I. Mondor, H. R. Gelderblom, and Q. J. Sattentau, “Cell Membrane Vesicles Are a Major Contaminant of Gradient-Enriched Human Immunodeficiency Virus Type-1 Preparations,” *Virology*, vol. 230, no. 1, pp. 125–133, Mar. 1997, doi: 10.1006/viro.1997.8453.
- [41] S. Welsch, B. Müller, and H.-G. Kräusslich, “More than one door - Budding of enveloped viruses through cellular membranes,” *FEBS Lett.*, vol. 581, no. 11, pp. 2089–2097, May 2007, doi: 10.1016/j.febslet.2007.03.060.
- [42] J. W. Bess, R. J. Gorelick, W. J. Bosche, L. E. Henderson, and L. O. Arthur, “Microvesicles Are a Source of Contaminating Cellular Proteins Found in Purified HIV-1 Preparations,” *Virology*, vol. 230, no. 1, pp. 134–144, Mar. 1997, doi: 10.1006/VIRO.1997.8499.
- [43] F. T. T. Borges, L. A. A. Reis, N. Schor, F. T. T. Borges, L. A. A. Reis, and N. Schor, “Extracellular vesicles: Structure, function, and potential clinical uses in renal diseases,” *Brazilian J. Med. Biol. Res.*, vol. 46, no. 10, pp. 824–830, Oct. 2013, doi: 10.1590/1414-431X20132964.
- [44] L. T. Brinton, H. S. Sloane, M. Kester, and K. A. Kelly, “Formation and role of exosomes in cancer,” *Cell. Mol. Life Sci.*, vol. 72, no. 4, pp. 659–671, Feb. 2015, doi: 10.1007/s00018-014-1764-3.
- [45] E. N.-t Hoen *et al.*, “Extracellular vesicles and viruses: Are they close relatives?,” *Proc. Natl. Acad. Sci.*, vol. 113, no. 33, pp. 9155–9161, Aug. 2016, doi: 10.1073/PNAS.1605146113.
- [46] J. J. Wang, R. Horton, V. Varthakavi, P. Spearman, and L. Ratner, “Formation and release of virus-like particles by HIV-1 matrix protein,” *AIDS*, vol. 13, no. 2, pp. 281–3, Feb. 1999.
- [47] R. S. Felberbaum, “The baculovirus expression vector system: A commercial manufacturing

- platform for viral vaccines and gene therapy vectors," *Biotechnol. J.*, vol. 10, no. 5, pp. 702–714, 2015, doi: 10.1002/biot.201400438.
- [48] F. Liu, X. Wu, L. Li, Z. Liu, and Z. Wang, "Use of baculovirus expression system for generation of virus-like particles: successes and challenges," *Protein Expr. Purif.*, vol. 90, no. 2, pp. 104–116, 2013.
- [49] N. Pelucchi *et al.*, "Production of recombinant HIV-1/HBV virus-like particles in *Nicotiana tabacum* and *Arabidopsis thaliana* plants for a bivalent plant-based vaccine," *Vaccine*, vol. 25, no. 49, pp. 8228–8240, 2007, doi: 10.1016/j.vaccine.2007.09.061.
- [50] Q. Chen and K. R. Davis, "The potential of plants as a system for the development and production of human biologics," *F1000Research*, vol. 5, no. 0, pp. 1–8, 2016.
- [51] J. Zhu, "Mammalian cell protein expression for biopharmaceutical production," *Biotechnol. Adv.*, vol. 30, no. 5, pp. 1158–1170, 2012, doi: 10.1016/j.biotechadv.2011.08.022.
- [52] M. G. Masavuli, D. K. Wijesundara, J. Torresi, E. J. Gowans, and B. Grubor-Bauk, "Preclinical development and production of virus-like particles as vaccine candidates for hepatitis C," *Front. Microbiol.*, vol. 8, no. DEC, pp. 1–11, 2017, doi: 10.3389/fmicb.2017.02413.
- [53] D. J. Hwang, I. M. Roberts, and T. M. Wilson, "Expression of tobacco mosaic virus coat protein and assembly of pseudovirus particles in *Escherichia coli*," *Proc. Natl. Acad. Sci.*, vol. 91, no. 19, pp. 9067–9071, 2006, doi: 10.1073/pnas.91.19.9067.
- [54] M. Tan, W. Zhong, D. Song, S. Thornton, and X. Jiang, "E. coli-expressed recombinant norovirus capsid proteins maintain authentic antigenicity and receptor binding capability," *J. Med. Virol.*, vol. 74, no. 4, pp. 641–649, 2004, doi: 10.1002/jmv.20228.
- [55] P. Valenzuela, A. Medina, W. J. Rutter, G. Ammerer, and B. D. Hall, "Synthesis and assembly of hepatitis B virus surface antigen particles in yeast," *Nature*, vol. 298, no. 5872, pp. 347–350, 1982, doi: 10.1038/298347a0.
- [56] K. J. Hofmann *et al.*, "Sequence determination of human papillomavirus type 6a and assembly of virus-like particles in *Saccharomyces cerevisiae*," *Virology*, vol. 209, no. 2, pp. 506–518, 1995.
- [57] J. K. C. Ma, P. M. W. Drake, and P. Christou, "The production of recombinant pharmaceutical proteins in plants," *Nat. Rev. Genet.*, vol. 4, no. 10, pp. 794–805, 2003, doi: 10.1038/nrg1177.
- [58] F. M. Wurm, "Production of recombinant protein therapeutics in cultivated mammalian cells," *Nat. Biotechnol.*, vol. 22, p. 1393, Nov. 2004.
- [59] K. P. Jayapal, K. F. Wlaschin, W. Hu, and M. G. S. Yap, "Recombinant protein therapeutics from CHO cells-20 years and counting," *Chem. Eng. Prog.*, vol. 103, no. 10, p. 40, 2007.
- [60] C. Li *et al.*, "Hantavirus-like particles generated in CHO cells induce specific immune responses in C57BL/6 mice," *Vaccine*, vol. 28, no. 26, pp. 4294–4300, 2010, doi: 10.1016/j.vaccine.2010.04.025.
- [61] P. Steppert *et al.*, "Purification of HIV-1 gag virus-like particles and separation of other extracellular particles," *J. Chromatogr. A*, vol. 1455, pp. 93–101, 2016, doi: 10.1016/j.chroma.2016.05.053.
- [62] G. W. Holzer *et al.*, "Overexpression of hepatitis B virus surface antigens including the preS1 region in a serum-free Chinese hamster ovary cell line," *Protein Expr. Purif.*, vol. 29, no. 1, pp.

- 58–69, 2003, doi: 10.1016/S1046-5928(03)00011-1.
- [63] E. Beaumont, R. Patient, C. Hourieux, I. Dimier-Poisson, and P. Roingard, “Chimeric hepatitis B virus/hepatitis C virus envelope proteins elicit broadly neutralizing antibodies and constitute a potential bivalent prophylactic vaccine,” *Hepatology*, vol. 57, no. 4, pp. 1303–1313, 2013, doi: 10.1002/hep.26132.
- [64] D. Fontana, R. Kratje, M. Etcheverrigaray, and C. Prieto, “Immunogenic virus-like particles continuously expressed in mammalian cells as a veterinary rabies vaccine candidate,” *Vaccine*, vol. 33, no. 35, pp. 4238–4246, 2015, doi: 10.1016/j.vaccine.2015.03.088.
- [65] C. M. Thompson, E. Petiot, A. Lennaertz, O. Henry, and A. A. Kamen, “Analytical technologies for influenza virus-like particle candidate vaccines: Challenges and emerging approaches,” *Viol. J.*, vol. 10, no. November 2012, 2013, doi: 10.1186/1743-422X-10-141.
- [66] G. E. Smith, M. D. Summers, and M. J. Fraser, “Production of human beta interferon in insect cells infected with a baculovirus expression vector.,” *Mol. Cell. Biol.*, vol. 3, no. 12, pp. 2156–2165, 1983.
- [67] J. A. Mena and A. A. Kamen, “Insect cell technology is a versatile and robust vaccine manufacturing platform,” *Expert Rev. Vaccines*, vol. 10, no. 7, pp. 1063–1081, 2011, doi: 10.1586/erv.11.24.
- [68] L. Buonaguro *et al.*, “Baculovirus-Derived Human Immunodeficiency Virus Type 1 Virus-Like Particles Activate Dendritic Cells and Induce Ex Vivo T-Cell Responses,” *J. Virol.*, vol. 80, no. 18, pp. 9134–9143, 2006, doi: 10.1128/jvi.00050-06.
- [69] S. W. Metz *et al.*, “Effective Chikungunya Virus-like Particle Vaccine Produced in Insect Cells,” *PLoS Negl. Trop. Dis.*, vol. 7, no. 3, 2013, doi: 10.1371/journal.pntd.0002124.
- [70] L. Maranga, T. F. Brazao, and M. J. T. Carrondo, “Virus-like particle production at low multiplicities of infection with the baculovirus insect cell system,” *Biotechnol. Bioeng.*, vol. 84, no. 2, pp. 245–253, 2003, doi: 10.1002/bit.10773.
- [71] C. M. Thompson, E. Petiot, A. Mullick, M. G. Aucoin, O. Henry, and A. A. Kamen, “Critical assessment of influenza VLP production in Sf9 and HEK293 expression systems,” *BMC Biotechnol.*, vol. 15, no. 1, 2015, doi: 10.1186/s12896-015-0152-x.
- [72] M. M. Van Oers, G. P. Pijlman, and J. M. Vlak, *Thirty years of baculovirus-insect cell protein expression: From dark horse to mainstream technology*, vol. 96, no. 1. 2015.
- [73] C. L. Effio and J. Hubbuch, “Next generation vaccines and vectors: Designing downstream processes for recombinant protein-based virus-like particles,” *Biotechnol. J.*, vol. 10, no. 5, pp. 715–727, 2015, doi: 10.1002/biot.201400392.
- [74] L. K. Pattenden, A. P. J. Middelberg, M. Niebert, and D. I. Lipin, “Towards the preparative and large-scale precision manufacture of virus-like particles,” *Trends Biotechnol.*, vol. 23, no. 10, pp. 523–529, 2005, doi: 10.1016/j.tibtech.2005.07.011.
- [75] K. Reiter, P. P. Aguilar, V. Wetter, P. Steppert, A. Tover, and A. Jungbauer, “Separation of virus-like particles and extracellular vesicles by flow-through and heparin affinity chromatography,” *J. Chromatogr. A*, 2018.
- [76] P. Nestola, C. Peixoto, R. R. J. S. J. S. Silva, P. M. Alves, J. P. B. B. Mota, and M. J. T. T. Carrondo, “Improved virus purification processes for vaccines and gene therapy,” *Biotechnol. Bioeng.*, vol. 112, no. 5, pp. 843–857, 2015, doi: 10.1002/bit.25545.

- [77] M. W. Wolf and U. Reichl, "Downstream processing of cell culture-derived virus particles," *Expert Rev. Vaccines*, vol. 10, no. 10, pp. 1451–1475, 2011, doi: 10.1586/erv.11.111.
- [78] P. Gerster *et al.*, "Purification of infective baculoviruses by monoliths," *J. Chromatogr. A*, vol. 1290, pp. 36–45, 2013, doi: 10.1016/j.chroma.2013.03.047.
- [79] G. Jagschies, E. Lindskog, K. Łącki, and P. Galliher, *Biopharmaceutical processing: development, design, and implementation of manufacturing processes*. .
- [80] G. Carta and A. Jungbauer, *Protein chromatography: process development and scale-up*. John Wiley & Sons, 2010.
- [81] A. Š. Podgornik, S. Yamamoto, M. Ž. Peterka, and N. L. Krajnc, "Fast separation of large biomolecules using short monolithic columns," *J. Chromatogr. B Anal. Technol. Biomed. Life Sci.*, vol. 927, pp. 80–89, 2013, doi: 10.1016/j.jchromb.2013.02.004.
- [82] F. Smrekar, M. Ciringier, A. Štrancar, and A. Podgornik, "Characterisation of methacrylate monoliths for bacteriophage purification," *J. Chromatogr. A*, vol. 1218, no. 17, pp. 2438–2444, 2011, doi: 10.1016/j.chroma.2010.12.083.
- [83] R. Hahn, A. Tscheliessnig, P. Bauerhansl, and A. Jungbauer, "Dispersion effects in preparative polymethacrylate monoliths operated in radial-flow columns," *J. Biochem. Biophys. Methods*, vol. 70, no. 1, pp. 87–94, 2007, doi: 10.1016/j.jbbm.2006.09.005.
- [84] C. Boi, "Membrane adsorbers as purification tools for monoclonal antibody purification," *J. Chromatogr. B Anal. Technol. Biomed. Life Sci.*, vol. 848, no. 1, pp. 19–27, 2007, doi: 10.1016/j.jchromb.2006.08.044.
- [85] S. Ahuja, *Handbook of bioseparations*, vol. 2. Elsevier, 2000.
- [86] R. Ghosh, "Ghosh et al 2002 Protein separation using membrane chromatography opportunities and challenges.pdf," vol. 952, pp. 13–27, 2002.
- [87] T. Vicente, M. F. Q. Sousa, C. Peixoto, J. P. B. Mota, P. M. Alves, and M. J. T. Carrondo, "Anion-exchange membrane chromatography for purification of rotavirus-like particles," *J. Memb. Sci.*, vol. 311, no. 1–2, pp. 270–283, 2008, doi: 10.1016/j.memsci.2007.12.021.
- [88] T. Vicente, A. Roldão, C. Peixoto, M. J. T. Carrondo, and P. M. Alves, "Large-scale production and purification of VLP-based vaccines," *J. Invertebr. Pathol.*, vol. 107, pp. S42–S48, 2011, doi: 10.1016/j.jip.2011.05.004.
- [89] S. B. Carvalho *et al.*, "Purification of influenza virus-like particles using sulfated cellulose membrane adsorbers," *J. Chem. Technol. Biotechnol.*, vol. 93, no. 7, pp. 1988–1996, 2018, doi: 10.1002/jctb.5474.
- [90] M. W. Wolff, C. Siewert, S. P. Hansen, R. Faber, and U. Reichl, "Purification of cell culture-derived modified vaccinia ankara virus by pseudo-affinity membrane adsorbers and hydrophobic interaction chromatography," *Biotechnol. Bioeng.*, vol. 107, no. 2, pp. 312–320, 2010, doi: 10.1002/bit.22797.
- [91] L. Urbas *et al.*, "Purification of recombinant adenovirus type 3 dodecahedral virus-like particles for biomedical applications using short monolithic columns," *J. Chromatogr. A*, vol. 1218, no. 17, pp. 2451–2459, 2011, doi: 10.1016/j.chroma.2011.01.032.
- [92] C. S. Burden, J. Jin, A. Podgornik, and D. G. Bracewell, "A monolith purification process for virus-like particles from yeast homogenate," *J. Chromatogr. B Anal. Technol. Biomed. Life Sci.*,

- vol. 880, no. 1, pp. 82–89, 2012, doi: 10.1016/j.jchromb.2011.10.044.
- [93] E. C. Peters, F. Svec, and J. M. J. Fréchet, "Preparation of Large-Diameter 'Molded' Porous Polymer Monoliths and the Control of Pore Structure Homogeneity," *Chem. Mater.*, vol. 9, no. 8, pp. 1898–1902, 1997, doi: 10.1021/cm970204n.
- [94] N. Tanaka, M. Motokawa, H. Kobayashi, K. Hosoya, and T. Ikegami, "Monolithic silica columns for capillary liquid chromatography," *J. Chromatogr. Libr.*, vol. 67, pp. 173–196, 2003.
- [95] A. Jungbauer and R. Hahn, "Polymethacrylate monoliths for preparative and industrial separation of biomolecular assemblies," *J. Chromatogr. A*, vol. 1184, no. 1–2, pp. 62–79, 2008, doi: 10.1016/j.chroma.2007.12.087.
- [96] R. Hahn, M. Panzer, E. Hansen, J. Møllerup, and A. Jungbauer, "Mass transfer properties of monoliths," *Sep. Sci. Technol.*, vol. 37, no. 7, pp. 1545–1565, 2002, doi: 10.1081/SS-120002736.
- [97] A. Strancar, A. Podgornik, M. Barut, and R. Necina, "Short monolithic columns as stationary phases for biochromatography," in *Modern Advances in Chromatography*, Springer, 2002, pp. 49–85.
- [98] S. Yamamoto and A. Kita, "Theoretical background of short chromatographic layers: optimization of gradient elution in short columns," *J. Chromatogr. A*, vol. 1065, no. 1, pp. 45–50, 2005.
- [99] M. Barut, A. Podgornik, P. Brne, and A. Štrancar, "Convective interaction media short monolithic columns: enabling chromatographic supports for the separation and purification of large biomolecules," *J. Sep. Sci.*, vol. 28, no. 15, pp. 1876–1892, 2005.
- [100] F. Svec, T. B. Tennikova, and Z. Deyl, *Monolithic materials: preparation, properties and applications*, vol. 67. Elsevier, 2003.
- [101] B. Mattiasson, A. Kumar, and I. Y. Galeaev, *Macroporous polymers: production properties and biotechnological/biomedical applications*. CRC Press, 2009.
- [102] P. G. Wang, *Monolithic chromatography and its modern applications*. ILM publications, 2010.
- [103] E. I. Trilisky and A. M. Lenhoff, "Flow-dependent entrapment of large bioparticles in porous process media," *Biotechnol. Bioeng.*, vol. 104, no. 1, pp. 127–133, 2009, doi: 10.1002/bit.22370.
- [104] A. Podgornik, A. Savnik, J. Jančar, and N. L. Krajnc, "Design of monoliths through their mechanical properties," *J. Chromatogr. A*, vol. 1333, pp. 9–17, 2014.
- [105] J. Urthaler, R. Schlegl, A. Podgornik, A. Strancar, A. Jungbauer, and R. Necina, "Application of monoliths for plasmid DNA purification: Development and transfer to production," *J. Chromatogr. A*, vol. 1065, no. 1, pp. 93–106, 2005, doi: 10.1016/j.chroma.2004.12.007.
- [106] S. Yamamoto, K. Nakanishi, and R. Matsuno, *Ion-exchange chromatography of proteins*. M. Dekker, 1988.
- [107] P. R. Haddad and P. E. Jackson, *Ion chromatography*, vol. 46. Elsevier, 1990.
- [108] A. Tiselius, "Chromatographic analysis. General introduction," *Discuss. Faraday Soc.*, vol. 7, pp. 7–11, 1949.
- [109] S. Hjertén, "Some general aspects of hydrophobic interaction chromatography," *J.*

- Chromatogr. A*, vol. 87, no. 2, pp. 325–331, 1973, doi: 10.1016/S0021-9673(01)91733-9.
- [110] J. A. Queiroz, C. T. Tomaz, and J. M. S. Cabral, “Hydrophobic interaction chromatography of proteins,” *J. Biotechnol.*, vol. 87, no. 2, pp. 143–159, 2001.
- [111] A. Tiselius, S. Hjerten, and Ö. Levin, “Protein chromatography on calcium phosphate columns,” *Arch. Biochem. Biophys.*, vol. 65, no. 1, pp. 132–155, 1956.
- [112] C. Jiang, L. Flansburg, S. Ghose, P. Jorjorian, and A. A. Shukla, “Defining process design space for a hydrophobic interaction chromatography (HIC) purification step: application of quality by design (QbD) principles,” *Biotechnol. Bioeng.*, vol. 107, no. 6, pp. 985–997, 2010.
- [113] F. Monteiro, N. Carinhas, M. J. T. Carrondo, V. Bernal, and P. M. Alves, “Toward system-level understanding of baculovirus–host cell interactions: from molecular fundamental studies to large-scale proteomics approaches,” *Front. Microbiol.*, vol. 3, p. 391, 2012, doi: 10.3389/fmicb.2012.00391.
- [114] M. M. Bradford, “A rapid and sensitive method for the quantitation of microgram quantities of protein utilizing the principle of protein-dye binding,” *Anal. Biochem.*, vol. 72, no. 1–2, pp. 248–254, 1976.
- [115] B. T. Kurien and R. H. Scofield, “Western blotting,” *Methods*, vol. 38, no. 4, pp. 283–293, 2006.
- [116] P. Steppert, D. Burgstaller, M. Klausberger, A. Tover, E. Berger, and A. Jungbauer, “Quantification and characterization of virus-like particles by size-exclusion chromatography and nanoparticle tracking analysis,” *J. Chromatogr. A*, vol. 1487, pp. 89–99, 2017, doi: 10.1016/j.chroma.2016.12.085.
- [117] S. J. Flint, V. R. (Vincent R. . Racaniello, G. F. Rall, A. M. Skalka, and L. W. (Lynn W. . Enquist, *Principles of virology*. .
- [118] B. Carr and M. Wright, *Nanoparticle Tracking Analysis: A review of applications and usage 2010-2012*. Nanosight, 2013.
- [119] P. Kramberger, M. Ciringer, A. Štrancar, and M. Peterka, “Evaluation of nanoparticle tracking analysis for total virus particle determination,” *Virology*, vol. 9, no. 1, p. 265, 2012, doi: 10.1186/1743-422x-9-265.
- [120] R. A. Dragovic *et al.*, “Sizing and phenotyping of cellular vesicles using Nanoparticle Tracking Analysis,” *Nanomedicine Nanotechnology, Biol. Med.*, vol. 7, no. 6, pp. 780–788, Dec. 2011, doi: 10.1016/j.nano.2011.04.003.
- [121] D. Griffiths, P. Hole, J. Smith, A. Malloy, and B. Carr, “Counting and sizing of virus and protein aggregates by nanoparticle tracking analysis (NTA),” *Nanotechnology*, vol. 3, pp. 176–179, 2010.
- [122] P. J. Wyatt, “Light scattering and the absolute characterization of macromolecules,” *Anal. Chim. Acta*, vol. 272, no. 1, pp. 1–40, 1993.
- [123] S. Podzimek, *Light scattering, size exclusion chromatography and asymmetric flow field flow fractionation: powerful tools for the characterization of polymers, proteins and nanoparticles*. John Wiley & Sons, 2011.
- [124] M. McEvoy, V. Razinkov, Z. Wei, J. R. Casas-Finet, G. I. Tous, and M. A. Schenerman, “Improved particle counting and size distribution determination of aggregated virus populations by asymmetric flow field-flow fractionation and multiangle light scattering

- techniques," *Biotechnol. Prog.*, vol. 27, no. 2, pp. 547–554, 2011.
- [125] P. J. Wyatt, "Measurement of special nanoparticle structures by light scattering," *Anal. Chem.*, vol. 86, no. 15, pp. 7171–7183, 2014.
- [126] B. H. Zimm, "The scattering of light and the radial distribution function of high polymer solutions," *J. Chem. Phys.*, vol. 16, no. 12, pp. 1093–1099, 1948.
- [127] C. Ladd Effio, S. A. Oelmeier, and J. Hubbuch, "High-throughput characterization of virus-like particles by interlaced size-exclusion chromatography," *Vaccine*, vol. 34, no. 10, pp. 1259–1267, 2016, doi: 10.1016/j.vaccine.2016.01.035.
- [128] J. Transfiguracion, A. P. Manceur, E. Petiot, C. M. Thompson, and A. A. Kamen, "Particle quantification of influenza viruses by high performance liquid chromatography," *Vaccine*, vol. 33, no. 1, pp. 78–84, 2015.
- [129] Y. Yang *et al.*, "Size-exclusion HPLC provides a simple, rapid, and versatile alternative method for quality control of vaccines by characterizing the assembly of antigens," *Vaccine*, vol. 33, no. 9, pp. 1143–1150, 2015.
- [130] J. Pérez and Y. Nishino, "Advances in X-ray scattering: from solution SAXS to achievements with coherent beams," *Curr. Opin. Struct. Biol.*, vol. 22, no. 5, pp. 670–678, 2012.
- [131] M. A. Graewert and D. I. Svergun, "Impact and progress in small and wide angle X-ray scattering (SAXS and WAXS)," *Curr. Opin. Struct. Biol.*, vol. 23, no. 5, pp. 748–754, 2013.
- [132] L. Boldon, F. Laliberte, and L. Liu, "Review of the fundamental theories behind small angle X-ray scattering, molecular dynamics simulations, and relevant integrated application," *Nano Rev.*, vol. 6, no. 1, p. 25661, 2015.
- [133] A. Guinier, G. Fournet, and K. L. Yudowitch, "Small-angle scattering of X-rays," 1955.
- [134] H. Schnablegger and Y. Singh, "The SAXS guide: getting acquainted with the principles," *Austria Ant. Paar GmbH*, 2011.
- [135] L. Li, "Structural analysis of cylindrical particles by small angle X-ray scattering." 2005.
- [136] C. Rochette, "Structural analysis of nanoparticles by small angle X-ray scattering." Dissertation. University of Bayreuth, 2011.
- [137] A. Guinier, "La diffraction des rayons X aux très petits angles: application à l'étude de phénomènes ultramicroscopiques," in *Annales de physique*, 1939, vol. 11, no. 12, pp. 161–237.
- [138] D. I. Svergun and M. H. J. Koch, "Small-angle scattering studies of biological macromolecules in solution," *Reports Prog. Phys.*, vol. 66, no. 10, p. 1735, 2003.
- [139] G. Porod, "The x-ray small-angle scattering of close-packed colloid systems," *Kolloid Z.*, vol. 124, p. 32, 1951.
- [140] P. J. Wyatt and M. J. Weida, "Method and apparatus for determining absolute number densities of particles in suspension." Google Patents, 10-Aug-2004.
- [141] P. J. Wyatt, "Measurement of Special Nanoparticle Structures by Light Scattering," *Anal. Chem.*, vol. 86, no. 15, pp. 7171–7183, Aug. 2014, doi: 10.1021/ac500185w.
- [142] F. Krammer *et al.*, "Evaluation of the influenza A replicon for transient expression of

- recombinant proteins in mammalian cells," *PLoS One*, vol. 5, no. 10, p. e13265, 2010.
- [143] S. Schwartz, M. Campbell, G. Nasioulas, J. Harrison, B. K. Felber, and G. N. Pavlakis, "Mutational Inactivation of an Inhibitory Sequence in Human Immunodeficiency Virus Type 1 Results in Rev- Independent gag Expression," *J. Virol.*, pp. 7176–7182, 1992.
- [144] M. M. Segura, A. Garnier, Y. Durocher, H. Coelho, and A. Kamen, "Production of lentiviral vectors by large-scale transient transfection of suspension cultures and affinity chromatography purification," *Biotechnol. Bioeng.*, vol. 98, no. 4, pp. 789–799, 2007, doi: 10.1002/bit.21467.
- [145] L. Cervera, I. González-Domínguez, M. M. Segura, and F. Gòdia, "Intracellular characterization of Gag VLP production by transient transfection of HEK 293 cells," *Biotechnol. Bioeng.*, vol. 114, no. 11, pp. 2507–2517, 2017, doi: 10.1002/bit.26367.
- [146] Y. Hu, X. Cheng, and H. Daniel Ou-Yang, "Enumerating virus-like particles in an optically concentrated suspension by fluorescence correlation spectroscopy," *Biomed. Opt. Express*, vol. 4, no. 9, p. 1646, 2013, doi: 10.1364/boe.4.001646.
- [147] L. J. REED and H. MUENCH, "A SIMPLE METHOD OF ESTIMATING FIFTY PER CENT ENDPOINTS¹²," *Am. J. Epidemiol.*, vol. 27, no. 3, pp. 493–497, May 1938, doi: 10.1093/oxfordjournals.aje.a118408.
- [148] P. Debye, "Zerstreuung von röntgenstrahlen," *Ann. Phys.*, vol. 351, no. 6, pp. 809–823, 1915.
- [149] R. Hine, *The facts on file dictionary of biology*. Infobase Publishing, 2009.
- [150] P. Pereira Aguilar, I. González-Domínguez, T. A. Schneider, F. Gòdia, L. Cervera, and A. Jungbauer, "At-line multi-angle light scattering detector for faster process development in enveloped virus-like particle purification," *J. Sep. Sci.*, no. June, pp. 1–10, 2019, doi: 10.1002/jssc.201900441.
- [151] G. Raposo and W. Stoorvogel, "Extracellular vesicles: Exosomes, microvesicles, and friends," *J. Cell Biol.*, vol. 200, no. 4, pp. 373–383, 2013, doi: 10.1083/jcb.201211138.
- [152] B. K. Thakur *et al.*, "Double-stranded DNA in exosomes: a novel biomarker in cancer detection," *Cell Res.*, vol. 24, no. 6, p. 766, 2014.
- [153] B. Kalbfuss, Y. Genzel, M. Wolff, A. Zimmermann, R. Morenweiser, and U. Reichl, "Harvesting and concentration of human influenza A virus produced in serum-free mammalian cell culture for the production of vaccines," *Biotechnol. Bioeng.*, vol. 97, no. 1, pp. 73–85, 2007.
- [154] G. G. Mironov, A. V. Chechik, R. Ozer, J. C. Bell, and M. V. Berezovski, "Viral Quantitative Capillary Electrophoresis for Counting Intact Viruses," *Anal. Chem.*, vol. 83, no. 13, pp. 5431–5435, Jul. 2011, doi: 10.1021/ac201006u.
- [155] T. Vicente, R. Fáber, P. M. Alves, M. J. T. Carrondo, and J. P. B. Mota, "Impact of ligand density on the optimization of ion-exchange membrane chromatography for viral vector purification," *Biotechnol. Bioeng.*, vol. 108, no. 6, pp. 1347–1359, 2011.
- [156] R. Wagner, L. Deml, H. Fließbach, G. Wanner, and H. Wolf, "Assembly and extracellular release of chimeric HIV-1 Pr55gag retrovirus-like particles," *Virology*, vol. 200, no. 1, pp. 162–175, 1994.
- [157] L. Deml, C. Speth, M. P. Dierich, H. Wolf, and R. Wagner, "Recombinant HIV-1 Pr55gag virus-like particles: Potent stimulators of innate and acquired immune responses," *Mol. Immunol.*,

- vol. 42, no. 2, pp. 259–277, 2005, doi: 10.1016/j.molimm.2004.06.028.
- [158] T. Vicente, C. Peixoto, M. J. T. Carrondo, and P. M. Alves, “Purification of recombinant baculoviruses for gene therapy using membrane processes,” *Gene Ther.*, vol. 16, no. 6, pp. 766–775, Jun. 2009, doi: 10.1038/gt.2009.33.
- [159] T. Vicente, C. Peixoto, P. M. Alves, and M. J. T. Carrondo, “Modeling electrostatic interactions of baculovirus vectors for ion-exchange process development,” *J. Chromatogr. A*, vol. 1217, no. 24, pp. 3754–3764, Jun. 2010, doi: 10.1016/j.chroma.2010.03.059.
- [160] A. Podgornik *et al.*, “Large-scale methacrylate monolithic columns: design and properties,” *J. Biochem. Biophys. Methods*, vol. 60, no. 3, pp. 179–189, Sep. 2004, doi: 10.1016/J.JBBM.2004.01.002.
- [161] M. O. Chang, T. Suzuki, N. Yamamoto, M. Watanabe, and H. Takaku, “HIV-1 Gag-Virus-Like Particles Inhibit HIV-1 Replication in Dendritic Cells and T Cells through IFN- α -Dependent Upregulation of APOBEC3G and 3F,” *J. Innate Immun.*, vol. 4, no. 5–6, pp. 579–590, 2012, doi: 10.1159/000339402.
- [162] Z. Valley-Omar, A. E. Meyers, E. G. Shephard, A.-L. Williamson, and E. P. Rybicki, “Abrogation of contaminating RNA activity in HIV-1 Gag VLPs,” *Virology*, vol. 8, p. 462, Oct. 2011, doi: 10.1186/1743-422X-8-462.
- [163] S. A. Monsma, A. G. Oomens, and G. W. Blissard, “The GP64 envelope fusion protein is an essential baculovirus protein required for cell-to-cell transmission of infection,” *J. Virol.*, vol. 70, no. 7, pp. 4607–4616, 1996.
- [164] I. Markovic, H. Pulyaeva, A. Sokoloff, and L. V. Chernomordik, “Membrane Fusion Mediated by Baculovirus gp64 Involves Assembly of Stable gp64 Trimers into Multiprotein Aggregates,” *J. Cell Biol.*, vol. 143, no. 5, pp. 1155–1166, Nov. 1998, doi: 10.1083/jcb.143.5.1155.
- [165] A. Venereo-Sanchez *et al.*, “Hemagglutinin and neuraminidase containing virus-like particles produced in HEK-293 suspension culture: An effective influenza vaccine candidate,” *Vaccine*, vol. 34, no. 29, pp. 3371–3380, 2016, doi: 10.1016/j.vaccine.2016.04.089.
- [166] D. R. O’Reilly, L. K. Miller, and V. A. Luckow, *Baculovirus expression vectors: a laboratory manual*. Oxford University Press on Demand, 1994.
- [167] C. for P. M. Products, “Virus validation studies: design, contribution and interpretation of studies validating the inactivation and removal of viruses,” CPMP/BWP/268/95, European Agency for the Evaluation of Medicinal Products ..., 1996.
- [168] N. Heath *et al.*, “Rapid isolation and enrichment of extracellular vesicle preparations using anion exchange chromatography,” *Sci. Rep.*, vol. 8, no. 1, p. 5730, Dec. 2018, doi: 10.1038/s41598-018-24163-y.
- [169] S. Gutiérrez-Granados, L. Cervera, F. Gòdia, J. Carrillo, and M. M. Segura, “Development and validation of a quantitation assay for fluorescently tagged HIV-1 virus-like particles,” *J. Virol. Methods*, vol. 193, no. 1, pp. 85–95, Oct. 2013, doi: 10.1016/j.jviromet.2013.05.010.